

**THIN FILM COMPOSITE MEMBRANES OF  
GLASSY POLYMERS FOR GAS SEPARATION -  
PREPARATION AND CHARACTERIZATION**



**KATRIN EBERT**



**THIN FILM COMPOSITE MEMBRANES OF GLASSY POLYMERS  
FOR GAS SEPARATION-  
PREPARATION AND CHARACTERIZATION**

PROEFSCHRIFT

ter verkrijging van  
de graad van doctor aan de Universiteit Twente,  
op gezag van de rector magnificus,  
prof. dr. Th. J. A. Popma,  
volgens besluit van het College voor Promoties  
in het openbaar te verdedigen  
op vrijdag 15 september 1995 te 13.15 uur.

door

Katrin Ebert  
geboren op 17 september 1965  
te Dresden

Dit proefschrift is goedgekeurd door de promotor Prof. Dr. H. Strathmann en de assistent-promotor Dr. M. H. V. Mulder.

*Für meine Mutter*

Air Products and Chemicals, Inc. is gratefully acknowledged for financial support.

CIP-DATA KONINKLIJKE BIBLIOTHEEK, DEN HAAG

Ebert, Katrin

Thin film composite membranes of glassy polymers for gas separation - Preparation and characterization / Katrin Ebert. - [S.l.: s.n.]. - III

Thesis Enschede. - With ref. - With summary in Dutch and German.

ISBN 90-9008341-3

Subject headings: composite membranes / gas separation / glassy polymers / dip-coating / stress measurements

Copyright © 1995 K. Ebert

All rights reserved.

Printed in the Netherlands by Ponsen & Looijen B. V., Wageningen.

## Preface

Mit der hier vorliegenden Arbeit geht für mich die Universitätszeit nun endgültig vorbei. Eine ganz besonders wichtige Stütze, Studium und Promotion zu absolvieren, war und ist für mich der Rückhalt in der Familie. In diesem Zusammenhang möchte ich ganz besonders meiner Mutter danken, die mich mit viel Liebe unterstützt, mir dabei aber immer meinen persönlichen Freiraum gewährt hat.

Weiterhin möchte ich allen meinen Freunden und Bekannten für ihre Freundschaft und ihr Interesse danken. Es ist herrlich, mit guten Freunden über "Gott und die Welt" schwatzen zu können.

Of course, such a PhD-study you cannot do alone. There were a number of people at the university who were involved in the project.

First of all, I have to thank Jose Nolten who worked the first three years in the project. In this time she carried out a lot of experimental work, which was the fundament of this thesis. Beside her practical help she fulfilled another delicate task: introducing me into the secrets of the dutch language.

Special thanks I want to give to Ljubo Germic and Andreja Kranjc from the University of Maribor in Slovenia. I enjoyed very much working together with you! Ljubo, you very enthusiastic carried out a lot of permoporometry and liquid-liquid displacement experiments. Your work was an excellent base for chapter 2. Andreja, preparing composite membranes and characterizing polymer solutions can be quite disappointing. Nevertheless, you always believed in the "break through".

Zandrie Borneman I want to thank for the stress measurements. With his specially created set-up the reproducibility of the measurements could be improved a lot.

Kitty Nijmeijer, who came in the very last period of the project, was the second student who had to prepare composite membranes. Her work added new aspects to chapter 4.

Herman Teunis took care of the gas permeation set-up which was the most important set-up during my work.

Marcel Mulder, the assistant promotor was a good support during the four years. If it was necessary he took time for discussion.

I want to thank Professor Strathmann for critical reading the concept of this thesis.

Dr. Puri and Jaap van't Hof from Air Products and Chemicals, Inc. I want to thank for cooperative support during the whole project.

Marjo Peeters, Alie Bos, Ingo Blume, Willem Kools and Erik Meuleman I want to thank for reading the concept of my thesis.

Finally, I want to thank all the members of the membrane group for help, discussions and fun.

Katje

# CONTENT

## CHAPTER 1

### Composite membranes for gas separation

1. 1. Introduction	1
1. 2. Commercial gas separation membranes	2
1. 3. Preparation of composite membranes - A short literature review	6
1. 4. The Dip-coating process	8
1. 5. Scope of this thesis	11
1. 6. References	12

## CHAPTER 2

### Characterization methods for support layers in composite membranes

Summary	15
2. 1. Introduction	16
2. 2. Theoretical aspects of the characterization techniques	16
2. 2. 1. Gas transport through porous membranes	16
2. 2. 2. Scanning electron microscopy	19
2. 2. 3. Permporometry	20
2. 2. 4. Liquid-liquid displacement	23
2. 3. Experimental	25
2. 3. 1. Materials	25
2. 3. 2. Gas fluxes	25
2. 3. 3. Field emission scanning electron microscopy (FESEM)	25
2. 3. 4. Permporometry	25
2. 3. 5. Liquid-liquid displacement	27
2. 4. Results and discussion	27
2. 4. 1. Pressure normalized gas fluxes	27
2. 4. 2. Field emission scanning electron microscopy	28
2. 4. 3. Permporometry	29
2. 4. 4. Liquid-liquid displacement	33
2. 5. General discussion - Comparison of the characterization techniques	37
2. 6. References	38



<b>Appendix A:</b> Derivation of the pore size distribution from permoporometry measurements	40
----------------------------------------------------------------------------------------------	----

<b>Appendix B:</b> Derivation of the pore size distribution from liquid-liquid displacement measurements	44
----------------------------------------------------------------------------------------------------------	----

### CHAPTER 3

#### **Composite membranes with a glassy polymer as toplayer; Part I: Polycarbonate as coating polymer**

Summary	47
3. 1. Introduction	48
3. 2. Theoretical aspects of the dip-coating process	48
3. 3. Polymers in solution - Influence on the coating process	52
3. 4. Gas transport through composite membranes	53
3. 5. Calculation with the resistance model	53
3. 6. Experimental	56
3. 6. 1. Support materials	56
3. 6. 2. Coating materials	57
3. 6. 3. Coating procedure	57
3. 6. 4. Characterization of the composite membranes	59
3. 7. Results and discussion	59
3. 7. 1. Coating experiments without impregnation	59
3. 7. 2. Coating experiments with impregnation	62
Influence of the coating velocity	66
Influence of the polymer concentration	67
3. 8. Conclusions	69
3. 9. References	69
<b>Appendix A:</b> Rheological properties of polymer solutions	71
<b>Appendix B:</b> Polymers in solution - Some aspects of characterization	76

## CHAPTER 4

### Composite membranes with a glassy polymer as toplayer; Part II: Poly(methyl methacrylate) as coating polymer

Summary	83
4. 1. Introduction	84
4. 2. Drying process	84
4. 3. Post treatment of coating layers	86
4. 4. Experimental	86
4. 4. 1. Support materials	86
4. 4. 2. Coating material	87
4. 4. 3. Coating procedure	88
4. 4. 4. Drying and post treatment of the composite membranes	89
4. 4. 5. Characterization of the composite membranes	89
4. 5. Results and discussion of the coating experiments	90
4. 5. 1. Influence of the coating velocity	90
Flat membranes	90
Hollow fibers without impregnation	91
Hollow fibers with impregnation	92
4. 5. 2. Influence of the polymer concentration	94
4. 5. 3. Influence of the coating solvent and molecular weight	95
4. 5. 4. Influence of the drying procedure	96
4. 5. 5. Influence of the post treatment procedure	97
4. 5. 6. Role of the support	98
4. 6. Conclusions	99
4. 7. References	99

## CHAPTER 5

### Stress measurements in coating layers upon drying

Summary	101
5. 1. Introduction	102
5. 2. Mechanical properties of polymers	102
5. 3. Methods for the determination of the stress in thin layers	107
5. 4. Principle of the new method	109
5. 5. Experimental	111
5. 6. Results and discussion	111
5. 6. 1. Influence of the support on the final stress	111

5. 6. 2. Influence of the molecular weight	112
5. 6. 3. Influence of the coating thickness	116
5. 6. 4. Influence of the drying procedure	117
5. 6. 5. Influence of post treatment	117
5. 7. Conclusions	118
5. 8. References	119

## **CHAPTER 6**

### **The preparation of composite membranes by dip-coating; A summary**

6. 1. Introduction	121
6. 2. General aspects	122
The support	122
The coating polymer	122
Prevention of pore penetration	123
Drying and post treatment	124
6. 3. Conclusions	125
6. 4. References	125
<b>Summary</b>	127
<b>Samenvatting</b>	129
<b>Zusammenfassung</b>	131
<b>Curriculum Vitae</b>	134



# 1

## COMPOSITE MEMBRANES FOR GAS SEPARATION

### 1. 1. INTRODUCTION

Mitchell<sup>[1]</sup> was one of the first who observed that natural rubber can separate gases. Later Graham<sup>[2]</sup> described the transport of gases through natural rubber by a simple solution-diffusion mechanism: first the gas dissolves in the membrane, diffuses through the membrane due to a driving force of a concentration gradient and, finally, desorbs at the other side of the membrane. This is schematically shown in Figure 1.1. The membrane functions as an interphase with permselective properties.

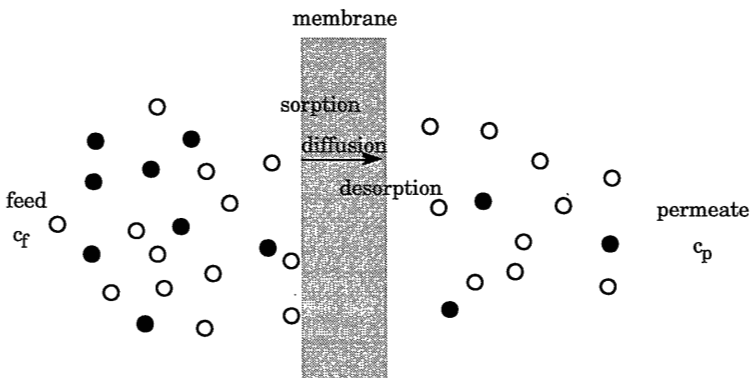


**Figure 1.1** Schematical drawing of the solution-diffusion mechanism of gases through a membrane ( $c_f$  and  $c_p$  represent the gas concentration in the feed and in the permeate, respectively)

Since the first experiments of Mitchell and Graham gas separation by means of membranes has become an increasing field of interest. Membranes are, however, not only used in gas separation but in many other fields, such as purification of liquids by ultrafiltration or microfiltration, desalination of seawater by reverse osmosis, separation of organic liquids and multivalent ions from water by nanofiltration, etc.. These applications indicate already that the term “membrane” is complex, since the different applications are based on different separation mechanisms. The definition of the “membrane” should include information about the nature of the membrane as well as about its function. A membrane can simply *“be considered as a permselective barrier between two phases”*<sup>[3]</sup>. A more extended definition of a membrane was given by Quinn<sup>[4]</sup>: *“A membrane is an interphase. It has distinct physicochemical properties and it is bounded by two surfaces, each of which joins it to a continuous bulk phase. Generally it is “thin” - in the sense that it has a large ratio of surface area to volume; as its thickness approaches molecular dimensions the interphase becomes an interface. The special separative/ barrier/contacting properties of membranes derive from the fact that an interphase can communicate simultaneously with its two adjacent phases; this permits the establishment and maintenance of gradients across the membrane and allows exchange to occur at both surfaces.”*

## 1. 2. COMMERCIAL GAS SEPARATION MEMBRANES

Today membrane technology must compete with other existing techniques such as pressure swing adsorption (PSA) and cryogenic distillation. Generally, membranes for the separation of air can be used to produce both, oxygen and nitrogen. In practice, however, the production of high-purity nitrogen can be achieved much easier than the production of high-purity oxygen<sup>[5]</sup>. Therefore, membranes are mainly used for the nitrogen enrichment from air. Nitrogen is used in the petrochemical and pharmaceutical industry and for food processing and packaging. Most of the oxygen is still produced by cryogenic distillation<sup>[6]</sup>. Economical considerations of the separation process, however, show that each of the processes PSA, cryogenic distillation and membrane technology can have advantages, depending on the requirements of purity of the gas and the amount required. Beaver et al.<sup>[6]</sup> showed that cryogenic distillation processes are useful if large amounts of high purity nitrogen are required. If moderate volumes of high purity nitrogen at modest pressure are required, PSA is the most economical method. Membranes are of commercial interest for purities of nitrogen up to 99.5 % and volume streames up to about 2800 liter /hour. In Figure 1.2 the different gas separation methods used for nitrogen enrichment are compared with respect to their economical feasibility<sup>[7]</sup>. It can be seen that membranes have benefits especially for lower volumes and lower purities of nitrogen.

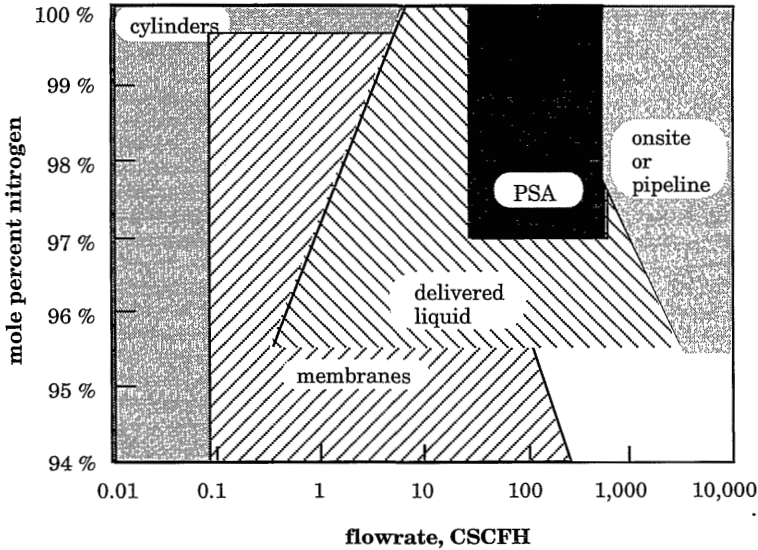


**Figure 1.2** Schematic drawing showing the commercially interesting area of application of gas separation techniques used for nitrogen enrichment from air as a function of gas purities and plant capacities<sup>[7]</sup>; 1 CSCFH ( hundred standard cubic feet per hour)=3 m<sup>3</sup>/hour

A number of polymeric membranes for the separation of air are on the market. Some of them are listed in table 1.1. Most of these membranes are in hollow fiber or spiral wound configuration. Furthermore, the membrane structure is either a composite or an integrally skinned asymmetric structure. In the case of a composite membrane generally an elastomeric sealing layer is applied on a (glassy) support material to repair possible defects in the support. This indicates already that the preparation of thin defect-free layers of glassy polymers provides difficulties. This is mainly due to the generation of stress during preparation which results in defects<sup>[8]</sup>. This occurs only with glassy polymers and not with elastomers since in the former case the glass transition temperature is passed.

The crucial parameters which determine the economical attractiveness of membranes are the flux and the separation factor. A high selectivity can be obtained by developing proper materials. Generally, there is a significant difference between glassy and rubbery polymers with respect to their gas separation performance. Characteristic for rubbery polymers is a quite high gas permeability combined with a quite low selectivity for the separation of certain gases. Glassy polymers are known for high selectivities, especially for the separation of oxygen from nitrogen, however, the permeability through these materials is extremely low. Table 1.2 summarizes the gas permeation properties and the glass transition temperatures of some polymers. Generally, it can be seen that the lower the glass transition temperature

the higher the oxygen permeability. In some cases the low permeability may also be caused by crystallinity of the material which leads to a drastic decrease in permeability.

**Table 1.1** Commercial gas separation membranes for the nitrogen enrichment from air<sup>[9,10]</sup>

supplier	membrane	material
A/G Technology	AVIR	ethylcellulose
Delair		PPO
Dow	Generon I	polymethylpentene
	Generon II	modified PC
	Cynara	cellulose triacetate
	Separex	cellulose acetate
Envirogenics	Gasep	cellulose acetate
Grace		cellulose acetate
MTR		PDMS coating
Oxygen Enrichment		PDMS/PC copolymer
Permea	Prism Alpha	PSf with PDMS
Ube		polyimide
Union Carbide Ind. Gases	NitroGEN	

PPO polyphenylene oxide  
 PC polycarbonate  
 PDMS polydimethylsiloxane  
 PSf polysulfone

For the use in gas separation it is absolutely necessary to have defect-free membranes because defects of 5 nm lead already to a drastical decrease in selectivity<sup>[11]</sup>.

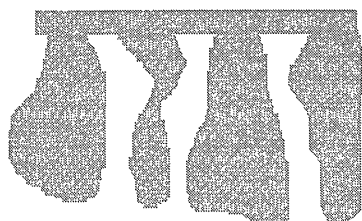


**Table 1.2** Glass transition temperatures and gas permeation properties of some polymers

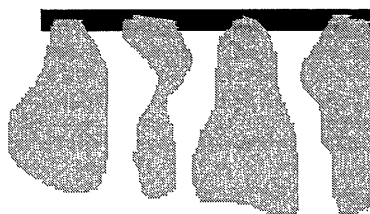
polymer	glass transition temperature [°C]	oxygen permeability [Barrer]*	selectivity (O <sub>2</sub> /N <sub>2</sub> )
polydimethylsiloxane[12]	- 123	600	2.1
polybutadiene[12]	85	24	3.0
polyethylene[12]	- 120	2.9	3.0
polyisoprene[12]	- 73	23.3	2.5
butyl rubber[13]	- 65	1.3	4.0
polymethylpentene[14]	30	32.3	4.1
polyvinylalcohol[12]	85	0.009	>9
polyvinylchloride[12]	87	0.045	3.8
polyacrylonitrile[15]	120	0.002	3.1
polycarbonate[16]	155	10.1	4.5
polysulfone[17]	190	1.05	6.36

\* 1 Barrer =  $10^{-10}$  cm<sup>3</sup> cm/cm<sup>2</sup> s cmHg

To enhance the transmembrane flux the thickness of the rate limiting toplayers must be decreased as much as possible. Improved mechanical stability in combination with good separation properties can be achieved by making either an integrally skinned membrane or a composite membrane (see Figure 1.3).



integrally skinned membrane with top layer and sublayer from the same material



composite membrane with top layer and sublayer from different materials

**Figure 1.3** Schematical drawings of an integrally skinned membrane and a composite membrane

From an economical point of view composite membranes are preferred because only a thin layer of the selective polymer is required. In this way the membrane costs can be kept low because a number of polymers which have been developed for special separation problems are quite expensive. Furthermore, most of these special polymers show good selectivities but very low permeabilities. To obtain economically

reasonable fluxes through membranes of these materials, very low layer thicknesses are required. Prasad et al.<sup>[5]</sup> calculated how the thickness of the membrane directly influences the product costs in the case of nitrogen production. The results are shown in Figure 1.4.

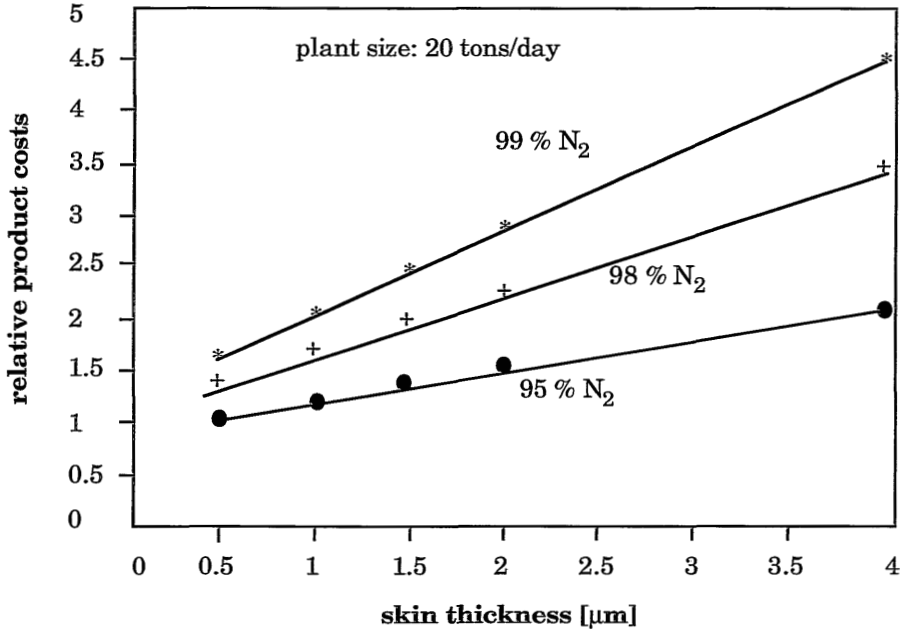


**Figure 1.4** Effect of membrane skin thickness on nitrogen product costs<sup>[5]</sup>

As can be seen from this figure the skin thickness has a drastic influence on the product costs. A decrease of the thickness of the separating layer from 4  $\mu\text{m}$  to 0.5  $\mu\text{m}$  results in a 300 % decrease of the product costs at high nitrogen purities.

### 1. 3. PREPARATION OF COMPOSITE MEMBRANES - A SHORT LITERATURE REVIEW

There is a large interest in the preparation of composite membranes with ultrathin defect-free layers. In the literature, especially in the patent literature, a number of methods can be found which describe the preparation of these membranes. Generally, there are different methods to apply a thin dense layer upon a porous support, e. g. plasma polymerization, interfacial polymerization, spin coating, Langmuir-Blodgett technique and dip-coating. Because most of the selective polymers can only be applied by a solution type coating and a continuous process is preferred dip-coating can be considered as the most suitable technique.

Very crucial for the preparation of composite membranes is the size of the pores at the surface of the support, the pore size distribution and the porosity. However, there are two conflicting structure-property requirements. On one hand, if just the flux through such a membrane is considered then the support must be as open as possible and may not contribute to transport<sup>[11]</sup>. On the other hand, if the pores at the surface are too big the thin coating layers do not have enough mechanical support to withstand the high pressures applied in gas separation processes. Furthermore, these big pores may cause defects during the coating process because the relatively low viscous coating solutions can easily penetrate into these pores. In this way not only defects are created, but it may also lead to a drastic decrease in the membrane flux due to pore blocking<sup>[11]</sup>. Rezac<sup>[18]</sup> prepared composite membranes consisting of a ceramic support and a polymeric coating layer. Defect-free layers could only be prepared if the diameter of the polymer coils in the coating solution were at least as large as the diameter of the maximum pores at the surface of the support. This can be achieved by the choice of a suitable solvent and a polymer with a high molecular weight<sup>[18]</sup>.

Pore penetration is one of the main problems in the preparation of composite membranes. Different approaches are known to prevent this and some of them will be discussed here briefly.

Williams et al.<sup>[19]</sup> described a method to coat ethylcellulose on polysulfone (PSf) hollow fibers. The PSf fibers were dried prior to the coating procedure in such a way that small amounts of liquid remained in the substrate. The pore filling liquid was chosen to be a nonsolvent for the coating polymer but miscible with the solvent of the coating solution. In this way composite membranes with slightly asymmetric structure of the coating layer and low effective thicknesses were obtained. Glycerine can be used as the pore filling liquid as well<sup>[20]</sup>. Ohyabu<sup>[21]</sup> used as a support hollow fibers, which were spun from a solution of PSf and polyvinylpyrrolidone (PVP) in dimethylformamide (DMF). Just after the coating process was finished the PVP was removed. The advantage of this approach is that during the coating process the surface is quite smooth and that the resistance of the final support to the transport is quite low. Bikson<sup>[22]</sup> annealed asymmetric PSf fibers near the glass transition temperature prior to the coating experiments. As a result of this temperature treatment the surface of the PSf fibers became smoother, however, also the flux through these annealed fibers decreased.

Pore penetration can be prevented as well by the preparation of a multilayer composite membrane, consisting of a porous support, a highly permeable intermediate layer (a 'gutter' layer) and on top the actual separation layer. The intermediate layers are often prepared of polydimethylsiloxane or its derivatives<sup>[14,16,23-28]</sup>, which exhibit a high gas permeability. A problem which often arises with these type of membranes is that adhesion between support and coating material becomes very important. If the adhesion is poor very typical defects can be created, which sometimes can have quite large dimensions<sup>[16]</sup>. Riley et al.<sup>[28]</sup> used

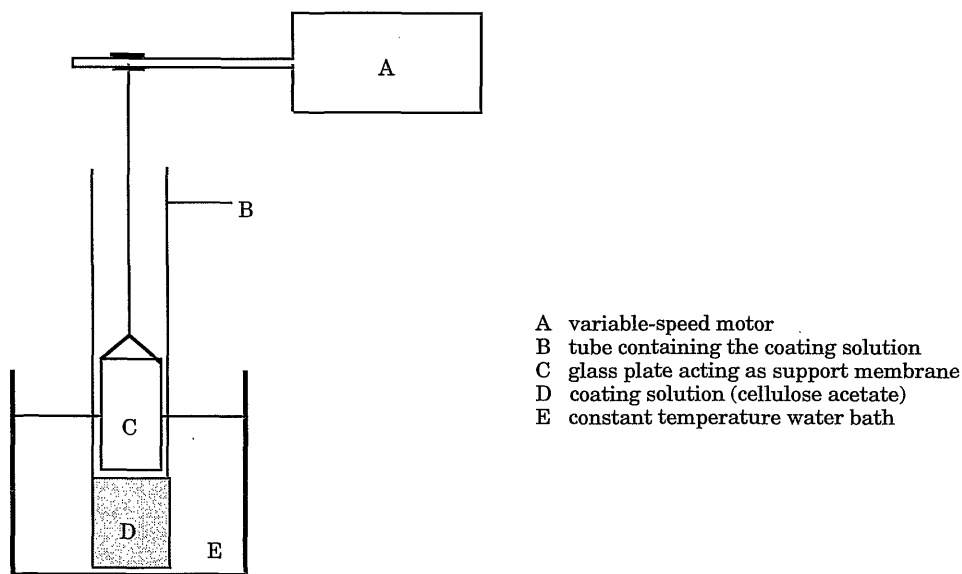
the effect of smoothing the surface by an intermediate layer during the coating process. However, after the coating layer has been solidified the intermediate layer was leached out.

Another possibility to overcome pore penetration is to make use of coating solutions which can gelate. Preferably, this gelation should already occur at low polymer concentrations, because higher concentrated solutions result in thicker coating layers. For the coating process a solution is used which is just at the border of gelation. Once, the solution is coated on the support, already a very small change in concentration, e. g. by evaporation of the solvent, will induce gelation leading to a drastic increase in viscosity which prevents the solution from penetrating into the pores of the support<sup>[14,25]</sup>.

When the coating layer has been formed several methods can be employed to repair existing defects. The treatment can be carried out either at the surface of the coating layer<sup>[15,29-32]</sup> or from the permeate side of the layer<sup>[29]</sup>. Bikson et al.<sup>[29]</sup> could improve the performance of composite membranes by contacting the permeate side of the coating layer with a volatile solvent or a solution of a volatile solvent and a prepolymer, which was crosslinked after the solvent was evaporated. Pinnau et al.<sup>[30]</sup> treated asymmetric polyetherimide (PEI) membranes either with a solvent or swelling agent or with a solution of PEI. The solutions were applied by immersion, spraying or painting. The post-treatment resulted in composite membranes with slightly decreased flux but increased selectivity. The same improvement of membrane performance was found by Rezac et al.<sup>[32]</sup>. The membranes were treated either in the vapour phase, by immersion or by treatment with a sponge. Surface treatment with a sponge appeared to give the best results with respect to membrane flux and selectivity.

#### 1. 4. THE DIP-COATING PROCESS

Dip-coating is a simple process in which a support is immersed in a solution containing the coating polymer and then withdrawn from this solution<sup>[33]</sup>. Thereby, a thin film adheres to the support which can be solidified by evaporating the solvent. With this method very thin layers, even lower than 0.01  $\mu\text{m}$ , can be prepared. In Figure 1.5 a schematical drawing of the coating set-up used by Riley and coworkers<sup>[33]</sup> is shown.



- A variable-speed motor
- B tube containing the coating solution
- C glass plate acting as support membrane
- D coating solution (cellulose acetate)
- E constant temperature water bath

**Figure 1.5** Schematical drawing of a set-up for the preparation of thin film composite membranes<sup>[33]</sup>

The coating velocity has to be chosen so that a continuous film can be formed on the support. If the velocity is too high then the film breaks due to effects of surface tension. A very low coating velocity may lead to inhomogeneities due to partial evaporation of the solvent. Preferred velocities as indicated in the literature are in the range of 0.25 to 5 cm/s<sup>[34-36]</sup>.

The coating solution (D) consisting of a dilute cellulose acetate solution was placed in a tube (B). The tube was then immersed in a water bath at 30 °C to keep the temperature during the coating experiment constant. The glass plate was immersed in the coating solution and remained there for about 5 minutes. After that the glass plate was withdrawn from the solution with a motor (A). After the membrane was allowed to dry for 20 minutes, the glass plate (with the coated membrane on it) was immersed into water and the membranes were floated off. Membranes with thicknesses of about 600 could be prepared reproducibly.

For the preparation of composite membranes by dip-coating a number of parameters have to be considered. They can roughly be divided into three groups. The first group are the polymer related parameters like permeability and solubility behaviour of a certain gas in a polymer. The second group are the process related coating parameters, e. g., coating velocity, concentration, viscosity, solvent, temperature of the coating solution, evaporation time. The support related parameters, such as surface porosity, pore size distribution and flux through the support, belong to the third group. Each of these parameters needs to be optimized to give a desired

composite membrane and to improve the reproducibility of the results which is one of the main problems in the preparation of composite membranes<sup>[15,16]</sup>.

The thickness of the coating layer depends mainly on the polymer concentration, the molecular weight, the solvent and the parameters of the coating process such as the coating velocity<sup>[33,37,38]</sup>. The dependence of the coating thickness on the concentration of the coating solution for cellulose membranes is shown in Figure 1.6<sup>[33]</sup>.

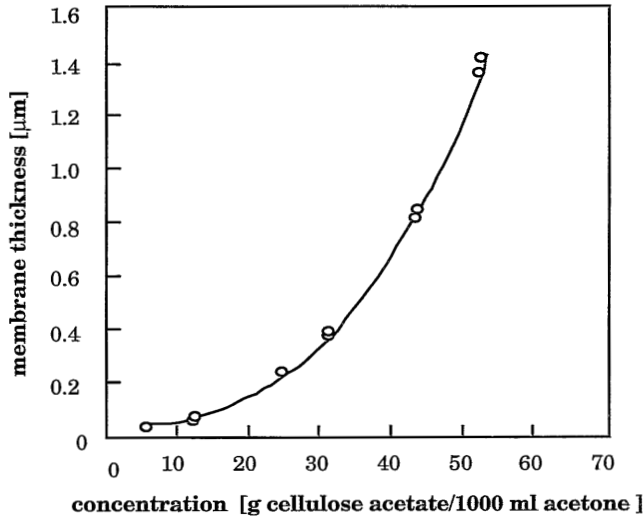


**Figure 1.6** Dependence of the coating thickness on the concentration of the coating solution.<sup>[33]</sup>

A problem which arises with layers prepared by dip-coating is the occurrence of defects which are mainly caused by mechanical stresses built up during the film formation process<sup>[39]</sup>. To obtain thin layers coating solutions with rather low polymer concentrations are used, ranging from 0.5 to 4 % polymer in the solution. During the film formation process, i. e. solidification of the coating layer, a volume contraction due to the evaporation of solvent occurs<sup>[8]</sup>. Because of adhesion to the support this volume reduction can not occur isotropically in all directions, but only in one direction. The volume reduction parallel to the support must be compensated by relaxation of the polymer or, if the stress becomes too high, cracks will be formed resulting in defects. A method where the nascent film is kept free of any tensile stress is the Langmuir-Blodgett technique. In Figure 1.7 a schematical drawing of a Langmuir-Blodgett set-up is shown<sup>[39]</sup>. The polymer solution is applied onto the liquid support between two barriers. It is important that firstly, the liquid support contains no contaminants and secondly, the polymer solution spreads spontaneously over the liquid support. Then one of the barriers is drawn away, resulting in a

controlled enlargement of the surface area on which the polymer solution can spread. After complete evaporation of the solvent solidification has occurred and the film is removed from the surface and deposited on a porous membrane support. Film thicknesses of less than  $0.1 \mu\text{m}$  can be obtained, however, films can only be prepared in a batch production mode<sup>[39-41]</sup>.

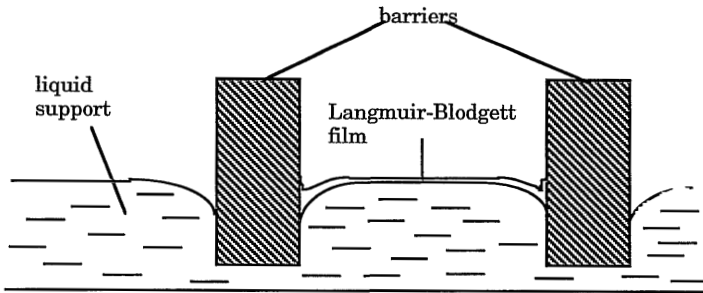


**Figure 1.7** Schematical drawing of a set up for the preparation of Langmuir-Blodgett films<sup>[39]</sup>

## 1. 5. SCOPE OF THIS THESIS

To make gas separation by means of polymeric membranes economically feasible, composite membranes with thin separation layers or integrally skinned asymmetric membranes are required. This work describes the preparation of a glassy toplayer on a glassy support by means of a dip-coating technique. A number of parameters may have an influence on the quality of the prepared layers, such as the coating velocity, the concentration of the coating solution, the molecular weight of the coating polymer, the coating solvent, the impregnation of the support, the drying and the post-treatment procedure, and these have been investigated in this work.

For the coating experiments different porous supports, in flat sheet as well as in hollow fiber configuration, have been used. These membranes have been characterized with respect to their morphology by different methods, such as gas permeation measurements, electron microscopy, permoporometry and liquid-liquid displacement. The results of the characterization methods are described in Chapter 2. The calculation of the pore size distributions from permoporometry and liquid-liquid displacement measurements has been described as well (see appendix A and B to Chapter 2).

The influence of some coating parameters as well as the role of the drying and post-treatment procedure have been investigated. The results are given in Chapter 3 for polycarbonate as the coating material, while in Chapter 4 coating experiments with poly(methyl methacrylate) are discussed. The prepared composite membranes were characterized by gas permeation measurements and electron microscopy. The

rheological properties of the coating solutions have been described in Appendix A to this chapter. To investigate the influence of the molecular dimension of the polymer in the coating solution with respect to the quality of the coating layer all coating solutions have been characterized by light scattering, viscosimetry and gel permeation chromatography. The results are shown in Appendix B to Chapter 3.

One of the reasons for defects in thin coating layers are mechanical stresses which are generated during the drying process. In Chapter 5 a new method is described to measure these stresses. The method can help to influence the film formation in such a way that no defects are formed.

Chapter 6 gives a general summary for the preparation of composite membranes as concluded from the results of this thesis.

## 1. 6. REFERENCES

- [1] J. K. Mitchell; *Am. J. Med.*, 7(1830), 36-67
- [2] T. Graham; *Phil. Mag.*, 32 (1866), 401-420
- [3] M. H. V. Mulder; *Basic principles of membrane technology*; Kluwer Academic Publishers, Dordrecht, the Netherlands (1991)
- [4] H. K. Lonsdale; *What is a membrane? Part II*; *J. Membr. Sci.*, 43 (1989), 1-3
- [5] R. Prasad, D. R. Thompson; *Evolution of membranes in commercial air separation*; *J. Membr. Sci.*, 94 (1994) 225-248
- [6] E. R. Beaver, P. Y. Bhat; *Integration of membranes with other air separation technologies*; *AIChE Symposium Series No. 261, Vol. 84*, 113-123
- [7] R. W. Spillman; *Economics of gas separation membranes*; *Chem. Eng. Progr.* 85 (1989) 41-62
- [8] chapter 5 of this thesis
- [9] W. Maaskant, M. H. V. Mulder, J. J. P. Tholen; *Nederlands membraangids, versie 1.0*; (1993), Haskoning, Nederland
- [10] T. Matsuura; *Synthetic membranes and membrane separation processes*; CRC Press, Inc. Boca Raton (1994)
- [11] J. M. S. Henis, M. K. Tripodi; *Multicomponent membranes for gas separation*; U. S. Patent 4,230,463  
J. M. S. Henis, M. K. Tripodi; *Composite hollow-fiber membranes for gas separation: the resistance model approach*; *J. Membr. Sci.*, 8 (1981) 233-246
- [12] H. Yasuda, V. Stannett; "Permeability coefficients" in *Polymer Handbook*, J. Brandrup (Ed.), John Wiley Interscience, NY (1975)
- [13] C. G. Wensly, G. Z. Jakabharz; *High performance gas separation membranes*; *AIChE Nat. Meeting, Atlanta (Georgia), March 1984*
- [14] I. Pinnau; *Ultrathin ethylcellulose/poly(4-methylpentene-1) permselective membranes*; U. S. Patent 4,871,378
- [15] chapter 4 of this thesis
- [16] chapter 3 of this thesis
- [17] I. Pinnau; *Skin formation of integral-asymmetric gas separation membranes made by dry/wet phase inversion*; PhD-thesis, University of Austin (Texas), (1991)
- [18] M. E. Rezac, W. J. Koros; *Preparation of polymeric-ceramic composite membranes with thin defect-free separating layers*, *J. Appl. Polym. Sci.*, 46 (1992), 1927-1938
- [19] S. C. Williams, B. Bikson, J. K. Nelson; *Composite membranes for enhanced fluid separation*; EP 0 286 091  
S. C. Williams, B. Bikson, J. K. Nelson, R. D. Burchesky; *Method for preparing composite membranes for enhanced gas separation*; U. S. Patent 4,840,819



- [20] E. R. Kafchinsky, T. Chung; Asymmetric fluoropolymer-coated polyolefine hollow fibers; U. S. Patent 5,213,689
- [21] S. Ohyabu, S. Kawai, T. Okamoto, T. Migaki; Composite hollow fibre-type separation membranes, process for the preparation thereof and their use; U. S. Patent 4,664,669
- [22] B. Bikson, J. E. Miller, J. K. Nelson; Permeable membranes for enhanced gas separation; U. S. Patent 4,881,954
- [23] A. v. d. Scheer; Composite dense membranes; U. S. Patent 4,581,043
- [24] I. Cabasso, K. A. Lundy; Method for making membranes for gas separation and the composite membranes; U. S. Patent 4,602,922  
K. A. Lundy, I. Cabasso; Analysis and construction of multilayer membranes for the separation of gas mixtures; *Ind. Eng. Chem. Res.*, 28(6) (1989), 742-756
- [25] I. Blume, I. Pinnau; Composite membranes, method of preparation and use; U. S. Patent 4,963,165
- [26] C. R. Gouchanour; Gas separation membranes with ultrathin layers; U. S. Patent 5,160,353
- [27] J. J. Chiou; Composite gas separation membrane having a gutter layer comprising a crosslinked polar phenyl-containing organopolysiloxane, and method for making the same; U. S. Patent 5,286,280
- [28] R. L. Riley, Thin film separation membranes and processes for making the same; U. S. Patent 3,648,845
- [29] B. Bikson, S. Gaglia, G. Kharas; Composite separation membranes and the preparation and use thereof; U. S. Patent 4,767,422
- [30] I. Pinnau, J. Wind; Process for increasing the selectivity of asymmetric membranes U. S. Patent 5,007,944
- [31] R. A. Hayes; Surfactant treatment of aromatic polyimide gas separation membranes; U. S. Patent 5,034,024  
R. A. Hayes; Surfactant treatment of polyaramide gas separation membranes; U. S. Patent 5,032,149
- [32] M. E. Rezac, J. D. LeRoux, H. Chen, D. R. Paul, W. J. Koros; Effect of mild solvent post-treatment on the gas transport properties of glassy polymer membranes; *J. Membr. Sci.*, 90 (1994), 213-229
- [33] R. L. Riley, H. K. Lonsdale, C. R. Lyons, U. Merten; The preparation of ultrathin reverse osmosis membranes and the attainment of "theoretical" salt rejection; *J. Appl. Polym. Sci.*, 11 (1967) 2143-2158
- [34] K. Matsumoto, X. Ping; Composite or asymmetric fluorine containing polyimide membrane, a process for manufacturing the same and a method for the separation and preparation of gas using the same; U. S. Patent 5,165,963
- [35] R. L. Riley, R. L. Grabowsky; Preparation of gas separation membranes; U. S. Patent 4,243,701
- [36] B. Bikson, J. K. Nelson; Composite membranes and their manufacture and their use; U. S. Patent 4,826,599
- [37] B. M. Deryagin, S. M. Levi; Film coating theory; The Focal Press, London New York (1959)
- [38] P. Groenveld; Dip-coating by withdrawal of liquid films; Ph-D thesis University of Delft (1970)
- [39] W. J. Ward; Ultrathin polymer membranes; U. S. Patent 4,374,891  
W. J. Ward; Method for casting of ultrathin polymer membranes; U. S. Patent 4,279,855
- [40] S. G. Kimura, R. G. Larigne, W. R. Browall; Method for casting ultrathin methylpentene polymer membranes; U. S. Patent 4,192,842  
S. G. Kimura, R. G. Larigne, W. R. Browall; Method for casting ultrathin methylpentene polymer membranes; U. S. Patent 4,132,824
- [41] T. Yamamada, S. Kurisu, S. Azuma, K. Sugie, T. Yamaji; Ultrathin solid membrane, process for production thereof, and use thereof for concentrating a specified gas in a gaseous mixture; U. S. Patent 4,406,673



# 2

---

## **CHARACTERIZATION METHODS FOR SUPPORT LAYERS IN COMPOSITE MEMBRANES**

---

### ***Summary***

*The development of a suitable support structure is the first step in the preparation of a composite membrane. Various methods have been used to characterize the support layers, such as gas flux measurements, (field emission) scanning electron microscopy, permoporometry and liquid-liquid displacement. Three different commercial polyacrylonitrile membranes have been characterized in this study and the results obtained from the different methods have been compared.*

*Significant differences in the pore size distributions determined from permoporometry and liquid-liquid displacement were obtained. A shift of the pore size distribution to higher pore radii was found with liquid-liquid displacement experiments.*

## 2. 1. INTRODUCTION

Composite membranes consist of a porous support on which a thin dense layer is deposited. In general, both layers originate from different materials. The advantage of such a membrane is that the dense layer as well as the support can be prepared and optimized independently. For an optimal composite membrane the support should only provide mechanical stability and should have no resistance to gas transport. Therefore, a very open structure and a narrow pore size distribution is required. On the other hand, the surface pores should not be too large because then the applied coating cannot bridge these pores and defects will be formed. An optimal structure-performance relationship must be found with respect to morphology and transport behaviour. Different methods to characterize the support can be used depending whether information about the morphology, the performance or the chemical composition are required<sup>[1]</sup>. Furthermore, it is also important for which purpose the final membrane will be used. Beerlage<sup>[2]</sup> showed that the morphology of ultrafiltration membranes are different in the dry and in the wet state. Therefore, the characterization technique should be chosen in such a way that the medium of characterization and final application are identical.

## 2.2. THEORETICAL ASPECTS OF THE CHARACTERIZATION TECHNIQUES

### 2. 2. 1. GAS TRANSPORT THROUGH POROUS MEMBRANES

The measurement of the gas fluxes is an important and simple method for the determination of the overall porosity of a membrane. The gas flux through a membrane can generally be expressed by:

$$J_i = \frac{P_i}{l} \Delta p_i, \quad (2.1)$$

where

$J_i$  flux of component  $i$  through the membrane [mol/m<sup>2</sup> s]

$P_i$  permeability coefficient of component  $i$  [mol/m s Pa]

$l$  membrane thickness (in the case of asymmetric membranes the thickness of the skin layer [m])

$\Delta p_i$  partial pressure difference of component  $i$  across the membrane [Pa]

In the case of porous membranes often the  $P/l$ -value is used to characterize the transport behaviour, because the determination of the skin layer thickness is rather difficult. Porous membranes which are used as supports in composite membranes for gas separation should have a  $P/l$  value which is at least three orders of

magnitude higher than that of the separation layer.

In a porous membrane pores of different sizes are present which all contribute to the transport. Dependent on the pore size different transport mechanisms can be distinguished in an asymmetric membrane (see figure 2.1).

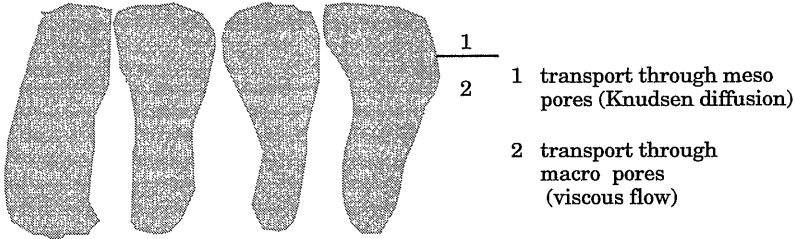


**Figure 2.1** *Schematical drawing of a porous support membrane with the corresponding transport mechanisms through the different parts of the membrane*

For pores with a radius  $> 10 \mu\text{m}$  Poisseuille or viscous flow occurs. In this case gas molecules only collide with each other (see figure 2.2). No separation of gases can be achieved with these membranes. The flux through such membranes can be estimated by the Hagen-Poiseuille equation (2.2) assuming cylindrically shaped pores<sup>[3-5]</sup>.

$$J = \frac{\varepsilon r^2 \Delta p}{8 \eta \tau l}, \quad (2.2)$$

where

$$\varepsilon = \frac{n \pi r^2}{A_m}, \quad (2.3)$$

with

- J flux through the membrane [m/s]
- $\varepsilon$  overall porosity [-]
- r pore radius [m]
- $\Delta p$  pressure difference [Pa]
- $\eta$  viscosity [Pa s]
- $\tau$  tortuosity [-]
- l membrane thickness (in the case of asymmetric membranes the thickness of the skin layer) [m]
- n number of pores [-]
- $A_m$  membrane area [m<sup>2</sup>]

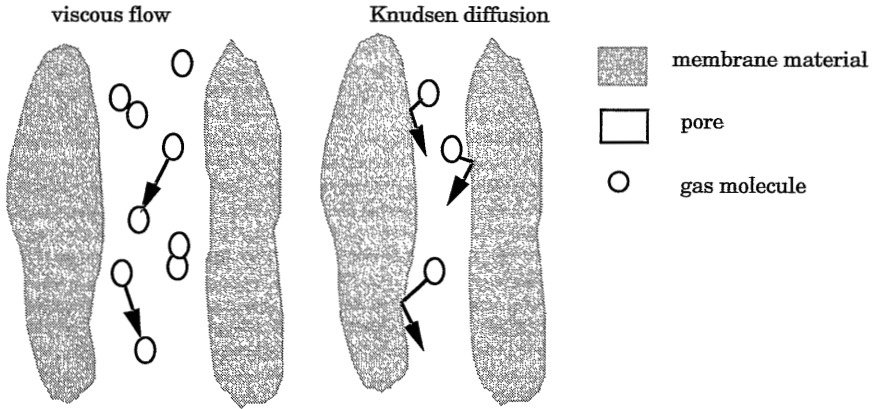


**Figure 2.2** Schematic drawing of the principles of viscous flow (left) and Knudsen diffusion (right)

In the case of smaller pores collisions of the gas molecules with the pore wall may become dominant (see figure 2.2) if the gas pressure is not too high. The mean free path length of the transported molecules may become comparable or even larger than the pore diameter. The flux through these pores is then given by Knudsen-flow (equation 2.4)<sup>[3,6]</sup>

$$J = \frac{\pi n r^2 D_k \Delta p}{A_m R T \tau l}, \quad (2.4)$$

where

$$D_k = \frac{2}{3} r \sqrt{\frac{8 R T}{\pi M_w}}, \quad (2.5)$$

with

$J$	flux through the membrane [mol/m <sup>2</sup> s]
$n$	number of pores [-]
$D_k$	Knudsen diffusion coefficient [m <sup>2</sup> /s]
$\Delta p$	pressure difference [Pa]
$A_m$	membrane surface [m <sup>2</sup> ]
$M_w$	molecular weight of the gas molecule [kg/mol]
$R$	gas constant [J/mol K]
$T$	temperature [K]
$\tau$	tortuosity [-]
$l$	thickness of the skin layer [m]

If the ratio of the fluxes of two gases through a membrane is equal to the reciprocal ratio of the square root of the molecular masses of the two gases (see equation 2.6) then it can be deduced that Knudsen diffusion occurs.

$$\frac{J_1}{J_2} = \frac{\sqrt{M_2}}{\sqrt{M_1}} \quad (2.6)$$

To characterize porous membranes with respect to their gas transport properties often the P/l value is determined. From the ratio of the P/l values for different gases the selectivity can be determined which may give an indication about the transport mechanism.

### **2. 2. 2. SCANNING ELECTRON MICROSCOPY**

Microscopic techniques are used to obtain both quantitative and qualitative information about the morphology of membranes<sup>[7]</sup>. However, it has to be noticed that the interpretation of the micrographs is often difficult. First of all the resolution of the method might be too low to detect pores with radii less than 20 nm and secondly, it cannot be concluded whether the pores observed on the surface are interconnected with the pores in the substructure. Finally, it should be noticed that artefacts might be created by the preparation technique of the samples.

The principle of scanning electron microscopy (SEM) can be described as follows<sup>[7]</sup>: The sample is exposed to a beam of electrons, which are called primary electrons, with kinetic energies up to 20 or 40 keV. On the surface of the sample two phenomena occur: firstly, the emission of secondary electrons with energies of a few tens of eV and secondly, re-emission or reflection of high-energy backscattered electrons from the primary electron beam. The resolution of scanning electron microscopy depends on the nature of the sample, its orientation in the microscope, the working distance of the sample from the final lens and the recording of the final image.

A disadvantage of the relatively high energy of the primary electrons is that the sample can be damaged. Therefore the sample is covered with, in the most cases, a thin gold layer to prevent the damage and charges. However, it should be noted that the gold layer may have an influence on the observed structures because of clustering effects of the gold. Information about very fine structures may be lost. Better results can be obtained from field emission scanning electron microscopy (FESEM)<sup>[8,9]</sup>. The kinetic energy of the electron beam is much smaller (< 5 keV is possible) compared to classical scanning electron microscopy. The resulting beam of secondary electrons is smaller in dimension and shows increased brightness and higher resolutions up to 5 nm can be reached. This microscopic technique may be employed to determine surface pores in ultrafiltration membranes.

### 2. 2. 3. PERMPOROMETRY

Permporometry is a useful method for the characterization of the active pores of ultrafiltration membranes. With this technique pores in the range of 3 to 100 nm can be determined. The method was first developed by Eyraud et al.<sup>[10]</sup> as gas-liquid permporometry. Later it has been improved to the gas-vapour permporometry<sup>[11,12]</sup>. Several authors reported recently on permporometry, e. g., Cuperus<sup>[13]</sup>, Cao et al.<sup>[14]</sup>, Beerlage<sup>[2]</sup> and Brinkman<sup>[15]</sup>.

Permporometry is based on the capillary condensation of a vapour in small pores in combination with the simultaneous measurement of the gas flux through the open pores. The used vapour should have a low interaction with the membrane material to avoid swelling. The membrane, which is placed in a cell, is contacted on both sides with vapour saturated gas streams. On one side, e. g., air and on the other side nitrogen saturated with cyclohexane are streaming along the membrane. In the beginning of the experiment the pores of the membrane are filled with the condensed vapour. By lowering the temperature of the saturated gas streams the vapour pressure decreases and pores start to open according to the Kelvin equation (equation 2.7)<sup>[3,16]</sup>

$$\ln p_r = - \frac{\gamma V_m}{RT} \left( \frac{1}{r_{K1}} + \frac{1}{r_{K2}} \right) \cos \Theta, \quad (2.7)$$

where

$p_r$	relative vapour pressure (=vapour pressure/saturated vapour pressure) [-]
$\gamma$	interfacial tension [N/m]
$V_m$	molar volume of the condensed vapour [m <sup>3</sup> /mol]
$R$	gas constant [J/mol K]
$T$	temperature [K]
$\Theta$	contact angle [°]
$r_{Ki}$	Kelvin-radii of the curvature of the vapour (1)-liquid (2) interface inside a pore [m].

The open pores allow the flow of both nitrogen and air and the oxygen concentration in the nitrogen stream is monitored. Dependent on the number of pores which are open the oxygen content in the nitrogen stream increases and this can be related to the pore size distribution. A schematical drawing of the measurement principle is given in figure 2.3.

For the calculation it is assumed that the condensed vapour wets the material completely. Hence, the contact angle  $\Theta$  becomes zero and therefore  $\cos \Theta$  becomes 1. During the desorption the interface between liquid and gas is hemispherical, so that  $r_1$  and  $r_2$  become equal<sup>[16-19]</sup> (see figure 2.4).



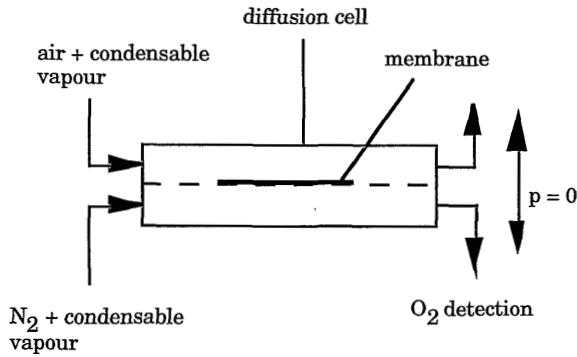


**Figure 2.3** Schematical drawing of the permoporometry principle

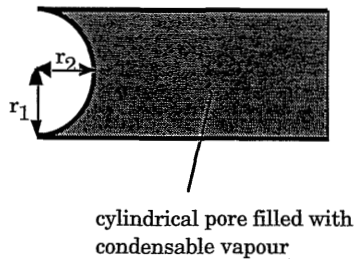


**Figure 2.4** Schematical drawing showing the meniscus of a condensable vapour during the desorption process in a cylindrical pore

The vapour pressure of a condensed liquid in a cylindrical pore is now given by a simplified form of the Kelvin equation<sup>[16]</sup>

$$\ln p_r = -\frac{2\gamma V_m}{RT} \frac{1}{r_K} \quad (2.8)$$

The Kelvin-radius  $r_K$  which can be calculated with equation (2.8) is not equal to the real pore radius. Due to adsorption of the condensed vapour at the pore walls a thin film of adsorbed condensate is present which disappears only if the relative vapour pressure of zero is reached. Under experimental conditions, however, this cannot be realized, so the thin adsorbed layer, the t-layer, is always present on the pore walls. Therefore, the radius calculated with the Kelvin equation (equation 2.8) must be corrected for the t-layer. The true pore radius can be obtained from equation (2.9)

$$r_p = r_K + t, \quad (2.9)$$

where  $t$  is the thickness of the adsorbed layer (t-layer) at the pore walls<sup>[14,17-19]</sup>.

$$J = \frac{\pi \sum_i (n_i r_i^4)}{8 A_m \eta \tau l} \Delta p, \quad (2.12)$$

where

$J$  flux [m/s]

$n_i$  number of pores [-]

$r_i$  pore radius [m]

$A_m$  membrane surface [m<sup>2</sup>]

$\eta$  viscosity of the permeating liquid [Pa s]

$\tau$  tortuosity [-]

$l$  effective membrane thickness, i. e., in the case of asymmetric membranes the thickness of toplayer [m]

$\Delta p$  pressure difference across the membrane [Pa].

This equation relates the liquid flow through the membranes to the applied pressure (see figure 2.6). If the stagnant liquid is replaced in all pores the pressure dependency of the liquid flow will become linear. If the two curves do not coincide then there still may be some pores which are filled with the stagnant liquid or there may be an interaction of the membrane material with one of the liquids causing swelling of the polymer matrix.

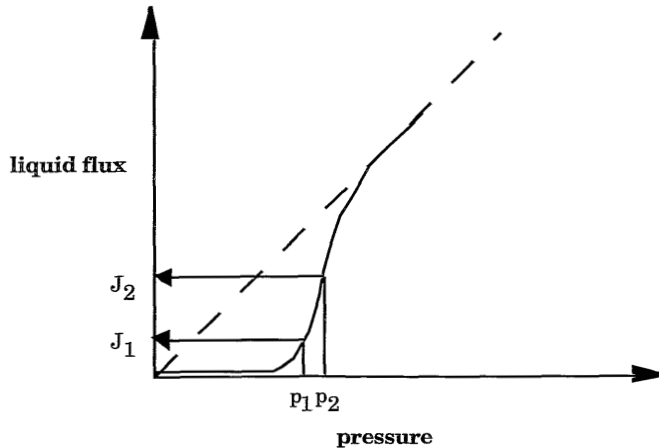


**Figure 2.6** Measurement principle of the liquid-liquid displacement: an applied pressure  $p_i$  causes the corresponding liquid flow  $J_i$ . The dashed line gives the dependency of the liquid flow on the pressure for the membrane with unfilled pores.

The pore size distribution can be obtained from the liquid-liquid displacement

experiments as described in appendix B to this chapter.

## **2. 3. EXPERIMENTAL**

### **2. 3. 1. MATERIALS**

Three commercial polyacrylonitrile membranes have been used as support membranes for the coating experiments (see chapters 3 and 4). Firstly, membranes supplied by GFT (Deutsche Carbone-Gesellschaft für Trenntechnik, Germany) have been used. These membranes are normally used as supports for GFT's composite membranes in pervaporation. Secondly, two types of ultrafiltration membranes obtained from Stork, Gorredijk, B. V. (the Netherlands) were used. These membranes, here referred to as Stork 3010 and 5010, are supplied in tubular form and are usually employed as UF membranes without a composite layer. The tubes were cut in such a way that after the drying procedure flat membranes were obtained. These membranes have been characterized with respect to their gas flow, morphology and pore size distributions. The GFT membranes were used without any pre-treatment procedure, while the Stork membranes first were rinsed with water for at least two days and then dried following the procedure of Macdonald et al.<sup>[22]</sup>: First, they were stored in ethanol for 24 hours and then in hexane again for 24 hours and finally they were dried in air under glass plates to keep them flat.

### **2. 3. 2. GAS FLUX MEASUREMENTS**

The membranes were cut in circles of 4.8 cm in diameter and placed in the cell. Nitrogen was applied at the feed side, while the permeate side of the cell was connected to a mass flow meter.

### **2. 3. 3. FIELD EMISSION SCANNING ELECTRON MICROSCOPY (FESEM)**

FESEM pictures were taken with a Hitachi S 800 apparatus. For the preparation of the surfaces the membranes were cut into small pieces and mounted on a sample holder. A thin carbon layer was placed on top of the samples with an argon sputter coater (Polaron Turbo Sputter Coater). The sputter time was 60 seconds. For the preparation of cross-sections pieces of membranes were wetted in a water/ethanol mixture and then frozen in liquid nitrogen followed by breaking.

### **2. 3. 4. PERMPOROMETRY**

A schematical drawing of the permoporometry set-up is given in figure 2.7. The membranes were placed in the diffusion cell (area 4.8 cm<sup>2</sup>) which was then placed

in a water bath at 34.5 °C. Along both sides of this cell the two gases were allowed to flow; technical air (21 % oxygen, 79 % nitrogen) on the top side of the membrane and pure nitrogen at the permeate side. Mass flow controllers (Brooks 5850TR) have been used to adjust the flow velocities of both gases to 0.67 ml/s for the Stork 5010 and 1.5 ml/s for the Stork 3010 and the GFT membranes. The gas streams are flowing through two vessels with cyclohexane at a temperature of 75 °C. Subsequently the cyclohexane saturated gas streams were led through a cooler at the same temperature as the water bath in which the membrane is placed (34.5 °C) in the beginning of the experiment. The membranes were saturated with cyclohexane vapour for at least 16 hours. The vapour pressure was then lowered by stepwise lowering the temperature of the coolers. The system was stabilized at each temperature for 30 minutes. After this time the oxygen content on the nitrogen side was determined using a gas chromatograph Varian 3400 equipped with a zeolite 13X column.

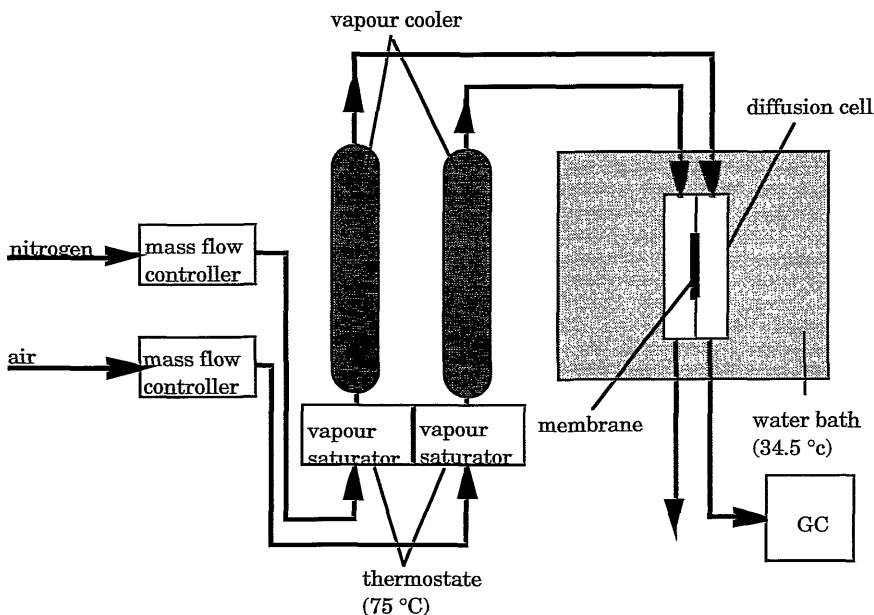


**Figure 2.7** Schematical drawing of the used permoporometry set-up

At a relative vapour pressure equal to unity all pores are blocked by the condensed vapour, i. e., no open pores are present and no oxygen flux is measured. By decreasing the relative vapour pressure, e. g. by lowering the temperature of the gas streams, some pores become open according to the Kelvin equation (equation 2.8). Now oxygen will diffuse through the open pores due to a concentration (partial pressure) gradient. In the beginning desorption takes place from the larger pores

and by further lowering of the relative vapour pressure more and more smaller pores become open (see figure 2.5).

### 2. 3. 5. LIQUID-LIQUID DISPLACEMENT

The liquid displacement experiments were carried out as described by Wienk<sup>[8]</sup>. Water and isobutanol were used as the two non-miscible liquids. After mixing of the two liquids the system was equilibrated for one night to obtain two saturated immiscible phases. To remove all the air bubbles this mixture was then kept for 30 minutes in an ultrasonic bath. Then the membrane was placed in isobutanol. Prior to the measurement the isobutanol has to be exchanged by water which acts as the stagnant liquid. The water wetted membrane was then placed in the cell of the liquid displacement set-up and then a certain flow of isobutanol through the membrane was adjusted by an HPLC pump (Waters 590) and the pressure necessary to obtain this flow was measured. Two sensors (Cerabar, 0-1 bar and 0-10 bar) have been used for the pressure measurement. A schematical drawing of the used set-up is given in figure 2.8.

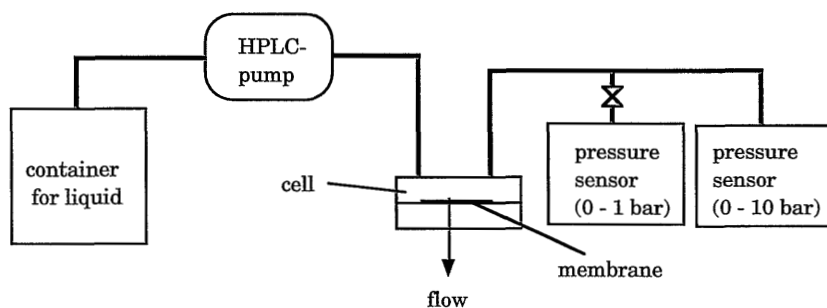


**Figure 2.8** Schematical drawing of the used liquid-liquid displacement set-up

## 2. 4. RESULTS AND DISCUSSION

### 2. 4. 1. PRESSURE NORMALIZED GAS FLUXES

The pressure normalized gas fluxes or  $P/l$  values of the commercial membranes are given in table 2.1.

**Table 2.1** *P/l values of commercial asymmetric PAN-membranes*

membrane	$P/l(N_2)$ [ $\text{cm}^3(\text{STP})/\text{cm}^2 \text{ s cmHg}$ ]
GFT	0.0029
Stork 3010	0.0033
Stork 5010	0.0017

Here the lowest  $P/l$  value belongs to the Stork 5010-membrane, while the highest flux was measured for Stork 3010. The  $P/l$  values through the GFT and Stork 3010 membranes are almost equal.

#### 2. 4. 2. FIELD EMISSION SCANNING MICROSCOPY

The surface of a GFT-membrane is shown in figure 2.9. The pore size distribution seems to be quite uniform. The mean pore diameter is about 12 nm diameter, while some bigger pores of about 30 nm diameter can be observed.

The Stork 3010-membrane shows a quite non-uniform pore size distribution (see figure 2.10a). The biggest pores on the surface are about 25 nm, while the mean pore size seems to be smaller than 4 nm. The Stork 5010 membrane shows some bigger pores of about 12 nm while the mean pore size is difficult to determine with this microscopic technique (see figure 2.10b). The results are summarized in table 2.2.

**Table 2.2** *Results of the microscopic study with the three commercial PAN membranes*

membrane	mean pore diameter [nm]	diameter of largest pores [nm]
GFT	12	32
Stork 3010	<4	25
Stork 5010	-	12

- smaller than the microscopic resolution

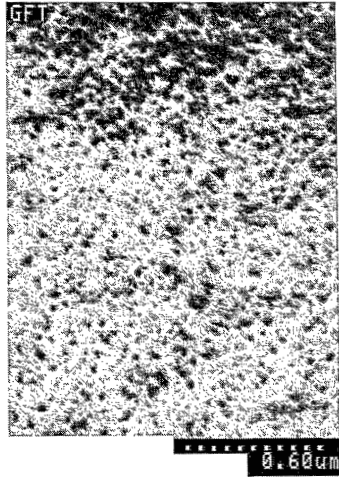


**Figure 2.9** FESEM-photograph showing the surface of a GFT-membrane

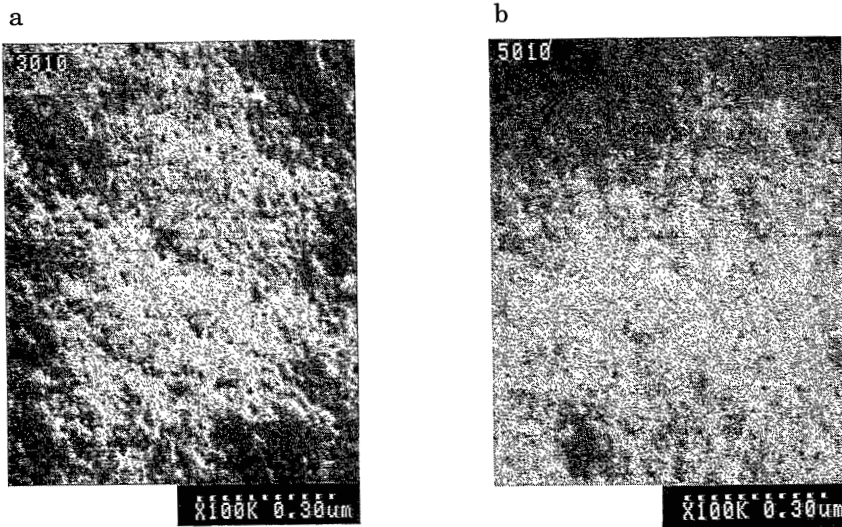


**Figure 2.10** FESEM-photograph showing the surface of a) Stork 3010-membrane and b) Stork 5010-membrane

### 2. 4. 3. PERMPOROMETRY

Permporometry measurements have been carried out with the three commercial flat membranes and the results are summarized in table 2.3. Unfortunately, it was

not possible to carry out successful permoporometry measurements with GFT membranes yet. Probably, the membranes have a structure which is just to open to close all the pores with condensed vapour. From Coulter<sup>®</sup> porosimetry experiments<sup>[23]</sup> no pores, neither for the GFT membranes nor for the Stork membranes, could be detected, which means that no pores bigger than 50 nm are present in the membranes.

**Table 2.3** Results from the permoporometry experiments for the commercial membranes

membrane	mean pore radius [nm]	largest pores radius [nm]
GFT	-	-
Stork 3010	(3)	(23)
Stork 5010	(2)	(17)

During a permoporometry experiment the oxygen content at the nitrogen side of the membrane is measured as a function of the relative vapour pressure of cyclohexane. The oxygen content can then be transferred into an oxygen flux and by plotting this versus the pore radius the pore size distribution can be obtained. The pore size distribution of a Stork 3010 membrane is shown in figure 2.11. Starting from high pore radii the cumulative oxygen flux, which is the sum of all separate fluxes, increases due to the fact that with every step more pores become open. The cumulative oxygen flux can be differentiated stepwise, resulting in a pore size distribution ( $dJ/dr_p$ ). The Stork 3010 membrane shows a relatively narrow pore size distribution with a mean pore radius of about 3 nm. In figure 2.12 the differential number of pores versus the pore radius is shown. It can be seen that, corresponding to figure 2.11, a high number of pores of about 3 nm is present in the membrane. However, it should be noted that it was not possible to close all the pores of the membrane with condensed vapour so that already in the beginning of the experiment an initial oxygen flux is present. This was observed to a different extent for all characterized Stork 3010 membranes. This might be an indication for the presence of pores between 25 nm and 50 nm. Table 2.4 gives the oxygen flux through the dry unfilled membrane (dry flux) and the initial oxygen flow at the beginning of the permoporometry experiment.



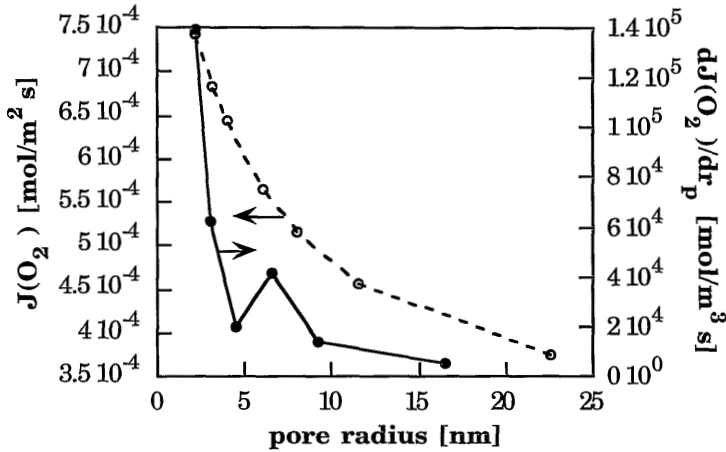


**Figure 2.11** Cumulative oxygen permeation curve (dashed line) and corresponding differential oxygen permeation curve (solid line) as a function of the pore radius of a Stork 3010 membrane

**Table 2.4** Dry and initial oxygen fluxes through the characterized membranes

membrane	dry oxygen flux [ $\text{cm}^3(\text{STP})/\text{cm}^2 \text{ s cmHg}$ ]	initial oxygen flux [ $\text{cm}^3(\text{STP})/\text{cm}^2 \text{ s cmHg}$ ]
GFT	0.0029	0.0023
Stork 3010	0.0033	0.0006
Stork 5010	0.0017	0.00067

As can be seen from these values the decrease in the oxygen flux differs quite significantly for the different membranes. In the case of the GFT membrane the flux just decreased for about 20 %, while for the Stork 3010 membrane this decrease was about 81 % and for Stork 5010 about 60 %.

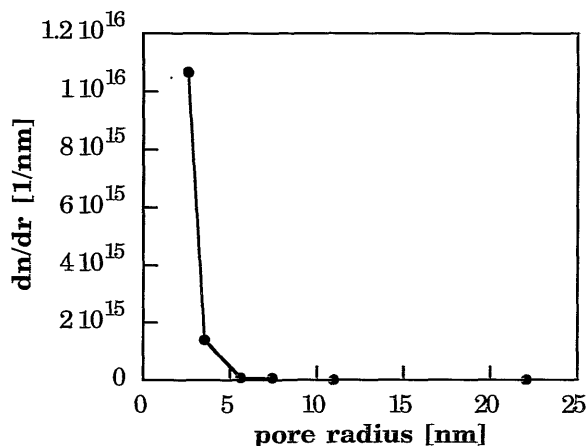


**Figure 2.12** Pore size distribution of a Stork 3010 membrane determined by permoporometry

In figure 2.13 the cumulative and differential oxygen flux are given for a Stork 5010 membrane. It can be seen that the mean pore size is about 2 nm. This corresponds with the pore size distribution of this membrane shown in figure 2.14. Because of experimental limitations it was not possible to determine the smallest pores. Probably, there are smaller pores present. For these membranes the initial oxygen flux in the beginning of the experiment was very low, so that it can be concluded that there might be a few bigger pores present.

The results of the permoporometry experiments are summarized in table 2.3. For both Stork membranes the presence of bigger pores can be expected. An indication therefore is the initial oxygen flux in the beginning of the experiments which shows that it was not possible to close all pores with cyclohexane vapour. The mean pore size for both membranes is about 2 to 3 nm, smaller pores cannot be detected with this method.

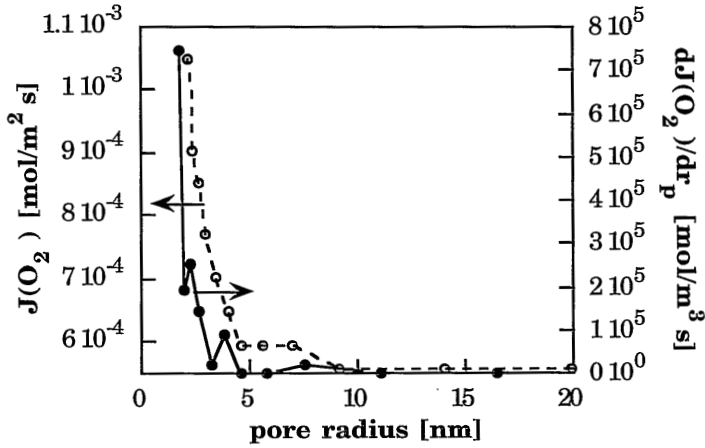


**Figure 2.13** Cumulative oxygen permeation curve (dashed line) and corresponding differential oxygen permeation curve (solid line) as a function of the pore radius of a Stork 5010 membrane

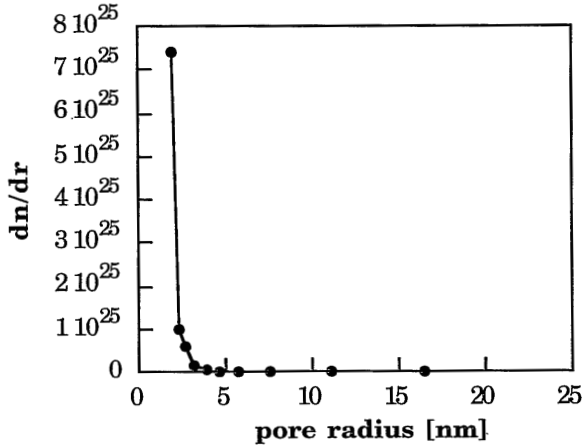


**Figure 2.14** Pore size distribution of a Stork 5010 membrane determined by permoporometry

#### 2. 4. 4. LIQUID-LIQUID DISPLACEMENT

Liquid-liquid displacement experiments were carried out with all three commercial membranes and the results are summarized in table 2.5.

The GFT-membrane shows a quite sharp pore size distribution with a mean pore size of about 14 nm, while the largest detected pores are about 17 nm (see figure 2.15 and 2.16). For the Stork 3010 membrane a relatively narrow pore size distribution was obtained with a mean pore radius of about 9 nm (see figures 2.17 and 2.18). Probably, there are pores larger than 20 nm, however, they could not be detected by this technique. The Stork 5010 membrane also shows a relatively narrow pore size distribution with the mean pore size at about 6 nm (see figure 2.19 and 2.20). Smaller pores could not be detected with this method.

From these figures it can be concluded that both GFT and Stork 3010 show a relatively narrow pore size distribution. However, the difference in mean pore radius is quite significant with about 14 nm for the GFT membrane and about 9 nm for the Stork 3010 membrane. For the Stork 5010 membrane a somewhat broader pore size distribution was determined, with the mean pore size of about 6 nm. It is remarkable that for the GFT membrane not only the largest mean pore radius was determined but also the highest number of pores. The lowest number of pores was determined for the Stork 5010 membrane which is about three orders of magnitude lower than for the GFT membrane and two orders of magnitude lower than for the Stork 3010 membrane.

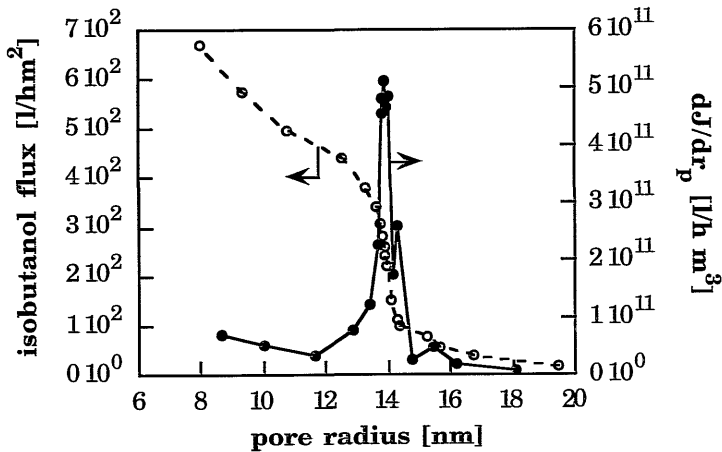


**Figure 2.15** Cumulative isobutanol flux curve and (dashed line) and corresponding differential isobutanol flux curve (solid line) as a function of the pore radius for a GFT membrane

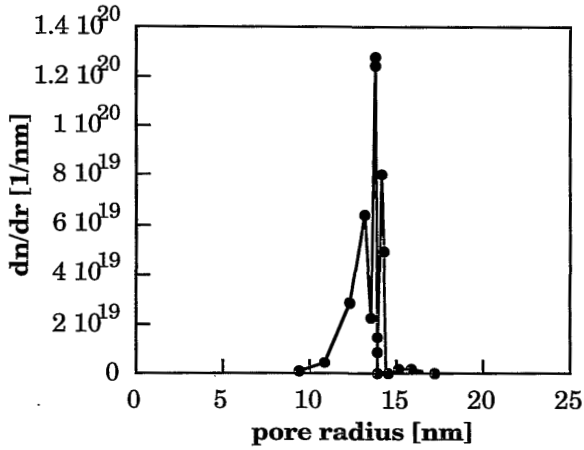


**Figure 2.16** Pore size distribution of a GFT membrane determined by liquid-liquid-displacement

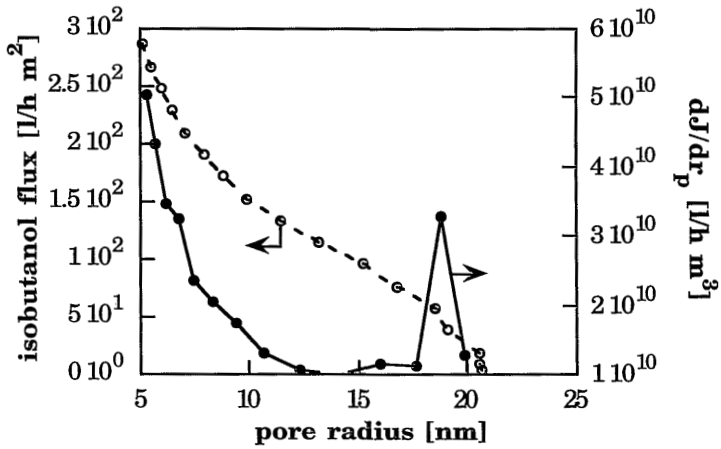


**Figure 2.17** Cumulative isobutanol flux curve and (dashed line) and corresponding differential isobutanol flux curve (solid line) as a function of the pore radius for a Stork 3010 membrane

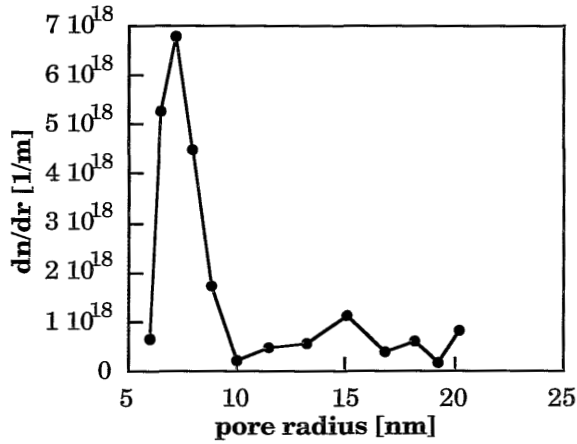


**Figure 2.18** Pore size distribution of a Stork 3010 membrane determined by liquid-liquid displacement

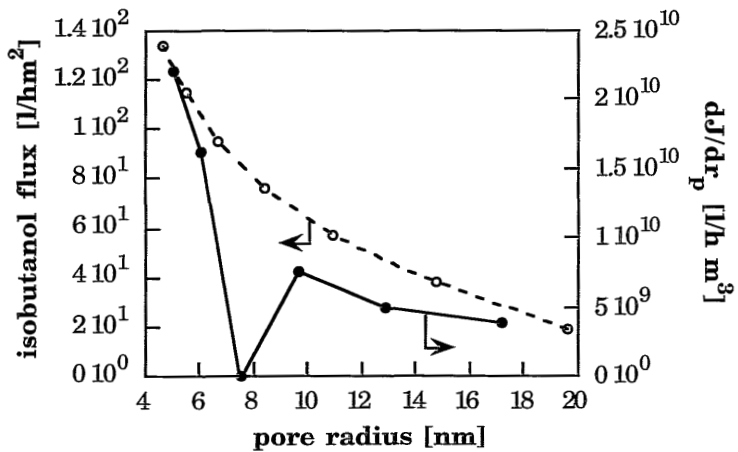


**Figure 2.19** Cumulative isobutanol flux curve and (dashed line) and corresponding differential isobutanol flux curve (solid line) as a function of the pore radius for a Stork 5010 membrane

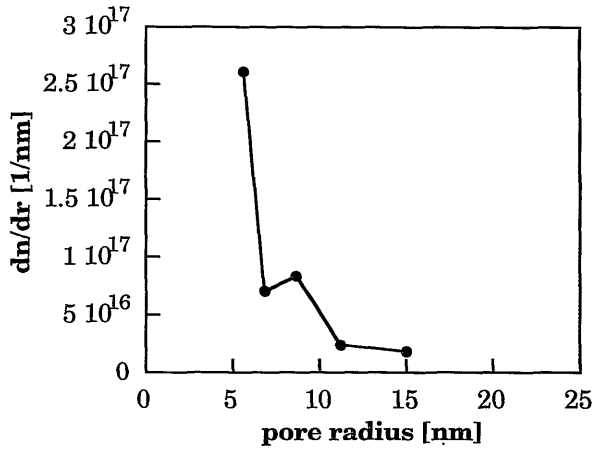


**Figure 2.20** Pore size distribution of a Stork 5010 membrane determined by liquid-liquid displacement

**Table 2.5** Results of the liquid-liquid displacement experiments

membrane	mean pore radius [nm]	largest pores [nm]
GFT	14	17
Stork 3010	9	>20
Stork 5010	(6)	>15

## 2. 5. COMPARISON OF THE CHARACTERIZATION TECHNIQUES - A GENERAL DISCUSSION

A number of methods are available to characterize support layers of composite membranes. The choice of the method which is applied depends strongly on the nature and the application of the membrane, i. e., whether the membrane is used in the dry or in the wet state.

From the gas fluxes (see table 2.1) it can be seen that the GFT membrane has the most open structure of the used membranes. The GFT membrane shows the biggest pores with a maximum size of about 30 nm and a mean pore size of about 12 nm. The mean pore sizes of the two Stork membranes are too small to be detected by this microscopic technique. Both membranes show some bigger pores of about 20 nm for Stork 3010 and 12 nm for Stork 5010. The trend can also be found in the results of the

liquid-liquid displacement. Again for the GFT membrane the largest mean pore size (28 nm pore diameter) and the highest number of pores were determined. The smallest mean pore size was determined for the Stork 5010 membrane (12 nm pore diameter), while this is about 18 nm for the Stork 3010 membrane. The number of pores with the mean pore size is about the same for the two Stork membranes. However, it seems that in the Stork 5010 membrane are pores bigger than 40 nm in diameter are present (see figure 2.10b). This might also explain the fact that in the permoporometry experiments the Stork 5010 membrane showed a higher initial oxygen flux than the Stork 3010 membrane (see table 2.3). This is an indication for the presence of bigger pores which cannot be blocked by the condensed cyclohexane vapour.

The main difference between the here described characterization methods is the medium in which the characterization takes place; the permoporometry is a partially dry method and the liquid-liquid displacement is a wet method. Beerlage<sup>[2]</sup> already found a large difference between characterization methods in the dry and in the wet state for ultrafiltration membranes of polyimide. She concluded in general that for characterization of support materials for composite membranes which are used in the dry state (gas separation) dry characterization methods are preferred concluded that the membranes change their morphology when being dried.

## 2. 6. REFERENCES

- [1] F. P. Cuperus, C. A. Smolders; Characterization of UF membranes, membrane characteristics and characterization techniques; *Adv. Colloid Interface Sci.*, 34 (1991) 135
- [2] M. A. M. Beerlage; Polyimide ultrafiltration membranes for non-aqueous systems; PhD-thesis, University of Twente (1994)
- [3] M. H. V. Mulder; Basic principles of membrane technology; Kluwer Academic Publishers, Dordrecht, the Netherlands (1991)
- [4] H. Yasuda, J. T. Tsai; Pore size of microporous polymer membranes; *J. Appl. Polym. Sci.*, 18(1974), 805-
- [5] F. W. Altena, H. A. M. Knoef, H. Heskamp, D. Bargeman, C. A. Smolders; Some comments on the applicability of gas permeation methods to characterize porous membranes based on improved data handling; *J. Membr. Sci.*, 12 (1983), 313-
- [6] E. A. Mason, A. P. Malinauskas; Gas transport in porous media: the dusty gas model; Elsevier, amsterdam (1983)
- [7] I. M. Watt; The principles and practice of electron microscopy; Cambridge University Press, Cambridge, 1985
- [8] I. M. Wienk; Ultrafiltration membranes from a polymer blend; PhD-thesis University of Twente (1993)
- [9] K. J. Kim, A. G. Fane, C. J. D. Fell, T. Suzuki, M. R. Dickson; Quantitative microscopic study of surface characteristics of ultrafiltration membranes; *J. Membr. Sci.*, 54 (1990) 89
- [10] C. Eyraud, M. Betemps, J. F. Quinson, F. Chatelut, M. Brun, B. Rasneur; *Bull. Soc. Chim. France*, 9-10 (1984) I-237
- [11] A. Mey-Marom, M. G. Katz; Measurement of active pore size distribution of microporous membranes - a new approach; *J. Membr. Sci.*, 27 (1986) 119
- [12] M. G. Katz, G. Baruch; New insights into the structure of microporous membranes obtained using a new pore size evaluation method; *Desal.*, 58 (1986) 199
- [13] F. P. Cuperus; Characterization of ultrafiltration membranes; PhD-thesis University of



Twente 1990

- [14] G. Z. Cao, J. Meijeringk, H. W. Brinkman, A. J. Burggraaf; Permporometry study on the size distribution of active pores in porous ceramic membranes; *J. Membr. Sci.*, 83 (1993) 221
- [15] H. W. Brinkman; Ceramic membranes by (electro)chemical vapour deposition; PhD-thesis University of Twente (1994)
- [16] A. W. Adamson; *Physical chemistry of surfaces*; Wiley, New York, 5th ed., 1990, p. 58
- [17] F. P. Cuperus, D. Bargeman, C. A. Smolders; Permporometry. The determination of the size distribution of active pores in UF membranes; *J. Membr. Sci.*, 71 (1992) 57
- [18] S. J. Gregg, K. S. W. Sing; *Adsorption, surface area and porosity*; 2nd ed., Academic Press, New York, 1992
- [19] D. M. Ruthven; *Principles of adsorption and desorption process*; J. Wiley & sons, New York, 172
- [20] H. Bechold, M. Schlesinger, K. Silbereisen; Porenweite von Ultrafiltern; *Koll. Z.* 55 (1931) 172
- [21] F. Erbe; Blockierungsphänomene bei Ultrafiltern; *Koll. Z.* 59 (1932) 195
- [22] W. Macdonald, S. Park, C. Y. Pan, E. Albata Method for drying water-wet membranes; U. S. Patent 3,842,515  
P. Manos; Gas separation membrane drying with water replacement liquid; U. S. Patent 4,080,744  
P. Manos; Solvent/exchange drying of membranes for gas separation; U. S. Patent 4,120,098
- [23] Reference Manual Coulter porometer II, Luton, England

## Appendix A to chapter 2

---

# Derivation of the pore size distribution from permoporometry

---

### 1. Introduction

In permoporometry the pores of a membrane are filled with condensed vapour. During the measurement the removal of the condensed vapour from the pores due to a stepwise change in the vapour pressure is followed by the diffusion of oxygen through the open pores. The results of the permoporometry measurements are often expressed in a pore size distribution where the number of pores is given as a function of the pore radius<sup>[1,2]</sup>. For a practical reason it is not possible to monitor this oxygen flux continuously but only in certain intervals. This oxygen flux is then related to the average pore size limiting the interval. For that reason a correct pore size distribution can only be given as the differential number of pores ( $dn/dr$ ) as a function of the pore radius. The derivation of this relation is given in this appendix.

### 2. Derivation

The gas flux through a porous membrane with pores in the nanometer range can be described by Knudsen flow<sup>[3]</sup>

$$J = \frac{n \pi r^2 D_k \Delta p}{A_m R T \tau l} \quad (\text{A1})$$

where

$$D_k = \frac{2}{3} r \sqrt{\frac{8 R T}{\pi M}} \quad (\text{A2})$$

with

J gas flux [mol/m<sup>2</sup>s]  
n number of pores [-]  
r pore radius [m]

- $D_k$  diffusion coefficient [m<sup>2</sup>/s]  
 $\Delta p$  pressure difference across the membrane [Pa]  
 $A_m$  membrane surface [m<sup>2</sup>]  
 $R$  ideal gas constant [J/K mol]  
 $T$  temperature [K]  
 $\tau$  tortuosity factor [-]  
 $l$  membrane thickness (in the case of asymmetric membranes the thickness of the toplayer [m]  
 $M$  molecular weight [kg/mol].

By combination of equation (A1) and (A2) equation (A3) the flux  $J_i$  through the pores with the radius  $r_i$  can be obtained

$$J_i = \frac{2}{3} \sqrt{\frac{8 \pi}{M R T}} \frac{\Delta p}{A_m \tau l} n_i r_i^3 \quad (\text{A3})$$

The total flux through the membrane can be obtained from the summation of equation (A3) over the entire distribution of the radii as given by equation (A4)

$$J = \sum_i J_i = \frac{2}{3} \sqrt{\frac{8 \pi}{M R T}} \frac{\Delta p}{A_m \tau l} \sum_i n_i r_i^3, \quad (\text{A4})$$

The summation term of this equation can be described by a continuous function

$$\sum_i n_i r_i^3 = \int_{r_{min}}^{\infty} \frac{\partial n}{\partial r} r^3 dr \quad (\text{A5})$$

$$J = -\frac{2}{3} \sqrt{\frac{8 \pi}{M R T}} \frac{\Delta p}{A_m \tau l} \int_{\infty}^{r_{min}} \left( \frac{\partial n}{\partial r} \right) r^3 dr$$

$$\frac{\partial J(r_{min})}{\partial r_{min}} = -\frac{2}{3} \sqrt{\frac{8 \pi}{M R T}} \frac{\Delta p}{A_m \tau l} \left[ r^3 \left( \frac{\partial n}{\partial r} \right) \right]_{r=r_{min}} \quad (\text{A6a})$$

$$\left( \frac{\partial n}{\partial r} \right)_{r_{min}} = - \left( \frac{\partial J(r_{min})}{\partial r_{min}} \right) \frac{2}{3} \sqrt{\frac{M R T}{8 \pi}} \frac{A_m \tau l}{\Delta p r_{min}^3} \quad (\text{A6b})$$

In permporometry the pores of a membrane are blocked by a condensed vapour. By changing the vapour pressure of the pore filling liquid the pores can open and take part in the gas transport. This is accomplished by changing the temperature at which the air or nitrogen stream is saturated with the vapour of the pore filling liquid. The temperature of the membrane is kept constant. The Kelvin equation gives

the relation between vapour pressure and pore radius.

$$\ln \frac{p(T_{sat})}{p(T_{membrane})} = - \frac{2 \gamma V_m}{R T_{membrane}} \frac{1}{r_{min}} \quad (A7)$$

There are various equations relating the temperature to the vapour pressure. Here the Antoine equation will be used

$$\lg p = A - \frac{B}{C + \Theta} \quad (A8a)$$

in which the pressure  $p$  is given in mmHg and the temperature  $\Theta$  in °C. A, B and C are constants specific for the liquid considered. Before applying equation (A8a) to the Kelvin equation the pressure must be given in Pa, the temperature in K and the  $^{10}\log$  is changed into the natural logarithm  $\ln$ . This is done in equation (A8b). Here K is an additional constant, which contains the conversion from mmHg to Pa.

$$\ln p = \ln K + A \ln 10 - \frac{B \ln 10}{C - 273.15 + T} \quad (A8b)$$

Combination of equation (A7) and (A8b) gives

$$r_{min} = \frac{2 \gamma V_m}{R T_{membrane}} \frac{(C - 273.15 + T_{sat})(C - 273.15 + T_{membrane})}{B(T_{membrane} - T_{sat}) \ln 10} \quad (A9)$$

The variation of the pore radius  $r_{min}$  with the temperature  $T_{sat}$  at which the nitrogen and the air stream are saturated with the vapour of the pore filling liquid is given by

$$\frac{dr_{min}}{dT_{sat}} = \frac{r_{min}}{T_{membrane} - T_{sat}} \frac{C - 273.15 + T_{membrane}}{C - 273.15 + T_{sat}} \quad (A10)$$

The combination of equations (A6b) and (A10) gives the relation between the pore size distribution and the derivative of the flux through the membrane with respect to the temperature  $T_{sat}$ .

$$\begin{aligned} \left(\frac{dn}{dr}\right)_{r_{min}} &= - \frac{dJ(T_{sat})}{dT_{sat}} \frac{dT_{sat}}{dr_{min}} \frac{3}{2} \frac{A_m \tau l}{r_{min}^3 \Delta p} \sqrt{\frac{R T_{membrane}}{8 \pi M}} \\ &\quad - \frac{dJ(T_{sat})}{dT_{sat}} \frac{(C - 273.15 + T_{sat})}{(C - 273.15 + T_{membrane})} (T_{membrane} - T_{sat}) \\ &\quad \cdot \frac{3}{2} \frac{A_m \tau l}{r_{min}^4 \Delta p} \sqrt{\frac{R T_{membrane}}{8 \pi M}} \end{aligned} \quad (A11)$$

The final equation to obtain the pore size distribution from permperometry

experiments is obtained by substitution of equation (A9) into (A11)

$$\left(\frac{dn}{dr}\right)_{r_{min}} = - \left(\frac{dJ(T_{sat})}{dT_{sat}}\right) \frac{(T_{membrane} - T_{sat})^5 (R T_{membrane} B \ln 10)^4}{(C - 273.15 + T_{sat})^3 (C - 273.15 + T_{membrane})^5} \frac{3A_m \tau l}{64(\gamma V_m)^4 \Delta p} \sqrt{\frac{R T_{membrane}}{2 \pi M}} \quad (A11)$$

By calculating the pore size distribution from experimental data according to equation (A11) and plotting it as a function of the pore radius, i. e. equation (A8) the correct pore size distribution of a membrane is obtained.

### 3. References

- [1] F. P. Cuperus; Characterization of ultrafiltration membranes; PhD-thesis University of Twente 1990
- [2] M. A. M. Beerlage; Polyimide ultrafiltration membranes for non-aqueous systems: PhD-thesis University of Twente 1994
- [3] M. H. V. Mulder; Basic principles of membrane technology; Kluwer Academic Publishers, Dordrecht, the Netherlands (1991)

# Derivation of the pore size distribution from liquid-liquid displacement

---

### 1. Introduction

In liquid-liquid displacement an increase in pressure difference across the membrane allows liquid permeation through smaller pores by the displacement of the pore filling liquid in these smaller pores. Furthermore there is an additional flow through already open pores due to the direct relation between flux and pressure difference. The results of liquid-liquid displacement experiments may be expressed in a pore size distribution<sup>[1]</sup> where the number of pores is given as a function of the pore radius. Because of practical limitations the liquid flux can not be followed continuously. The pressure is increased in certain intervals and the corresponding fluxes are measured. If the experiment is carried out in this way then one has to realize that the measured flux is not only caused by the open pores corresponding to the pressure but by also by pores which continuously opened in the interval. Therefore, for the calculation of the pore size distribution the width of the interval of in which the pressure is increased has to be taken into account. The derivation of the correct pore size distribution from liquid-liquid displacement experiments,  $dn/dr$  as a function of the pore radius, is given in this appendix.

### 2. Derivation

The liquid flux through a porous membrane in case of laminar flow through straight cylindrical capillaries with only one pore radius<sup>[2]</sup> is described by the Hagen-Poiseuille equation

$$J = \frac{\pi n r^4}{8 \eta A_m \tau l} \Delta p, \quad (\text{B1})$$

with

$J$  flux [m/s]  
 $n$  number of pores [1/m<sup>2</sup>]  
 $r$  pore radius [m]  
 $\eta$  viscosity of the permeating liquid [Pa s]  
 $A_m$  membrane surface [m<sup>2</sup>]  
 $\tau$  tortuosity [-]  
 $l$  membrane thickness, i. e. in the case of asymmetric membranes the thickness of toplayer [m].

The total flux in case of a pore size distribution  $dn/dr$  is described by the following equation

$$J = \int_{r=r_{min}}^{r=\infty} dJ = \int_{r=r_{min}}^{r=\infty} \frac{\pi \Delta p}{8 \eta \tau l} \frac{dn}{dr} r^4 dr. \quad (B2)$$

The integration is carried out from  $r = r_{min}$ , the pore radius just accessible for permeation, until  $r = \infty$ . Both the lower boundary  $r_{min}$  and the integrand are a function of the pressure difference  $\Delta p$ . The pore size distribution is found by twice differentiating the flux with respect to the pressure difference, applying Leibnitz' theorem<sup>[3]</sup>. The first derivative gives:

$$\frac{dJ(\Delta p)}{d\Delta p} = \int_{r=r_{min}(\Delta p)}^{r=\infty} \frac{dn}{dr} \frac{\pi r^4}{8 \eta \tau l} dr - \left[ \frac{dn}{dr} \frac{\pi r^4 \Delta p}{8 \eta \tau l} \right]_{r_{min}(\Delta p)} \cdot \frac{dr_{min}(\Delta p)}{d\Delta p}. \quad (B3)$$

The relation between the pressure difference across the membrane and the pore radius is given by the Laplace equation for cylindrical pores and complete wetting of the pore walls by the stagnant liquid (see also section 2.1.4).

$$\Delta p = \frac{2 \gamma}{r_{min}}, \quad (B4)$$

with

$\gamma$  interfacial tension between stagnant and displacing liquid [N/m].

The variation of the minimum pore radius with the pressure difference is given by equation (B5):

$$\frac{dr_{min}}{d\Delta p} = - \frac{2 \gamma}{\Delta p^2} \quad (B5)$$

The combination of equations (B3) and (B.5) gives:

$$\frac{dJ(\Delta p)}{d\Delta p} = \int_{\frac{2\gamma}{\Delta p}}^{r=\infty} \frac{\frac{dn}{dr} \pi r^4 dr}{8 \eta \tau l} + \frac{\pi \left(\frac{dn}{dr}\right)_{r_{min}} \frac{16 \gamma^4}{\Delta p^3} \left(\frac{2 \gamma}{\Delta p^2}\right)}{8 \eta \tau l} \quad (B6a)$$

$$= \frac{\pi}{8 \eta \tau l} \left[ \int_{\frac{2\gamma}{\Delta p}}^{r=\infty} \frac{dn}{dr} r^4 dr + \left(\frac{dn}{dr}\right)_{r_{min}} \frac{32 \gamma^5}{\Delta p^5} \right]. \quad (B6b)$$

Twice differentiating the flux with respect to the pressure difference gives:

$$\frac{d^2J(\Delta p)}{d(\Delta p)^2} = \frac{\pi}{8 \eta \tau l} \left[ \left(\frac{dn}{dr} r^4\right)_{r_{min}} \left(-\frac{2 \gamma}{\Delta p^2}\right) + \left(\frac{dn}{dr}\right)_{r_{min}} \left(-\frac{160 \gamma^5}{\Delta p^6}\right) \right] \quad (B7a)$$

$$= -\frac{\pi 16 \gamma^5}{\eta \tau l \Delta p^6} \left(\frac{dn}{dr}\right)_{r_{min}} \quad (B7b)$$

Rearranging equation (B7b) gives

$$\left(\frac{dn}{dr}\right)_{r_{min}} = -\frac{\eta \tau l \Delta p^6}{16 \pi \gamma^5} \cdot \frac{d^2J(\Delta p)}{d(\Delta p)^2}. \quad (B8)$$

From the measurement of the flux as a function of the pressure difference the pore size distribution can be calculated.

### 3. REFERENCES

- [1] I. M. Wienk; Ultrafiltration membranes from a polymer blend; PhD-thesis University of Twente (1993)
- [2] M. H. V. Mulder; Basic Principles of Membrane Technology; Kluwer Academic Publishers, Dordrecht, the Netherlands (1991)
- [3] M. Abramowitz, I. A. Stegun; Handbook of mathematical functions with formulas, graphs and mathematical tables; 10th printing, Wiley, New York, 1972; p. 11, nr. (3.3.7)



# 3

---

## COMPOSITE MEMBRANES WITH A GLASSY POLYMER AS TOPLAYER

### PART I: POLYCARBONATE AS COATING POLYMER

---

#### *Summary*

*Composite membranes have been prepared with polycarbonate (Makrolon 3200) as coating polymer and polyacrylonitrile as supporting structure. The influence of the coating velocity of the barrier polymer, its concentration and the viscosity of the coating solution have been investigated in relation to the membrane performance. A significant improvement of the quality and the reproducibility of the toplayer was obtained by impregnation of the support prior to the coating procedure thereby preventing pore penetration. For some of these membranes selectivities were obtained higher than the intrinsic value of Makrolon 3200.*

*The results have been discussed with respect to the coating theory and the resistance model. An increase in layer thickness could be observed with increasing coating velocity. The effective thicknesses, however, decrease with increasing coating velocity. This effect might be caused by the fact that the coating solution has less time to penetrate into the pores at higher coating velocities.*

### 3.1. INTRODUCTION

A number of special polymers have been developed for gas separation with improved selectivities, but their permeabilities are still quite low. In order to enhance the flux through membranes made from these polymers the separating layer should be as thin as possible. This can be achieved by preparing either a composite membrane or an integrally skinned asymmetric membrane. Composite membranes are prepared by the deposition of a thin layer upon a suitable support. Various methods can be applied to achieve this, e. g. dip-coating, spin-coating, plasma polymerization, interfacial polymerization and Langmuir-Blodgett technique. In this work we have used dip-coating as the process to prepare composite membranes where a support membrane is immersed in a polymer solution which contains the rate determining polymer.

### 3. 2. THEORETICAL ASPECTS OF THE DIP-COATING PROCESS

In the literature a number of articles can be found which describe the theory of the dip-coating process. Previous work in this field was mainly based on systems from the photographic industry where flat and nonporous supports were coated with an optical sensitive layer. On the other hand, in membrane systems *porous* supports are coated with solutions containing (glassy) polymers. However, the basic concepts are similar. The parameters of the coating process can be divided into three groups<sup>[1]</sup>. To the first group belong the parameters which are related to the flow conditions during the coating process. These parameters which are included in the Reynolds (Re) and Capillary (Ca) numbers (see Equations 3.1 and 3.2) give information which forces (viscous, capillary or inertial forces) contribute to the coating process. The capillary number shows the relative importance of viscous and capillary forces, while the Reynolds number shows the relative importance of inertial and viscous forces. The coating experiments described in this thesis are carried out at low Reynolds and Capillary numbers, i. e.  $Re \ll 1$ ,  $Ca \ll 1$ <sup>[2]</sup>.

$$Ca = \frac{\eta u}{\sigma}, \quad (3.1)$$

with

$\eta$  dynamic viscosity [Pa s]  
 $u$  coating velocity [m/s]  
 $\sigma$  surface tension [N/m]

$$Re = \frac{\rho u H}{\eta}, \quad (3.2)$$

with

$\rho$  density [ $\text{kg/m}^3$ ]  
 $H$  coating thickness [m]

The second group includes parameters which describe geometrical aspects of the coating process, i. e. whether the coating is applied on flat or cylindrical supports.

The third group contains the parameters which give information about the rheology of the coating solution, i. e. whether the solution behaves as a Newtonian or non-Newtonian fluid. In the appendix A it is shown that under process conditions the polymer solutions show Newtonian behaviour.

In a dip-coating process a support membrane is immersed and then withdrawn from a polymer solution. Middleman<sup>[3]</sup> defined three regions which represent the different properties of the coating layer ( see figure 3.1). In region 1 the properties are mainly determined by surface tension effects. In region 2 the properties of the coating layer are determined by surface tension as well as gravitational and viscosity related effects. In region 3 an equilibrium is reached between the effect of gravity and the drag of the layer. At a certain distance  $x$  the thickness of the coated layer reaches a constant final value  $H_\infty$ .

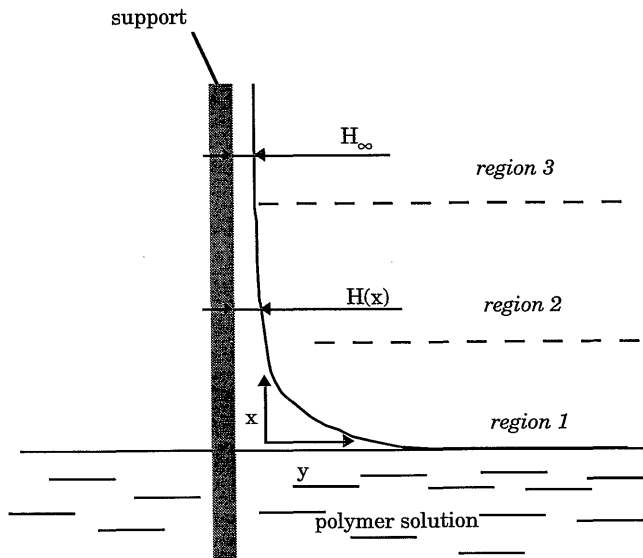


**Figure 3.1** Schematical drawing of the coating process showing the three different regions<sup>[3]</sup>.  $H_\infty$  is the final thickness of the coating layer.

If a support is coated with a liquid by dip-coating at a certain coating velocity the coated layer will lag behind the movement of the support due to gravity. The lag increases throughout the film, i. e., the maximum lag occurs in the outer region of

the film (see figure 3.2).

To describe the flow of a coated film under the influence of gravity (at constant temperature) the simplified Navier-Stokes equation can be used (see equation 3.3). Because in our experiments the support is vertically withdrawn from the coating solution the angle between interface coating solution and the support is  $90^\circ$  and can therefore, be neglected.

$$\eta \left( \frac{\partial^2 u}{\partial y^2} \right) = \rho g . \tag{3.3}$$

The boundary conditions for the described systems are given below:

$$1. u = U \quad \text{when } y = 0, \tag{3.4}$$

$$2. \frac{\partial u}{\partial y} = 0 \quad \text{when } y = H_\infty \tag{3.5}$$

With the first boundary condition the absence of slipping between the coating layer and the support is defined. The second limiting condition defines that along the layer of thickness  $H$  no other force than the air pressure is acting.

From equation (3.3) a parabolic velocity profile in the coated film is obtained (see figure 3.2).

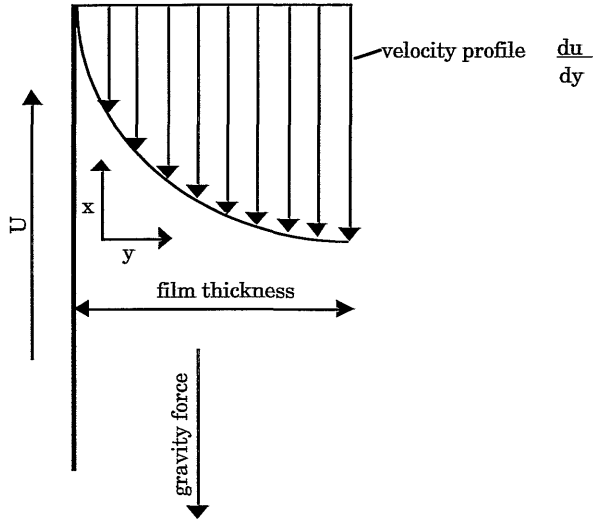


**Figure 3.2** Schematical drawing of the velocity profile in a coating layer

Integration of equation (3.3) gives

$$\int_H^y \frac{\partial^2 u}{\partial y^2} dy = \int_H^y \frac{\rho g}{\eta} dy \quad (3.6)$$

By incorporating equation (3.5) the solution of this integral is given by equation (3.7)

$$\frac{\partial u(y)}{\partial y} = \frac{\rho g}{\eta} (y - H) \quad (3.7)$$

By further integration of equation (3.7) under consideration of the boundary condition 1 (equation 3.4) equation (3.8) is obtained

$$u(y) = U + \frac{\rho g}{2 \eta} (y^2 - 2Hy) \quad (3.8)$$

The entrainment flux  $Q$  can be obtained by the integration of the velocity profile in the coating layer<sup>[4]</sup>

$$Q = \int_0^H u(y) dy. \quad (3.9)$$

The flux in the coating layer is then given by equation (3.10)

$$Q = UH - \frac{1}{3} \frac{\rho g}{\eta} H^3. \quad (3.10)$$

The maximum flux in the layer would be obtained if the gravity force would not act on the layer, i. e.,  $g=0$ . Under this condition the maximal possible coating thickness can be obtained according to

$$\frac{\partial Q}{\partial H} = U - \frac{\rho g}{\eta} H^2 = 0. \quad (3.11)$$

Equation (3.11) yields the maximum possible coating thickness  $H_m$

$$H_m = \sqrt{\frac{\eta U}{\rho g}}. \quad (3.12)$$

Equation (3.12) and equation (3.10) are combined to yield the final coating thickness  $H_\infty$

$$H_\infty = \frac{2}{3} \sqrt{\frac{\eta U}{\rho g}}. \quad (3.13)$$

### 3. 3. POLYMERS IN SOLUTION - INFLUENCE ON THE COATING PROCESS

One major problem in the preparation of composite membranes by solution coating is the penetration of polymer solution into the pores of the support. In this way pore blocking occurs which has a drastic effect on the permeation behaviour of the composite membranes. One possibility to prevent pore penetration is the impregnation of the support with a liquid<sup>[5]</sup>. Another possibility is the use of polymer solutions in which the dimensions of the polymer chains are greater than the pore diameter of the support. An important parameter, therefore, is the radius of gyration  $\langle R^{1/2} \rangle^2$ , which gives the dimension of a random coil in a certain solvent. The radius of gyration depends on the interaction between polymer chain and solvent. A good solvent will force the chains to interact with the solvent, leading to more extended chains. In a poor solvent the polymer excludes the solvent due to polymer-polymer interaction and this leads to a densification of the polymer chain. The two different conformations are schematically shown in figure 3.3.

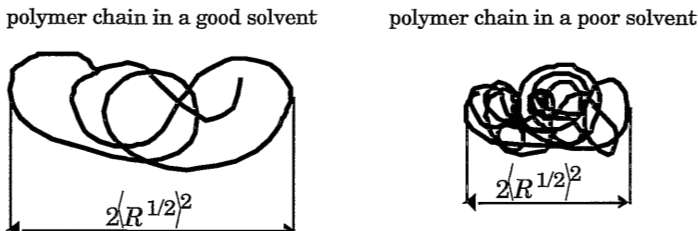


**Figure 3.3** Schematic drawing of a polymer coil in a good and in a poor solvent

Rezac<sup>[6]</sup> investigated the relation between coil diameter of the polymer chains, pore size of the support and performance of the composite membrane for a series of polymers. Solutions in which the dimension of the polymer coils was at least as big as the pores of the support resulted in defect-free coating layers. Polymers with a broad molecular weight distribution did not form defect-free layers, since the low molecular weight parts have a smaller coil dimension and could therefore penetrate into the pores. Since the polymer solutions used for coating experiments have usually a low polymer content, already a small amount of solution penetrating into the pores can lead to defects in the coating because the amount of residual solution on the support is not enough to cover the support.

Various methods can be used to determine the radius of gyration such as static light scattering<sup>[7,8]</sup>, gel permeation chromatography and viscosimetry<sup>[7,8]</sup>. A brief description of these methods is given in appendix B.

### 3. 4. GAS TRANSPORT THROUGH COMPOSITE MEMBRANES

The transport through dense membranes can be described by a solution-diffusion model. The flux through such a membrane can be described by the following equation

$$J_i = \frac{P_i}{l} * \Delta p_i, \tag{3.14}$$

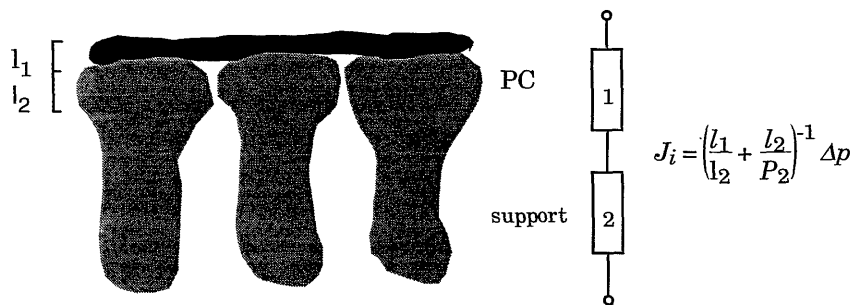
where

- $J_i$  flux of the species i through the membrane [ $\text{cm}^3(\text{STP})/\text{cm}^2 \text{ s}$ ]
- $P_i$  permeability of the species in the membrane [ $\text{cm}^3(\text{STP}) \text{ cm}/\text{cm}^2 \text{ s cmHg}$ ]
- $l$  thickness of the membrane [cm]
- $\Delta p_i$  partial pressure difference across the membrane [cmHg].

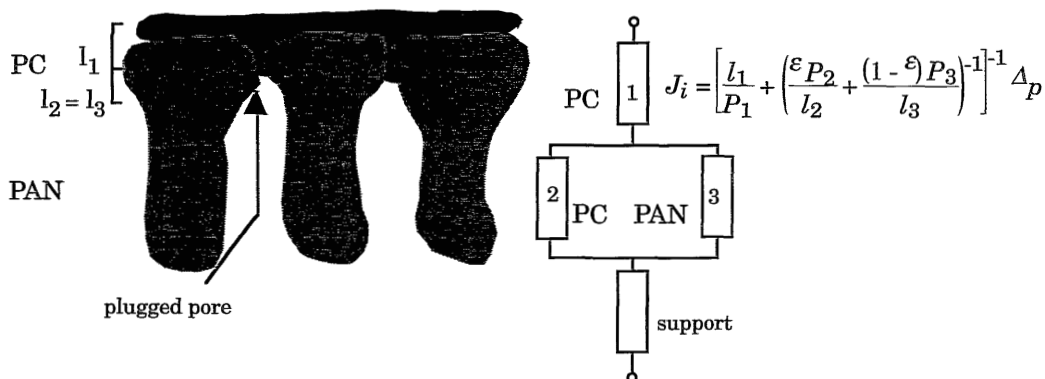
### 3. 5. CALCULATION WITH THE RESISTANCE MODEL

The flux through a composite membrane depends on the contributions of the different parts of the membrane and this can be described by the resistance model developed by Henis and Tripodi<sup>[9]</sup>. This model compares the flow through a membrane with an electrical circuit analogue. With this model the influence of different types of composite membranes (1-layer or multilayer membranes) or the influence of the support as well the influence of the penetration depth of polymer into the pores of the support can be estimated (see figure 3.4).

#### I: no pore penetration



**II: pore penetration**



**III: 2-layer membrane, no pore penetration**

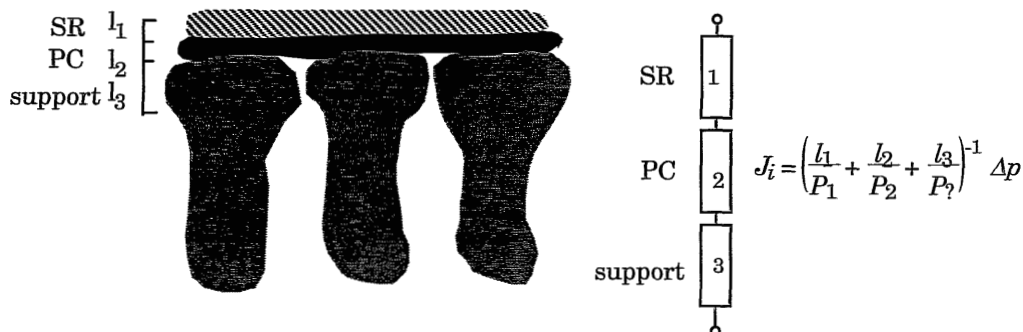


**Figure 3.4** Different types of composite membranes modelled with the resistance model; Case I: 1-layer composite membrane, no pore penetration; case II: 1-layer composite membrane with pore penetration; case III: 2-layer composite membrane, no pore penetration

I: In the ideal case a thin rate-determining layer has been deposited onto a support without the occurrence of pore penetration. Because the resistance of the selective layer is much higher than that of the porous support, the transport is determined by this selective layer (see figure 3.4I).  $l_1$  and  $l_2$  refer here to the thickness of the selective layer and the thickness of the skin layer of the porous support, respectively.

II: In the case that the coating polymer penetrates into the pores of the support the resistance to transport increases drastically, especially in the case of glassy toplayer. The flow through this membrane can be described by a combination of series and parallel resistances (figure 3.4II). Here  $l_1$  is the thickness of the selective polymer on the support,  $l_2$  is the penetration depth of selective polymer in the support pores and  $l_3$  is the thickness of the skin layer of the support.



III: Because the preparation of defect-free thin coating layers is difficult to achieve the membranes can be coated by an additional layer of a highly permeable polymer. This sealing layer should plug the defects in the actual selective layer to ensure that the transport of gases through these membranes occurs by the solution-diffusion mechanism. The resistance of the sealing layer should be low or negligible compared to that of the selective layer. The performance of such a membrane can be calculated by assuming that sealing layer, selective layer and porous support act as resistances in series (see figure 3.4III). In this example it is assumed that no pore penetration takes place.  $l_1$  represents the thickness of the silicon rubber layer,  $l_2$  the thickness of the selective polymer and  $l_3$  the thickness of the skin layer of the support.

The fluxes through the membranes can now be calculated with the transport equations given above. Herefrom, the effective thickness of the membranes can be determined. It gives an indication how, for example, the penetration depth of the coating polymer, influences the membrane performance. The calculations have been carried out for the materials used in this work (see section 3. 4.) and they are given in table 3.1.

**Table 3.1** *Oxygen permeation characteristics for the polymers used for the coating experiments. These values were used for the calculations of the resistance model*

---

polycarbonate (selective polymer):	$P(O_2) = 9.5$ Barrer
PDMS (sealing layer):	$P(O_2) = 600$ Barrer
PAN (support):	$P(O_2) = 0.002$ Barrer
Support (GFT):	$P/l (O_2) = 0.00315$ cm <sup>3</sup> /cm <sup>2</sup> s cmHg
surface porosity:	$\varepsilon = 2$ %
feed pressure:	$p = 1$ bar

---

### I: no pore penetration

thickness of the selective layer:  $l_1 = 1$  μm

$$J_{O_2} = \left[ \frac{l_1}{P_1} + \frac{l_2}{P_2} \right]^{-1} \Delta p_{O_2} \quad (3.15)$$

$$J_{(O_2)} = 7.22 \cdot 10^{-4} \text{ cm}^3/\text{cm}^2 \text{ s}$$

$$l_{\text{eff}} = 1 \text{ μm}$$

**II: pore penetration**

thickness of the selective layer:  $l_1 = 1 \mu\text{m}$   
 penetration depth of the selective polymer:  $l_2 = 1 \mu\text{m}$   
 skin layer thickness  $l_3=l_2$

$$J_{O_2} = \left[ \frac{l_1}{P_1} + \left( \frac{\varepsilon P_2}{l_2} + \frac{(1-\varepsilon)P_3}{l_3} \right)^{-1} \right]^{-1} \Delta p_{O_2} \quad (3.16)$$

$$J_{(O_2)} = 1.43 \cdot 10^{-5} \text{ cm}^3/\text{cm}^2$$

$$l_{\text{eff}} = 50 \mu\text{m}$$

**III: 2-layer membrane, no pore penetration**

thickness of the sealing layer:  $l_1 = 1 \mu\text{m}$   
 thickness of the selective layer :  $l_2 = 1 \mu\text{m}$

$$J_{O_2} = \left[ \frac{l_1}{P_1} + \frac{l_2}{P_2} + \frac{l_3}{P_3} \right]^{-1} \Delta p_{O_2} \quad (3.17)$$

$$J_{(O_2)} = 7.1 \cdot 10^{-4} \text{ cm}^3/\text{cm}^2$$

$$l_{\text{eff}} = 1.02 \mu\text{m}$$

These simple calculations nicely show the different effects on the flux and the effective thickness. A penetration depth of only  $1 \mu\text{m}$  into the support causes a drastical decrease in flux (see example II). Sealing a selective layer with a highly permeable polymer has negligible effects on the flux. Clearly, pore penetration should be avoided as much as possible in the case of a glassy toplayer coating on a glassy polymer support. The effective thickness shows the effectiveness of the coating process of the difference between the coating thickness as determined by SEM and the actual thickness.

**3. 6. EXPERIMENTAL****3. 6. 1. SUPPORT MATERIALS**

Flat asymmetric PAN-membranes from Deutsche Carbone (GFT), Germany were used for the coating experiments. The GFT-membranes are normally employed as support in pervaporation composite membranes with polyvinylalcohol (PVA) as toplayer. They have been used without any further treatment. The gas permeation properties of these porous membranes are given in table 3.2.

**Table 3.2** Gas permeation properties of the used support membranes

membrane	P/I O <sub>2</sub> *	P/I N <sub>2</sub> *	selectivity (O <sub>2</sub> /N <sub>2</sub> )
GFT	0.315	0.29	1.09

\*  $\cdot 10^{-2}$  cm<sup>3</sup>/cm<sup>2</sup> s cmHg

### 3. 6. 2. COATING MATERIAL

Polycarbonate (PC), Makrolon 3200 from Bayer, AG was used as selective polymer. The chemical structure of the polymer is given in figure 3.5. The gas separation properties of the polymer for oxygen and nitrogen are given in table 3.3.

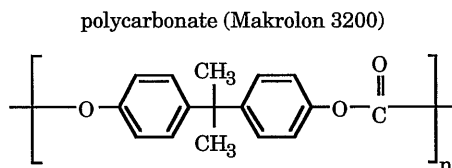


**Figure 3.5** Chemical structure of 4,4'-isopropylidene bisphenol polycarbonate (Makrolon 3200)

**Table 3.3** Intrinsic permeation properties of Makrolon 3200

polymer	M <sub>w</sub> [g/mol]	P(O <sub>2</sub> ) [Barrer]*	P(N <sub>2</sub> ) [Barrer]*	selectivity (O <sub>2</sub> /N <sub>2</sub> )
Makrolon 3200	32,000	9.5	2.25	4.5

\* Barrer =  $10^{-10}$  cm<sup>3</sup>(STP) cm/cm<sup>2</sup> s cmHg

### 3. 6. 3. COATING PROCEDURE

The flat supports were glued on glass plates with polyvinyl alcohol and then placed in a coating vessel which contains the coating solution (see figure 3.6). This vessel is allowed to empty by opening a tap at the bottom. By opening the tap to different extends the coating velocity was varied. On the top of the vessel the drying gas, which in our case was nitrogen, was introduced.

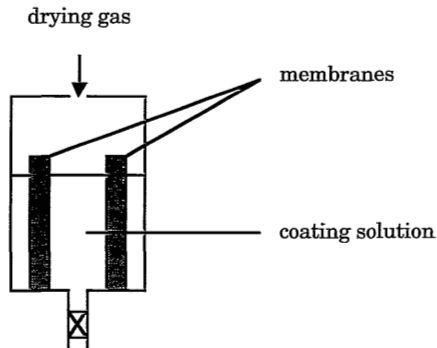


**Figure 3.6** Schematical drawing of the coating set-up

Some of the PAN-membranes were impregnated with water by a procedure illustrated in figure 3.7. Therefore a small cut was applied to the support membrane through which the needle of a syringe could be introduced and water be injected (see figure 3.7). For some experiments the pore filling water was applied on the surface of the support membranes. After penetration of the water into the pores the excessive water on the membrane surface was carefully removed with a tissue. The hollow fibers were impregnated by suction of water through the bore side of the fiber with a vacuum pump. After this impregnation procedure the fibers were closed at one end by a heat treatment with a soldering-iron.

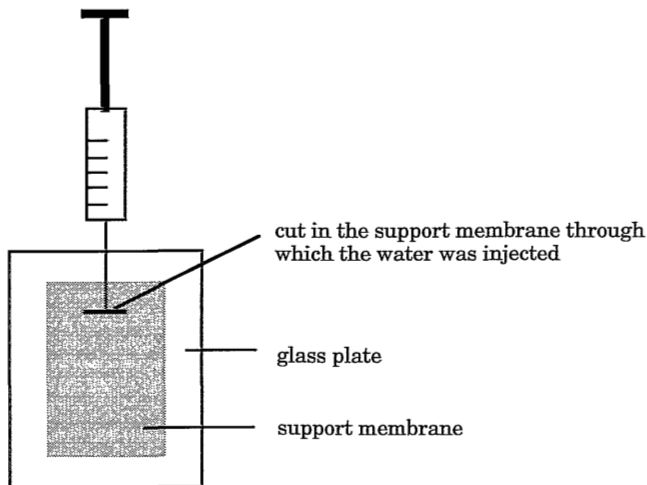


**Figure 3.7** Schematic drawing of the impregnation procedure of flat membranes

Solutions of 2 % and 5 % (by weight) Makrolon 3200 in chloroform were used to prepare the composite membranes. Coating velocities were varied between 0.05 and 0.5 cm/s.

After the coating procedure the prepared composite membranes were dried in air at room temperature in the vertical position. The coating angle was in all cases 90°. For the gas permeation experiments the membranes were coated with a thin layer of silicone rubber to plug defects<sup>[9]</sup>. Therefore the coated membranes were dipped in a solution of 3 % polydimethylsiloxane (PDMS) and a curing agent in iso-octane<sup>[10]</sup>. After withdrawing the membranes from the PDMS solution the membranes were dried in the horizontal position in an oven at 80 °C for 24 hours. This procedure was carried out at least twice.

### **3. 6. 4. CHARACTERIZATION OF THE COMPOSITE MEMBRANES**

The prepared composite membranes have been characterized by gas permeation measurements and electron microscopy. For the permeation measurements the set-up described by van't Hof<sup>[11]</sup> has been used. The fluxes of the pure gases (nitrogen and oxygen) have been measured at pressures between 3 and 5 bar. The membranes have been conditioned in each gas for several hours, i. e., at least 14 hours in N<sub>2</sub> and 6 to 8 hours in O<sub>2</sub>.

The microscopic studies have been performed on either a Field Emission Scanning Electron Microscope (FESEM) Hitachi S 800 and on a Scanning Electron Microscope (SEM) Jeol JSM-T 220A. The samples were wetted in a water/ethanol mixture and then broken in liquid nitrogen. After drying for at least 4 hours in a vacuum oven at 30 °C the samples were sputtered with carbon for the FESEM- and with gold for the SEM-investigations.

## **3. 7. RESULTS AND DISCUSSION**

### **3. 7. 1. COATING EXPERIMENTS WITHOUT IMPREGNATION**

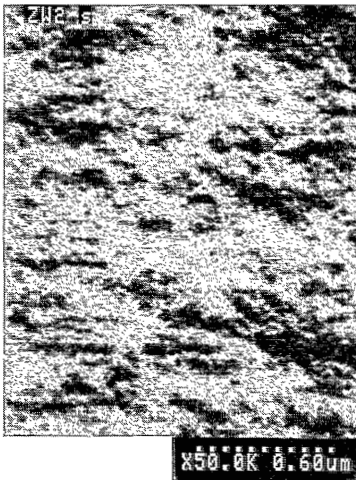
The cross-section of a GFT-membrane coated with 2 % solution of Makrolon 3200 in chloroform is shown in figure 3.8. The coating solution was applied on a dry support membrane. No clear toplayer can be observed.



**Figure 3.8** SEM-photograph showing the cross-section of a composite membrane made by dip-coating on a non-impregnated GFT-support (coating velocity: 0.5 cm/s, coating layer dried in air)

The surface of the coating layer is shown in figure 3.9a. If the surface of the coated and the uncoated support is compared (figure 3.9) then it seems that most of the pores of the support are covered.

a)



b)

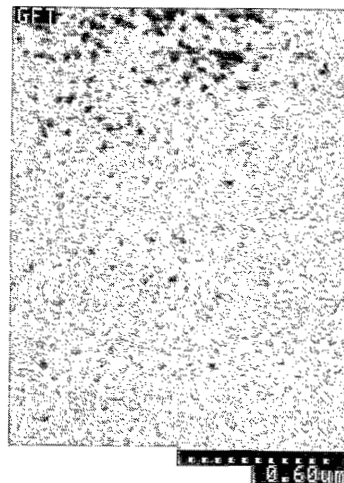


**Figure 3.9** SEM-photographs showing the surfaces of a) the composite membrane shown in figure 3.8 and b) an uncoated GFT membrane

This is also indicated by the decreased P/l-values of the prepared composite membranes in comparison to the uncoated support-membranes. From the gas

permeation experiments the effective thicknesses have been calculated (equation 3.18) by assuming that the transport is completely determined by the toplayer.

$$(P/l)_{\text{composite}} = \frac{P_{\text{toplayer}}}{l_{\text{eff}}}, \quad (3.18)$$

with

$(P/l)_{\text{composite}}$  P/l-value of the composite membrane [ $\text{cm}^3/\text{cm}^2 \text{ s cmHg}$ ]  
 $P_{\text{toplayer}}$  intrinsic permeability coefficient of the toplayer polymer [ $\text{cm}^3 \text{ cm}/\text{cm}^2 \text{ s cmHg}$ ]  
 $l_{\text{eff}}$  effective thickness [cm].

The selectivities as a function of the effective thickness are given in figure 3.10. It shows big effective thicknesses with a large scatter. It should be noted that no dependence of the effective thickness on the coating velocity could be observed which gives an indication of the rather poor reproducibility of the experiments.

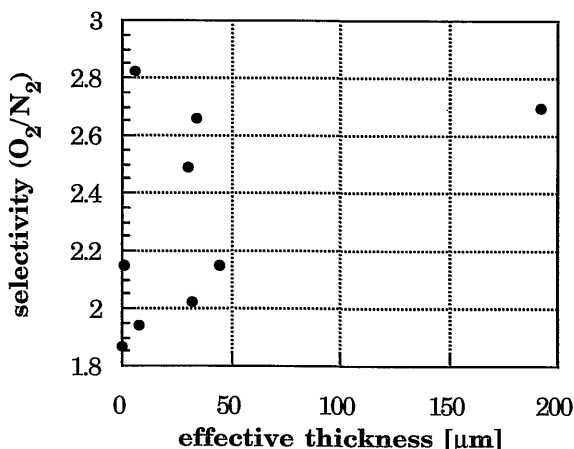


**Figure 3.10** Comparison of the calculated effective thicknesses and obtained selectivities for composite membranes prepared from solutions of 2 % Makrolon 3200 in chloroform on non-impregnated GFT-supports . The effective thicknesses were calculated according to equation (3.18)

Furthermore, it can be observed that a maximum value for the selectivity of  $\alpha=2.8$  has been obtained, far below the intrinsic value of 4.5. From these results it can be concluded that the polymer solution has penetrated into the pores of the support and blocked these pores and leakages must occur. From the relatively high effective thicknesses and the fact that practically no toplayer could be observed by electron microscopy it can be concluded that the solution penetrates into the support and blocked the pores. This result could be predicted by the resistance model assuming

pore penetration (see section 3. 4.). The characterization of the GFT support (see chapter 2) showed that pores are present with a maximum radius of about 20 nm. A parameter which gives information whether the polymer molecules can penetrate into the pores is the radius of gyration. The radius of gyration of Makrolon 3200 which has been determined by GPC and light scattering (see Appendix B to chapter 3) is about 9.4 nm and therefore, much smaller than the maximum pore size of the GFT membranes.

### 3. 7. 2. COATING EXPERIMENTS WITH IMPREGNATION

In the previous section it was shown that by immersion of a PAN support into a polymer solution a composite membrane with defects and a rather high effective thickness is obtained. Since the used polymer solutions have rather low viscosities and the polymer coil has a small dimension it will easily penetrate into the pores of the support due to capillary forces, resulting in a very high resistance of the support layer. Different approaches have been followed to prevent this. One possibility is to apply an intermediate layer of a highly permeable polymer<sup>[12,13]</sup>. Figure 3.11 shows the surface of a membrane where a layer of Makrolon 3200 was coated onto a silicone rubber layer. The obtained membranes showed typical defects caused by bad adhesion between the two materials.

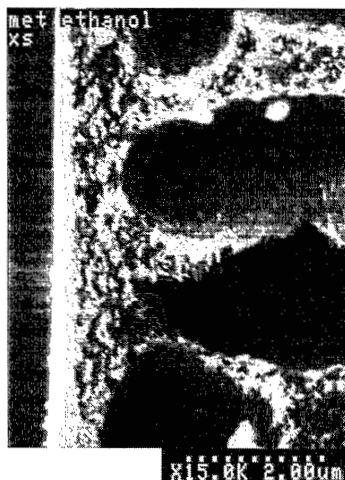


**Figure 3.11** Defects in the Makrolon 3200 layer caused by bad adhesion between the Makrolon 3200 and the intermediate PDMS layer

Filling of the pores of the support membrane with a liquid, which must be a nonsolvent for the coating polymer is another approach. Two different liquids have been selected, being ethanol and water. Both are nonsolvents for the coating polymer, however, ethanol is miscible with the solvent chloroform whereas water is immiscible with chloroform. The advantage of using these liquids is that they can be removed very easily from the support pores, e. g., by evaporation.

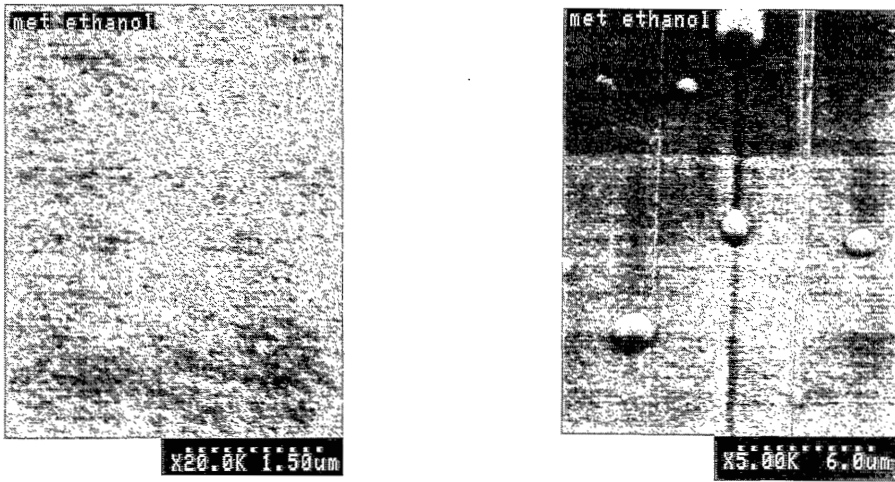


The cross-section of a composite membrane where the coating layer was applied onto a support membrane impregnated with ethanol is shown in figure 3.12. As soon as the support membrane was placed in the coating solution mixing of ethanol and chloroform took place, which was visible by turbulences near the membrane surface.



**Figure 3.12** *FESEM-photograph showing the cross-section of a composite membrane where the coating layer was applied onto an impregnated GFT support. The pores of the support membrane have been filled with ethanol.*

The surface of the coating layer is shown in Figure 3.13. The surface is very rough and some bigger holes can be observed which might be caused by mixing of ethanol and chloroform. The surface roughness of the coated layer is comparable to that of the layer prepared on a dry support (see Figure 3.9a). This shows that ethanol is not suitable to be used as pore filling liquid.



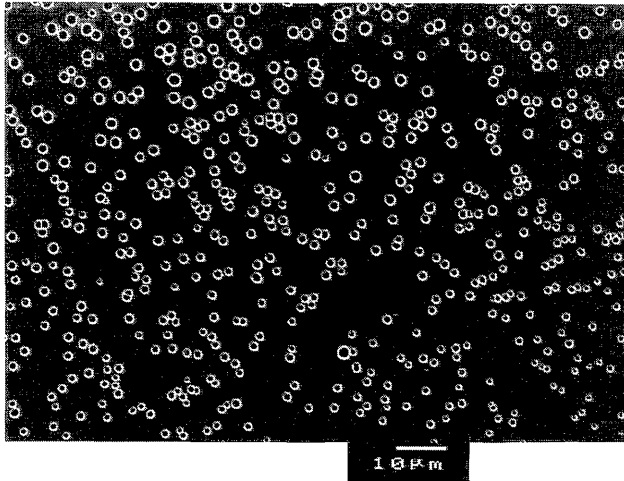
**Figure 3.13** FESEM-photographs showing the surfaces of a composite membrane where the pores of the support membrane were filled with ethanol prior to the coating procedure (left magnification 20,000x, right magnification 5,000x)

Figure 3.14 shows the cross-section of a coated GFT-membrane in which the pores were filled with water. The water was applied from the top of the support membrane. The membrane was coated in the same coating experiment as the membrane shown in Figure 3.8. It can be seen clearly that the coating layer shows a bad adhesion onto the support and that probably no pore penetration took place.



**Figure 3.14** FESEM-photographs showing the cross-sections of a composite membrane where the impregnating water was applied from the top of the GFT-membrane prior to the coating procedure

Figure 3.15 shows the surface of a coated membrane where the pore filling water was applied from the top of the support. Very typical and regularly distributed defects can be seen. This might be caused by water droplets on the support surface since the water was applied from the top surface. The surface of the coating layers looks very smooth.



**Figure 3.15** FESEM-photographs showing the surfaces of a coated layer prepared by dip-coating on an impregnated PAN-support where the pore filling water was applied from the top of the support

By applying the water from the bottom surface very smooth layers were obtained with only a few defects. From Figure 3.16 a very thin layer can be observed with a thickness of less than 100 nm. From equation (3.13) a theoretical thickness of 40.5  $\mu\text{m}$  can be calculated resulting in a final thickness after drying of 2  $\mu\text{m}$ . The difference between the observed and the calculated thickness of the coating layer is quite significant.

Figure 3.17 shows the surfaces of membranes which were coated with and without impregnation (see Figure 3.9). Relatively high surface roughness can be observed for non-impregnated supports, whereas in the case of impregnated supports perfectly smooth surfaces were obtained.



**Figure 3.16** SEM-photograph showing the cross-section of composite membranes where the water for the pore filling was applied from the bottom of the membrane (polymer concentration: 5 % ; coating velocity: 0.5 cm / s)

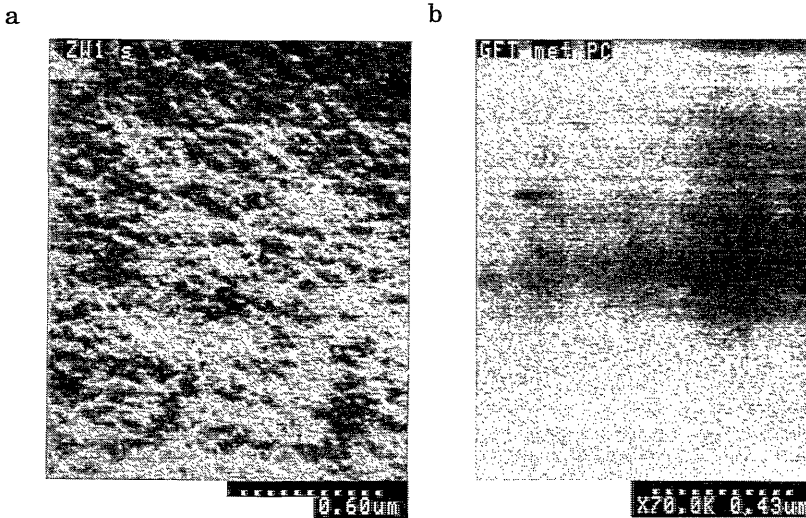


**Figure 3.17** SEM-photographs showing the surfaces of coating layers using a) dry PAN-supports and b) water impregnated PAN-support (in this case the water was applied from the bottom of the support membranes)

### ***Influence of the coating velocity***

The dependency of the selectivity on the effective thickness is shown in Figure 3.18. It can be observed that membranes with a high effective thickness show low selectivities. It should be noted that for some composite membranes higher selectivities were obtained than the intrinsic selectivity of Makrolon 3200 (see table 3.2). This behaviour has already been observed by Rezac<sup>[6]</sup>, Pfromm<sup>[14]</sup> and Pinnau<sup>[15,16]</sup>.

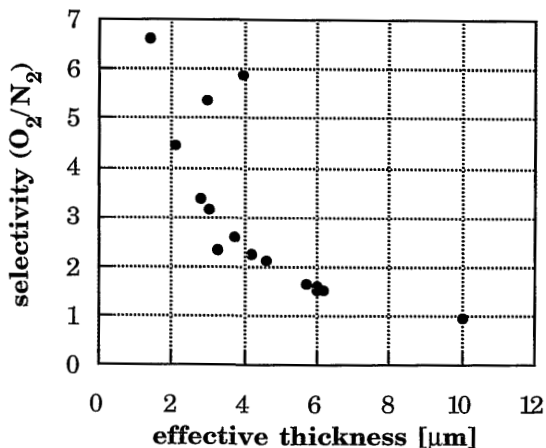


**Figure 3.18** Comparison of effective thicknesses and obtained selectivities for composite membranes prepared from solutions of 2 % Makrolon 3200 in chloroform on impregnated GFT supports. The membranes have been prepared with different coating velocities.

### ***Influence of the polymer concentration***

To investigate the influence of the Makrolon 3200 concentration, two different concentrations were used for the coating solutions. The results for the 2 % solutions were already shown in the previous section. The influence of the coating velocity on the gas separation performance of composite membranes prepared from solutions of 5 % Makrolon 3200 in chloroform on impregnated supports is shown in Figure 3.19. Like for the 2 % Makrolon 3200 solution an increase in the P/I-values can be observed with increasing coating velocity.

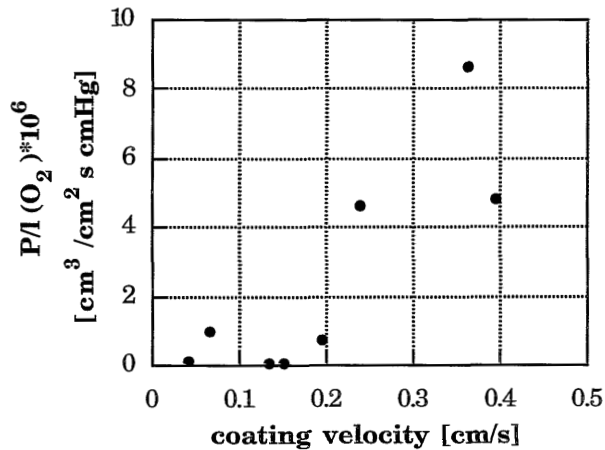


**Figure 3.19** Influence of the coating velocity on the  $P/l$ -values of composite membranes prepared from solutions of 5 % Makrolon 3200 in chloroform on impregnated GFT supports

Figure 3.20 compares the effective thicknesses of the various composite membranes prepared from the two different polymer solutions (2 % and 5 % Makrolon in chloroform). Generally, the membranes prepared from the solution of 5 % Makrolon 3200 in chloroform show lower effective thicknesses. This is rather surprising because one would expect an increase in the coating layer thickness with increasing polymer concentration. One reason for this behaviour might be that due to an increased viscosity of the higher concentrated solution pore penetration is more hindered leading to a decreased effective thickness. Nevertheless, there are membranes with relatively high effective thicknesses which indicates one of the major problems in preparing composite membranes: the reproducibility of the membranes is not satisfactory, although it should be considered that the variation in effective thicknesses is much smaller (1 - 15  $\mu\text{m}$ ) than in the case of non-impregnated supports (1 - 50 $\mu\text{m}$ ). The theoretical thicknesses have been calculated from equation (3.13) and corrected for the polymer concentration in the coating solution. Comparison of the effective thicknesses and theoretical thicknesses reveals that membranes prepared from solutions with 2 % Makrolon in chloroform show a higher effective thickness. This is most probably caused by penetration of the solution into the pores of the support.

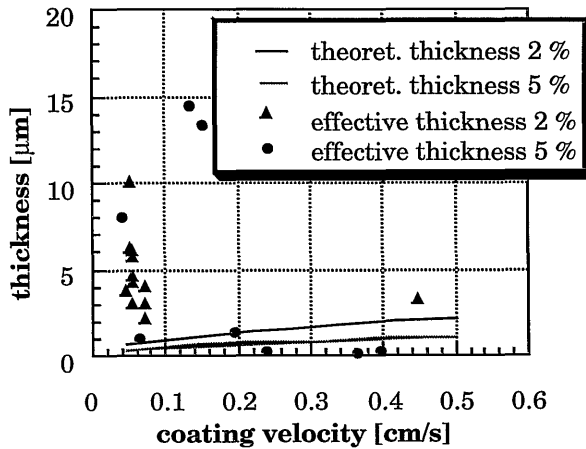


**Figure 3.20** Comparison of effective and theoretical thicknesses for composite membranes prepared from solutions of 2 % and 5 % Makrolon 3200 in chloroform on impregnated GFT supports. The effective thicknesses were calculated from the  $P/l$  values for oxygen. The theoretical thicknesses were calculated with equation (3.13) using the characteristics of the coating solutions given in Appendix A to this chapter.

### 3. 8. CONCLUSIONS

Impregnation of the pores of the support leads to a much better reproducibility of the coating process in preparing composite membranes, although it should be noted that it is still not satisfying. Comparison of Figures 3.8 and 3.16 shows very clearly that in the case of water impregnated supports a toplayer on the support was obtained, while in the case of non-impregnated supports no layer could be observed. Furthermore, in the case of water impregnated membranes much lower effective thicknesses from the gas permeation results were determined (see Figures 3.10 and 3.18). Impregnation of the support with ethanol did not yield in significant improvement of the quality of the coating layer compared to non-impregnated supports. From these results it can be concluded that impregnation should preferably be carried out with an liquid immiscible with the solvent of the coating solution.

Composite membranes prepared from a solution of 5 % Makrolon 3200 in chloroform show lower effective thicknesses compared to membranes prepared from solutions with 2 % Makrolon 3200. This effect is caused by pore penetration of the 2 % solution, whereas the higher viscous 5 % solution cannot so easily penetrate into the pores of the support. However, pore penetration takes place in both cases. This pore penetration might be prevented by using coating polymers with a high molecular

weight and good solvents so that their molecular dimensions in solutions are larger than the pore dimension.

### 3. 9. REFERENCES

- [1] P. Groenveld; Dip-coating by withdrawal of liquid films; PhD-thesis University of Delft (1970)
- [2] Appendix A to Chapter 3
- [3] S. Middleman; Fundamentals of polymer processing (chapter 8); Mc Graw-Hill Book Company (1977)
- [4] Deryagin, B. M., Levi, S. M.; Film coating theory; The Focal Press, London New York (1959)
- [5] Williams, S. C., Bikson, B., Nelson, J. K.; Composite membranes for enhanced fluid separation; EP 0 286 091  
Williams, S. C., Bikson, B., Nelson, J. K., Burchesky, R. D.; Method for preparing composite membranes for enhanced gas separation; U. S. Patent 4,840,819
- [6] Rezac, M. E., Koros, W. J.; Preparation of polymer-ceramic composite membranes with thin defect-free separating layers; J. Appl. Pol. Sc., Vol. 46, 1927-1938 (1992)
- [7] H.-G. Elias; Makromoleküle; Hüthig & Wepf Verlag Basel (1971)
- [8] P. J. Flory; Principles of polymer chemistry; Cornell University Press, NY (1953)
- [9] Henis, J. M., Tripodi, M. K.; Multicomponent membranes for gas separation; U. S. Patent 4,230,463  
Henis, J. M., Tripodi, M. K.; Composite hollow-fibre membranes for gas separation: The resistance model approach; J. Membr. Sci., 8 (1981) 233
- [10] I. Blume, R. W. Baker; U. S. Patent 4,952,751 (1990)
- [11] J. A. van't Hof; Wet spinning of asymmetric hollow fibre membranes for gas separation; PhD-thesis University of Twente (1988)
- [12] A. v. d. Scheer; Composite dense membranes; U. S. Patent 4,581,043
- [13] I. Cabasso; K. A. Lundy; Method of making membranes for gas separation and the composite membranes; U. S. Patent 4,602,922
- [14] P. H. Pfromm, I. Pinnau, W. J. Koros; Gas transport through integral-asymmetric membranes: A comparison to isotropic film transport properties; J. Appl. Pol. Sci., 48, 2161-2117
- [15] I. Pinnau; Skin formation of integral-asymmetric gas separation membranes made by dry/wet phase inversion; PhD-thesis University of Austin (1991)
- [16] I. Pinnau; M. W. Hellums, W. J. Koros; Gas transport through homogenous and asymmetric polystyrene carbonate membranes; Polymer, 32, 2612-2617 (1993)



# APPENDIX A TO CHAPTER 3

---

## Rheological properties of polymer solutions

---

### 1. Introduction

The thickness of a coated film depends on the rheological properties of the used coating solution and on the process conditions which can be expressed by a Capillary number and a Reynolds number<sup>[1,2]</sup>. The basic equation which relates the coating thickness  $H_\infty$  with the rheological properties is given below<sup>[1,2]</sup>

$$H_\infty = \frac{2}{3} \sqrt{\frac{\eta u}{\rho g}} \quad (\text{A1})$$

with

- H thickness of the coated wet film [m]
- $\eta$  viscosity of the coating solution [Pa s]
- u coating velocity [m/s]
- $\rho$  density of the coating solution [kg/m<sup>3</sup>]
- g gravitational constant [m/s<sup>2</sup>].

In this work solutions of polycarbonate and poly(methyl methacrylate) have been used for the coating experiments. In order to apply the correct coating theory it should be investigated whether the solutions show Newtonian or non-Newtonian behaviour<sup>[1,2]</sup>. In the case the coating solutions show Newtonian behaviour equation (A1) can be applied. This appendix describes the viscoelastic behaviour of the used coating solutions<sup>[3]</sup>. A schematical drawing of the experimental set-up is shown in figure A1. The solution is placed between the cone and plate. The plate is stationary and the torque  $T$  on the cone which is necessary to rotate the cone at a certain rotational velocity  $\omega$  is measured. The viscosity is then obtained by

$$\eta = \frac{3 T \Theta}{2 \pi R^3 \omega} \quad (\text{A2})$$

with

- $\eta$  viscosity of the solution [Pa s]
- T torque [Pa m<sup>3</sup>]
- $\Theta$  angle between cone and plate [°]
- R radius of cone and plate [m]
- $\omega$  rotational velocity [s<sup>-1</sup>]

At a certain characteristic shear rate the solution viscosity decreases. This is schematically shown in figure A2. A solution which has a shear rate below the characteristic one shows Newtonian behaviour while solutions with higher shear rates behave non-Newtonian.

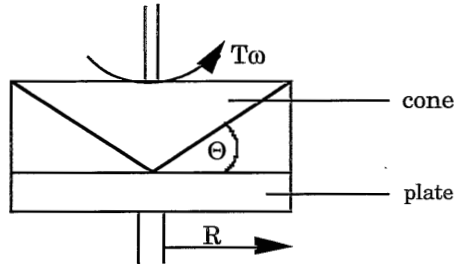


**Figure A1** Schematic drawing of the experimental set-up for the determination of the flow curve

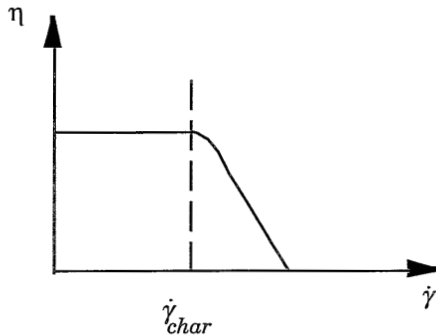


**Figure A2** Schematic drawing of a shear rate - viscosity diagram; The dashed line gives the point  $\dot{\gamma}_{char}$  at which the rheological behaviour changes from Newtonian to non-Newtonian

The shear rate  $\dot{\gamma}$  can be calculated according to equation A3

$$\dot{\gamma} = \frac{\Omega}{\Theta} \tag{A3}$$

Estimation of the process conditions

In the dip-coating process a thin polymer solution is deposited on a suitable support. In this process hydrodynamic and rheological parameters must be considered. Therefore, the Capillary number (Ca), the Reynolds number (Re) and the viscoelastic behaviour must be determined. The Capillary number and Reynolds number can be determined with equations (A4) and (A5), respectively. The results are summarized in table A1.

$$Ca = \frac{\eta u}{\sigma} \quad (A4)$$

$$Re = \frac{\rho u H_{\infty}}{\eta} \quad (A5)$$

**Table A1** *Some characteristics of the used polymer solutions for the calculation of the Capillary and Reynolds number*

	Makrolon 3200	PMMA 350	PMMA 100	PMMA 75
$\eta$ [Pa s]	0.01175	0.0664	0.00187	0.0017
$u$ [cm/s]	0.5	0.5	0.5	0.5
$\sigma$ $10^3$ [N/m]	28.5	29.55	29.37	29.14
$h$ $10^3$ [cm]	4.28	0.01	1.7	1.65
Ca [-]	0.0021	0.0112	0.00032	0.00029
Re [-]	0.026	0.0106	0.064	0.069

Under process conditions both the Capillary and the Reynolds number are quite low. Hence, it can be concluded that the coating theory can be applied for conditions with low Capillary and Reynolds numbers.

Comparison of the maximum shear rate under process conditions with the characteristic time of the polymer solution

The shear rate under process conditions can be estimated<sup>[5]</sup> from

$$\gamma = \frac{u}{H_{\infty}}, \quad (A6)$$

where

$u$  coating velocity [cm/s]

$H_{\infty}$  thickness of the coated film [cm].

For the estimation of the maximum shear rate the maximum values of the coating velocity and the minimum coating thickness which could be reached in our experiments have been taken:

$$u = 0.5 \text{ cm/s}$$

$$H_{\infty} = 4.28 \cdot 10^{-3} \text{ cm}$$

$$\gamma_{max} \approx 116.8 \text{ s}^{-1}$$

To estimate the characteristic shear rate at which a polymer solution starts to behave non-Newtonian the characteristic time  $\tau_{char}$  can be calculated according to equation A7<sup>[5]</sup>

$$\tau_{char} \approx \frac{1}{2} \frac{(\eta_0 - \eta_s) M}{c R T}, \quad (\text{A7})$$

where

- $\eta_0$  viscosity of the solution at zero shear rate [Pa s]
- $\eta_s$  viscosity of the solvent [Pa s]
- M molecular weight of the coating polymer [g/mol]
- c concentration of the polymer solution [g/m<sup>3</sup>]
- R gas constant [J/mol K]
- T temperature [K].

The shear rate under the experimental conditions of the coating process can be estimated using equation (A3). Comparison of this shear rate and the characteristic shear rate gives information whether the solution behaves either Newtonian or non-Newtonian.

**Table A2** *Some characteristics of the polymer solutions for the calculation of the characteristic shear rate*

	<i>Makrolon 3200</i>	<i>PMMA 350</i>	<i>PMMA 100</i>	<i>PMMA 75</i>
$\eta_0$ [Pa s]	0.01175	0.04637	0.00187	0.0017
$\eta_s$ [Pa s]	0.000798	0.000798	0.000798	0.000798
c 10 <sup>4</sup> [g/m <sup>3</sup> ]	7.74	7.74	10.0	10.0
M [g/mol]	32,000	430,000	85,000	84,000
$\tau$ [s]	9.136 10 <sup>-7</sup>	4.16 10 <sup>-5</sup>	1.67 10 <sup>-7</sup>	1.41 10 <sup>-7</sup>
$\gamma_{char}$ [s <sup>-1</sup> ]	1.09 10 <sup>6</sup>	2.41 10 <sup>4</sup>	5.89 10 <sup>6</sup>	7.1 10 <sup>6</sup>

$$R = 8.314 \text{ J/K mol}$$

$$T = 323.15 \text{ K}$$

The characteristic times for both polymers, polycarbonate and poly(methyl methacrylate), are higher than the shear rate calculated from the experimental conditions (equation (A2)). From these results it can be concluded that for all polymer solutions under the chosen experimental coating conditions Newtonian behaviour can be expected.

## **2. References**

- [1] B. M. Deryagin, S. M. Levi; Film coating theory; The Focal Press, London New York (1959)
- [2] P. Groenveld; Dip-coating by withdrawal of liquid films; PhD-thesis University Delft (1970)
- [3] J. D. Ferry; Viscoelastic properties of polymers; Wiley & Sons, Inc., 2. edition (1970)
- [4] chapter 3 of this thesis
- [5] T. C. Patton; Paint flow and pigment dispersion; Wiley & Sons, Inc., 2. edition (1979)

## APPENDIX B TO CHAPTER 3

---

# POLYMERS IN SOLUTION - SOME ASPECTS OF CHARACTERIZATION

---

### 1. Introduction

The properties of the polymer solutions are important for the preparation of composite membranes by solution coating. The dimension as well as the form of the polymer chains depend on the interaction of the polymer and the solvent. Rezac and Koros<sup>[1]</sup> showed that the molecular weight and related to this, the dimensions of the chains, may have a large influence on the quality of the coated layer. The dimensions of the chain should be a maximum in order to prevent pore penetration. The radius of gyration is a measure for the dimensions of a polymer coil in solution. For a random coil the radius of gyration can be related to the end-to-end distance.

$$\langle R_g^2 \rangle^{1/2} = \frac{\langle h^2 \rangle}{6} \quad (\text{B1})$$

with

$$\begin{array}{ll} \langle R_g^2 \rangle^{1/2} & \text{radius of gyration [nm]} \\ \langle h^2 \rangle^{1/2} & \text{root-mean-square-end-to-end distance [nm]} \end{array}$$

The radii of gyration have been determined by viscosimetry and gel permeation chromatography (GPC). The association behaviour of the solutions has been investigated by static light scattering.

### 2. Characterization methods

#### 2. 1. Viscosimetry

Viscosimetric measurements are very useful to obtain a quick information about various physical properties of polymers in solution. From these measurements

several molecular parameters can be calculated such as the radius of gyration, the interaction parameters between polymer and solvent and the influence of branching and association of the polymer molecules. A measure for the properties of polymers in solution is the intrinsic viscosity  $[\eta]$ , which is defined as

$$[\eta] \equiv \left( \frac{\eta_{sp}}{c} \right)_{c \rightarrow 0} \quad (\text{B2})$$

For the determination of the intrinsic viscosity the specific viscosity (see equation B3) is plotted as a function of the polymer concentration. The times necessary to pass a certain distance in a capillary of e. g. an Ubbelohde viscosimeter<sup>[2,3]</sup>, are measured for solvent ( $t_{\text{solvent}}$ ) and polymer solutions at different concentrations ( $t_{\text{solution}}$ ). For dilute solutions the following approximation can be made

$$\eta_{sp} = \frac{\eta_{\text{solution}} - \eta_{\text{solvent}}}{\eta_{\text{solvent}}} \approx \frac{t_{\text{solution}} - t_{\text{solvent}}}{t_{\text{solvent}}} \quad (\text{B3})$$

From these measurements the intrinsic viscosity  $[\eta]$  of the polymer in a certain solvent can be determined by plotting  $\eta_{sp}/c$  versus the concentration (see figure B1).

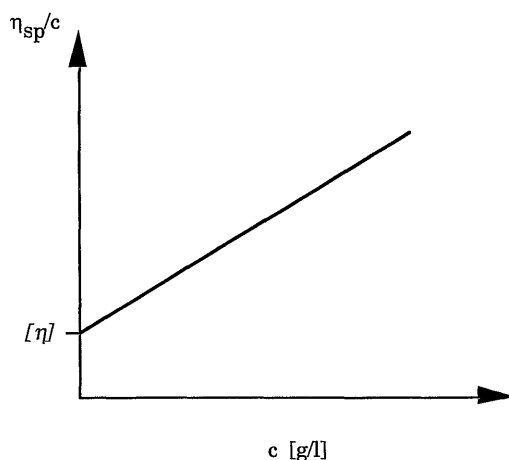


**Figure B1** Schematic drawing for the determination of the intrinsic viscosity from viscosity measurements

### 2. 1. 1. Experimental

An Ubbelohde viscosimeter with a capillary constant of 0.05027 was used for the measurements. Polymer solutions with different concentrations of 1 g/cm<sup>3</sup> to 10 g/cm<sup>3</sup> in chloroform, toluene, tetrahydrofurane (THF) and 1,2-dichloroethane (1,2-DCE) were used.

## 2. 1. 2. Results and discussion

The results of the viscosity measurements are summarized in table B1. As can be seen from these results the highest radii of gyration were obtained for PMMA 350 in toluene (12.7 nm) and 1,2-dichloroethane (15.4 nm). The radii are of about the same size as the largest pore size in the support membranes as determined by scanning electron microscopy (see chapter 2). For all other polymer/solvent systems investigated much lower radii of gyration were determined. For these systems, if used for coating experiments, pore penetration can be expected.

**Table B1** Results of the viscosity measurements for the different polymers in different solvents

polymer	solvent	$[\eta]$ [cm <sup>3</sup> /g]	$\langle R_g \rangle$ [nm]*
Makrolon 3200	chloroform	7.1	-
PMMA 350	chloroform	24.44	-
	toluene	80.47	12.7
	THF	15.25	10.9
	1,2-DCE	43.55	15.4
	chloroform	26.58	7.2
PMMA 100	toluene	15.38	8.6
	THF	29.43	8.9
	1,2-DCE	25	8.4
	chloroform	18.98	6.9
PMMA 75	toluene	18.35	7.0
	THF	29.71	8.2
	1,2-DCE	25.7	7.8
	chloroform	7.1	-

\* calculated after equation (B4)

## 2. 2. Gel permeation chromatography

Gel permeation chromatography allows the determination of the molecular weight and the radius of gyration<sup>[2,3]</sup>. The basic equation of the GPC relates the molecular weight of the polymer and the hydrodynamic volume is given below

$$[\eta] M = K V. \quad (B4)$$

with

$[\eta]$  intrinsic viscosity [cm<sup>3</sup>/g]

M molecular weight [kg/mol]



- V hydrodynamic volume [cm<sup>3</sup>]  
 K constant from Kuhn-Mark-Houwink equation

The hydrodynamic volume can be related to the root-mean-square-end-to-end distance of the polymer coil according to equation (B5). This equation is valid for polymers with a molecular weight higher than 10,000 g/mol<sup>[2]</sup>.

$$[\eta]M = \Phi \langle h^2 \rangle^{3/2} \quad (\text{B5})$$

with<sup>[4]</sup>  $\Phi = 2.84 \cdot 10^{23}$

where

- $\eta$  intrinsic viscosity of the polymer in a certain solvent [dl/g]  
 M molecular weight of the polymer [g/mol]  
 $\langle h^2 \rangle^{1/2}$  root mean square end to end distance of the polymer coil [m]  
 $\Phi$  universal constant [-].

From the root-mean-square-end-to-end distance of the polymer coil  $\langle h^2 \rangle^{1/2}$  the radius of gyration can be calculated according to equation (B1)

### 2. 2. 1. Experimental

The GPC measurements have been carried out using a Waters 510 HPLC-pump and a Viscometer detector H502 from Viscotek Corporation.

### 2. 2. 2. Results and discussion

The results obtained from GPC measurements are summarized in table B2. For Makrolon 3200 a molecular weight of 35,410 g/mol was determined which is in rather good agreement with the value given by the supplier (32,000 g/mol). For PMMA 100 and PMMA 75 almost the same molecular weights were determined. The highest radii of gyration were obtained for PMMA 350 in tetrahydrofurane and 1,2-dichloroethane. These radii are of about the same order as the biggest pores of the support membranes (see chapter 2). From these results it can be concluded that solutions of PMMA 350 in THF or 1,2-dichloroethane should give the best results for the coating experiments because the molecules can not penetrate into the pores of the support. However, one has to realize that these values are average values, which means that polymer chains with lower molecular weight and smaller chain dimensions are present in the solution, too.

**Table B2** Results from GPC measurements for the different polymers in different solvents

polymer	solvent	Mw[g/mol]	<R <sub>g</sub> > [nm]
Makrolon 3200	chloroform	35,410	9.4
	1,2-DCE	36,310	8.7
PMMA 350	chloroform	(436,500)	18.9
	toluene	544,500	14.9
	THF	485,600	23.1
	1,2-DCE	439,600	24.3
PMMA 100	chloroform	88,650	12.2
	toluene	81,510	8.9
	THF	80,590	9.7
	1,2-DCE	90,600	10.7
PMMA 75	chloroform	99,820	12.4
	toluene	86,550	8.3
	THF	87,730	9.9
	1,2-DCE	78,920	9.9

### 2. 3. Static light scattering

Static light scattering is a method from which the molecular weight of a polymer, the radius of gyration and the second virial coefficient of a polymer in a certain solvent can be obtained. The theory of the method is described in many literature sources<sup>[2,5,6]</sup>, therefore it will be explained here only very briefly.

The basic equation of light scattering is given below

$$\frac{Kc}{R} = \frac{1}{M_w P} + 2A_2c \dots \quad (\text{B.6})$$

with

- K optical constant [mol cm<sup>3</sup>/g<sup>2</sup>]
- c concentration of the polymer solution [g/l]
- R scattering intensity of the solution [-]
- M<sub>w</sub> molecular weight of the polymer [g/mol]
- P particle scattering function [-]
- A<sub>2</sub> second virial coefficient [cm<sup>3</sup>mol/g<sup>2</sup>]

For the calculation of the molecular weight a Zimm plot or a Berry plot can be used. For the Zimm plot Kc/R is plotted against sin<sup>2</sup>Θ+kc (k being an imaginary constant).

In some cases the angular dependence of the scattered light is not linear. Therefore in these cases the Berry plot is used<sup>[7,8]</sup>. For the Berry plot  $\sqrt{Kc/R}$  is plotted against  $\sin Q+kc$ . If the molecular weight determined from the Zimm plot is higher than that obtained from the Berry plot it can be concluded that the polymer tends to associate in the solvent investigated<sup>[5]</sup>.

### 2. 3. 1. Experimental

The light scattering experiments have been carried out using a photo-gonio-diffusiometer Sophica 42000M. Solutions of 1 gram/liter to 10 grams/liter have been prepared to measure the concentration dependent scattering.

### 2. 3. 2. Results and discussion

The results of the light scattering experiments are summarized in tables B3 and B4. The measurements could not be carried out for all polymer-solvent systems given in table B1 because for some of these solutions the refractive increments were too low.

The results show for the most polymer-solvent systems a rather good agreement between the molecular weights obtained from the Zimm and Berry plots. Quite significant differences were obtained for PMMA 350 in chloroform and THF. The large differences between the calculated molecular weights from light scattering and GPC indicate a great tendency to form high molecular weight associates.

**Table B.3** Results of static light scattering for the different polymers obtained from Zimm-plots

polymer	solvent	$M_w$ [g/mol]	$\langle R_g \rangle$ [nm]	$A_2 \cdot 10^{-4}$ [cm <sup>3</sup> mol/g <sup>2</sup> ]
Makrolon 3200	chloroform	41,900±7%	37	27.5
PMMA 350	chloroform	1,430,000±8%	92.3	8.28
	toluene	424,000±8%	-	2.72
	THF	1,920,000±70%	77.1	4.76
	1,2-DCE	409,000±8%	44.2	9.34
PMMA 100	chloroform	67,300±5%	-	11.4
	THF	82,400±2%	21.8	7.03
PMMA 75	THF	95,600±2%	17.5	6.33

- measurement was not possible because refractive increments were too low

**Table B.4** Results obtained from static light scattering for the different polymers obtained from Berry-plots

polymer	solvent	$M_w$ [g/mol]	$\langle R_g \rangle$ [nm]	$A_2 \cdot 10^{-4}$ [cm <sup>3</sup> mol/g <sup>2</sup> ]
Makrolon 3200	chloroform	37,500±2%	32.9	19.4
PMMA 350	chloroform	471,000±0.8%	42.5	4.33
	toluene	384,000±3%	-	1.85
	THF	448,000±55%	32.9	2.56
	1,2-DCE	223,000±1%	13.7	5.98
PMMA 100	chloroform	62,200±2%	-	8.52
	THF	77,600±0.7%	18	5.63
PMMA 75	THF	89,300±1%	14.2	5.04
	1,2-DCE	228,000±0.7%	56.3	5.96

### 3. Conclusions

Differences in the molecular weights determined by static light scattering and GPC can be observed. The determined molecular weights for the three different PMMA are higher than those given by the supplier. Comparison of results obtained from GPC measurements and from light scattering shows that PMMA 350 in 1,2-dichloroethane should give the best coating results. The molecular dimension of the chains in the solution has been estimated to be 24.3 nm which is as big as the maximum pores in the support membranes (see chapter 2). This may prevent the molecules from penetration into the pores. Furthermore, this solution does not form associates and homogeneous solutions can be obtained. For all other investigated polymer-solvent systems the radii of gyration were much lower. In these cases the molecules may penetrate very easily into the pores of the support which may lead to a high effective thickness and defects in the coating layer.

### 5. References

- [1] M. E. Rezac, W. J. Koros; Preparation of polymer-ceramic composite membranes with thin defect-free separating layers; *J. Appl. Sci.*, 46, 1927-1938 (1992)
- [2] P. J. Flory; *Principles of Polymer Chemistry*; Cornell University Press, NY (1953)
- [3] F. W. Billmeyer, Jr.; *Textbook of polymer science*; 3rd ed., Wiley, NY (1984)
- [4] G. Bodor; *Structural investigations of polymers*; Ellis Horwood, New York (1991)
- [5] H. G. Elias; *Makromoleküle*; Hüthig & Wepf Verlag Basel (1971)
- [6] M. B. Huglin; *Light Scattering from polymer solutions*; Academic Press, London (1972)
- [7] G. C. Berry; *J. Chem. Phys.*, 44, 4550 (1966)
- [8] W. Burchardt; *Adv. Polym. Sci.*, 48, 1 (1983)

# 4

---

## COMPOSITE MEMBRANES WITH A GLASSY POLYMER AS TOPLAYER

### PART II: POLY(METHYL METHACRYLATE) AS COATING POLYMER

---

#### **Summary**

*Composite membranes have been prepared by dip-coating with poly(methyl methacrylate) (PMMA) as the coating polymer. Three different molecular weights of PMMA, 430,000 g/mol, 85,000 g/mol and 84,000 g/mol, have been used. Commercial polyacrylonitrile supports in flat sheet and hollow fiber form have been used as supports. Furthermore, the influence of the coating solvent, the drying procedure and a post-treatment have been investigated. Better coating layers with a low effective thicknesses were obtained if high molecular weight polymers were used in combination with good solvents. In this case the radius of gyration of the polymer in solution was increased and this reduces the extend of pore penetration. Post-treatment with solvent vapour resulted in slightly improved performance of the prepared composite membranes.*

## 4. 1. INTRODUCTION

The pore penetration of the polymer solution into the porous support is one of the major problems connected with coating of a glassy toplayer onto a glassy support by dip-coating. Due to this penetration the effective thickness becomes much higher than the actual toplayer thickness. Therefore, it is absolutely necessary to avoid pore penetration. The molecular weight of the polymer and the type of the solvent are two parameters of importance to reduce the phenomenon of pore penetration. In this chapter the preparation of composite membranes with poly(methyl methacrylates) (PMMA) with different molecular weights will be discussed. To improve the performance of the prepared membranes the influence of the drying procedure and a post-treatment has been investigated as well. Additionally to flat sheets, hollow fibers have been used as support.

## 4. 2. DRYING PROCESS

In the dip-coating process the support is immersed in the polymer solution and after withdrawal from this solution the solvent is allowed to evaporate. Two phases of the drying process can be distinguished: firstly, there is evaporation of solvent at the surface of the film and secondly, there is transport of solvent from the bulk to the surface where evaporation occurs<sup>[1]</sup>. The latter process is diffusion controlled and depends mainly on the rate to which the solvent is supplied to the evaporating surface by diffusion<sup>[2]</sup>. A concentration profile develops as described schematically in Figure 4.1. Starting from a coated film of thickness  $H$  at time zero the polymer concentration is constant over the film thickness. At time  $t_1$  evaporation has been proceeded for a short period leading to a drastic increase in polymer concentration in the outer region of the film. A concentration profile has now been developed with a high polymer concentration at the outer surface and a relatively low polymer concentration at the support side. Due to diffusion and evaporation of the solvent the profile will change continuously. Equation (4.1) describes the transport with respect to the total volume and is based on the solvent volume fraction. Furthermore, it must be realized that the film thickness decreases constantly and that the concept of the moving boundary must be included. In addition to this concentration profile a glass transition profile is developed as well. If the solution reaches its glass transition, a drastic decrease in the diffusion of solvent to the surface will occur (see Figure 4.2). When the evaporation time proceeds further the concentration gradient in the layer becomes smaller until all solvent is removed (at time  $t$ ) and a constant polymer concentration through the film is reached, i. e., a dry film of thickness  $l$  (see Figure 4.1).

$$\frac{\partial \phi}{\partial t} = \frac{\partial}{\partial x} \left( D(\phi) \frac{\partial \phi}{\partial x} \right), \quad (4.1)$$

with

$\phi$  volume fraction of solvent [-]  
 $t$  time [sec]  
 $x$  directional coordinate perpendicular to the plane of the film [m]  
 $D$  diffusion coefficient [ $m^2/s$ ]

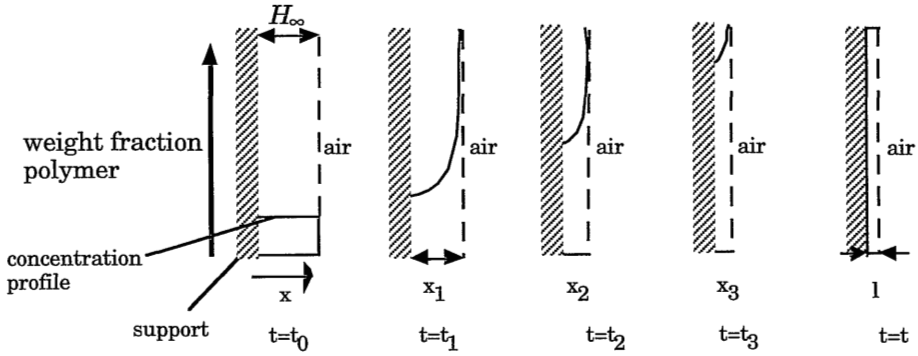


**Figure 4.1** Schematical drawing of the concentration profile in a film during the drying process.  $H$  is the thickness of the coated film,  $l$  is the thickness of the dried film.

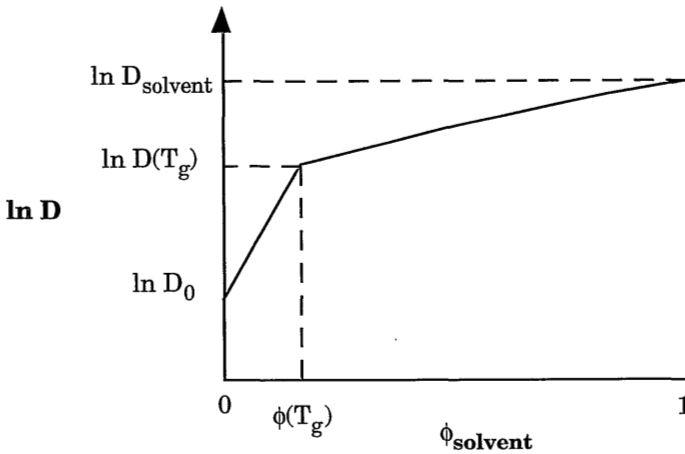


**Figure 4.2** Schematical drawing of the dependency of the diffusion coefficient on the solvent concentration in the polymer solution.  $D_0$ ,  $D(T_g)$  and  $D_{solvent}$  represent the diffusion coefficients at zero solvent concentration, at the glass transition and of the pure solvent, respectively<sup>[3]</sup>.

### 4. 3. POST-TREATMENT OF COATING LAYERS

Once a coating layer has formed a post-treatment procedure may be applied to “repair” existing defects. Different methods are possible to achieve this, e. g. by applying a liquid<sup>[4,5]</sup> or by contacting the coating layer with a vapour stream<sup>[4]</sup>. In this work the latter method was used. The mechanism of the post-treatment is schematically shown in Figure 4.3. Due to the contact with the vapour, the polymer of the coating layer is dissolved partially resulting in increased mobility of the re-dissolved polymer chains, i. e., the glass transition of the polymer “solution” is passed. These chains may then close defects by entanglement with other chains.

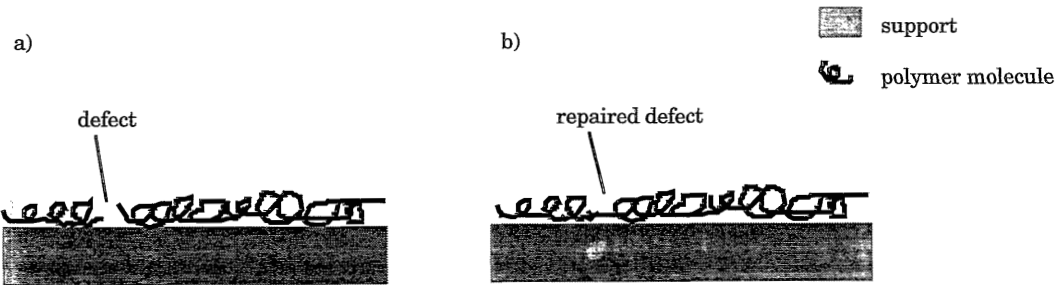


*Figure 4.3 Schematical drawing of the mechanism for repairing defects in a coating layer by post-treatment with solvent vapour: a) coating layer contains defects; b) repairing of the defect due to increased mobility of the polymer chains*

### 4. 4. EXPERIMENTAL

The experimental work includes both the preparation of the coating solution and the actual coating procedures as well as the drying and post-treatment procedures.

#### 4. 4. 1. SUPPORT MATERIALS

Flat asymmetric PAN-membranes from Deutsche Carbone (GFT), Germany and from Stork B. V., Gorredijk, the Netherlands, were used for the coating experiments. The GFT-membranes are normally employed as support in pervaporation composite membranes. They have been used without a further drying procedure. The Stork-membranes are used in ultrafiltration in a tubular configuration. For the coating experiments these tubes were cut and rinsed in water for 3 days and then dried by the following procedure<sup>[6]</sup>: first they were stored for 24 h in ethanol, then for 24 h in hexane and finally they were dried in the air between glass plates in order to obtain smooth membranes. The gas permeation properties of these membranes are given in table 4.1. Additionally, PAN hollow fibers with an outer diameter of 300  $\mu\text{m}$  and a pore wall thickness of about 50  $\mu\text{m}$ , referred here as APCI 1 from Air Products and



Chemicals Inc., have been used. These fibers have been used without further treatment. Its gas permeation properties are given in Table 4.1 as well. The Knudsen selectivity for a mixture of CO<sub>2</sub> and N<sub>2</sub> is 0.94.

**Table 4.1** Gas permeation properties of the used support membranes

membrane	P/I CO <sub>2</sub> *	P/I N <sub>2</sub> *	selectivity (CO <sub>2</sub> /N <sub>2</sub> )
GFT	0.0031	0.0029	1.06
Stork 3010	0.0039	0.0033	1.18
Stork 5010	0.0018	0.0017	1.05
APCI 1	0.0084	0.0083	1.01

\* cm<sup>3</sup>(STP)/cm<sup>2</sup> s cmHg

#### 4. 4. 2. COATING MATERIAL

Atactic poly(methyl methacrylate) with different molecular weights from Polyscience was used as selective polymers. The chemical structure of the polymer is given in Figure 4.4 and the gas separation properties of the polymers are given in table 4.2.

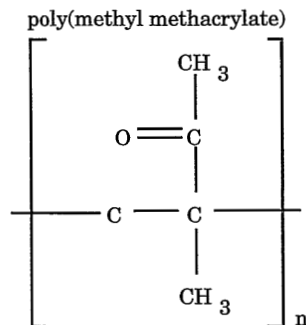


**Figure 4.4** Chemical structure of poly(methyl methacrylate)

As can be seen from these results the permeabilities of the polymers are quite low combined with relatively high selectivities for carbon dioxide/nitrogen. PMMA 350 shows the lowest CO<sub>2</sub> permeability, the selectivities for PMMA 350 and PMMA 100 are about the same, while the intrinsic selectivity for PMMA 75 is much lower.

**Table 4.2** *Intrinsic permeability properties of the three different poly(methyl methacrylate) samples*

polymer	$M_w$ [g/mol] <sup>#</sup>	$P(\text{CO}_2)$ [Barrer]*	$P(\text{N}_2)$ [Barrer]*	selectivity ( $\text{CO}_2/\text{N}_2$ )
PMMA 350	436,500	$3.1 \pm 3 \%$	$0.088 \pm 4 \%$	61.3
PMMA 100	85,000	$3.8 \pm 7 \%$	$0.064 \pm 7.5 \%$	58.3
PMMA 75	84,000	$1.9 \pm 9 \%$	$0.031 \pm 10 \%$	35.2

\* 1 Barrer =  $10^{-10} \text{ cm}^3(\text{STP}) \text{ cm/cm}^2 \text{ s cmHg}$

# determined by gel permeation chromatography with chloroform as solvent<sup>[7]</sup>

#### 4. 4. 3. COATING PROCEDURE

The flat supports were glued on glass plates and then placed in a coating vessel which contains the coating solution. This vessel is allowed to empty by opening a tap at the bottom. The procedure has been described in chapter 3. The hollow fiber supports were potted at the ends and placed in a holder which is schematically shown in Figure 4.5. The length of the fibers was between 10 to 14 cm.

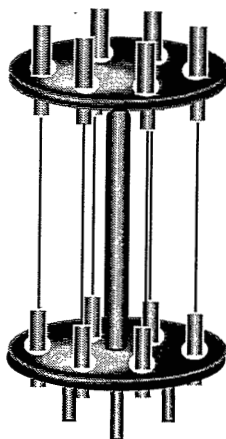


**Figure 4.5** *Schematic drawing of the coating set-up for hollow fibers*

In some cases the flat PAN-membranes were impregnated with water with help of a syringe. Therefore a small cut was made in the support membrane through which a syringe could be introduced and the water could be applied (see chapter 3). The hollow fibers were impregnated by sucking water through the bore side of the fiber

with a vacuum pump. After this impregnation procedure the fibers were closed at one end by a heat treatment with a soldering iron.

After the coating procedure the prepared composite membranes were dried in air at room temperature in the vertical position. The coating angle was in all cases 90°. For the gas permeation experiments the membranes were coated with a thin layer of silicone rubber to plug defects<sup>[8]</sup>. Therefore, the coated membranes were dipped in a solution of 3 % polydimethylsiloxane (PDMS) and a crosslinking agent (RTV 615B from General Electric Silicones, ratio polymer:crosslinking agent 9:1) in iso-octane<sup>[9]</sup>. After withdrawing from the solution, the membranes were dried in the horizontal position in an oven at 80 °C for 24 hours. This procedure was carried out at least twice.

#### **4. 4. 4. DRYING AND POST-TREATMENT OF THE COMPOSITE MEMBRANES**

To investigate the influence of the drying conditions different procedures have been carried out. Some of the coated membranes were dried in air in the horizontal position. The evaporation rate of the solvent was controlled in an atmosphere of nitrogen with a monitored solvent concentration.

A number of membranes were exposed to a post-treatment after drying. The membranes were placed again in the coating vessel shown in Figure 3.8. A vapour stream of a solvent or swelling agent was flowing through the vessel for a given period of time. Also in this case solvent of the coating solution and vapour were identical. The membranes were dried in air after this procedure. The experimental post-treatment conditions will be given in combination with the results.

#### **4. 4. 5. CHARACTERIZATION OF THE COMPOSITE MEMBRANES**

The prepared composite membranes were characterized by gas permeation measurements and electron microscopy. The set-up as described by van 't Hof<sup>[10]</sup> was used for the permeation measurements. The fluxes of the pure gases (nitrogen, oxygen and carbon dioxide) were measured at pressures between 3 and 5 bar. The membranes were conditioned in each gas for several hours, i. e. at least 14 hours in N<sub>2</sub> and 6 to 8 hours in O<sub>2</sub> and CO<sub>2</sub>.

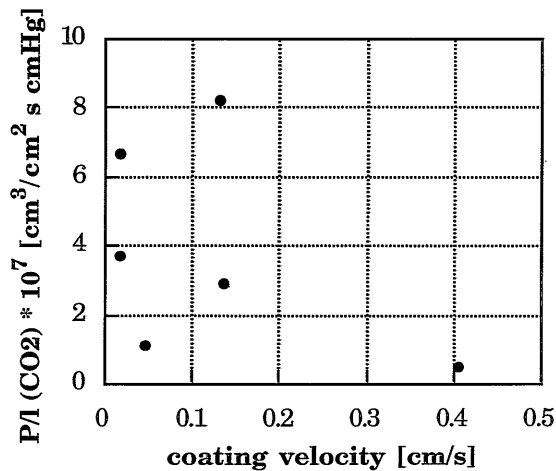
The microscopic studies were performed on either a Field Emission Scanning Electron Microscope (FESEM) Hitachi S 800 or on a Scanning Electron Microscope (SEM) Jeol JSM-T 220A. The samples were wetted in a water/ethanol mixture and then broken in liquid nitrogen. After drying of the samples for at least 4 hours in a vacuum oven at 30 °C they were sputtered with carbon for the FESEM- and with gold for the SEM-investigations.

## 4. 5. RESULTS AND DISCUSSION OF THE COATING EXPERIMENTS

### 4. 5. 1. INFLUENCE OF THE COATING VELOCITY

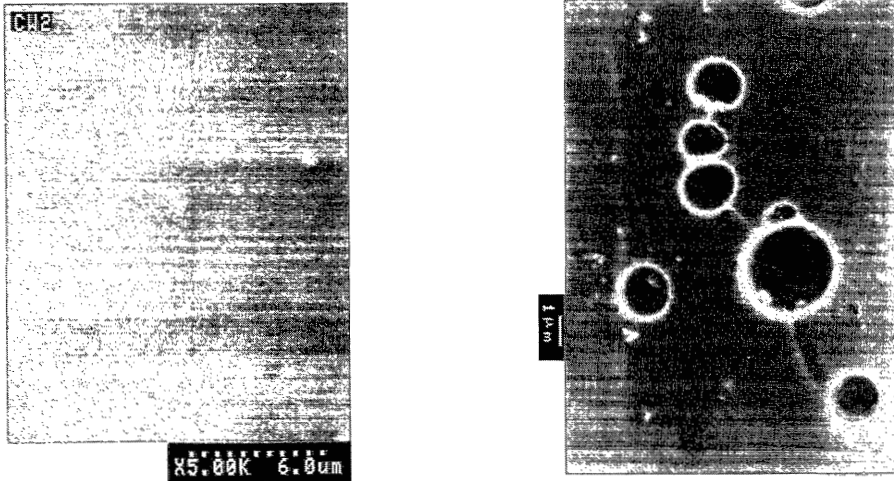
#### *Flat membranes*

Figure 4.6 shows the influence of the coating velocity on the P/l-values of the prepared composite membranes. It should be noted that the P/l-values given here do not represent the real thickness but the effective thickness. Furthermore, although not too many experiments were performed a rather scattered result was obtained.



**Figure 4.6** Influence of the coating velocity on the P/l-values of composite membranes prepared from solutions of 6.7 % PMMA 350 in chloroform on impregnated GFT supports

Figure 4.7 shows the surfaces of a coating layer of PMMA 350 prepared from a solution of 6.5 % PMMA in chloroform. Big parts of coating layers are smooth and seem to be defect free. However, at some places very typical circular defects of about 1.3  $\mu\text{m}$  in diameter can be observed, which are similar to the defects observed for layers of Makrolon 3200 (see chapter 3). It should be noted that these defects are present both in the case of impregnated supports and dry supports. Therefore, it is definitely not caused by the presence of water. It is difficult to distinguish which effects are responsible for the observed defects. Most probably they are caused by the large gradients in surface tension which occur during the evaporation of the solvent.



**Figure 4.7** SEM-photographs showing the surface of a coating layer prepared from a solution of PMMA 350 in chloroform

Hollow fibers without impregnation

The dependence of the P/l-values as a function of the coating velocity for composite membranes prepared from solutions of 6.5 % PMMA 350 in chloroform on non-impregnated APCI1 fibers is shown in Figure 4.8. A decrease in the P/l-values can be observed very clearly with increasing coating velocities. This is caused by the increase in thickness of the coating layer with increasing coating velocity as described by the coating theory (see chapter 3), but also by an influence of the support.

The dependence of the selectivity on the effective thickness of the hollow fiber composite membranes is shown in Figure 4.9. Similar to composite membranes with layers of polycarbonate (see section 3. 7. 1. and 3. 7. 2.), membranes with higher effective thicknesses show lower selectivities. Very low effective thicknesses below 1  $\mu\text{m}$  could be obtained. This indicates that the penetration of polymer into the pores of the support could be prevented. The reason for this is the relatively high molecular weight of the PMMA 350 (430,000 g/mol) and the hydrodynamic dimensions of the polymer chains in the coating solvent chloroform. From viscosity measurements a radius of gyration of 18.9 nm was determined (see Appendix B to Chapter 3). Light scattering experiments, however, indicate that this solution has a strong tendency to form associates, which are bigger than a single chain. The formed associates are probably too big to penetrate into the pores of the fibers, which have a maximum pore radius of about 50 nm determined by field emission scanning electron microscopy (FESEM).

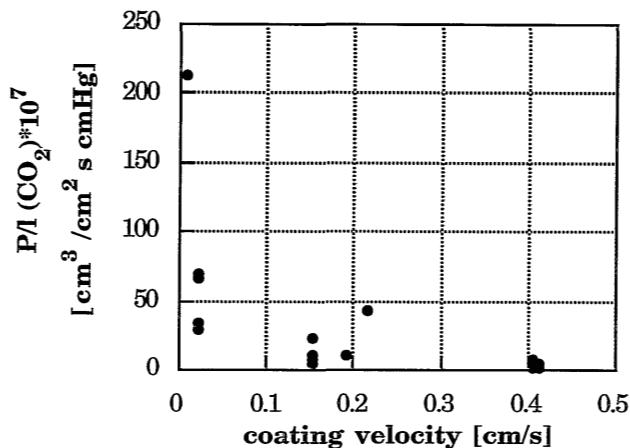


**Figure 4.8** Influence of the coating velocity on the  $P/l$ -values of composite membranes prepared from solutions of 6.5 % PMMA 350 in chloroform on non-impregnated APC11 fibers

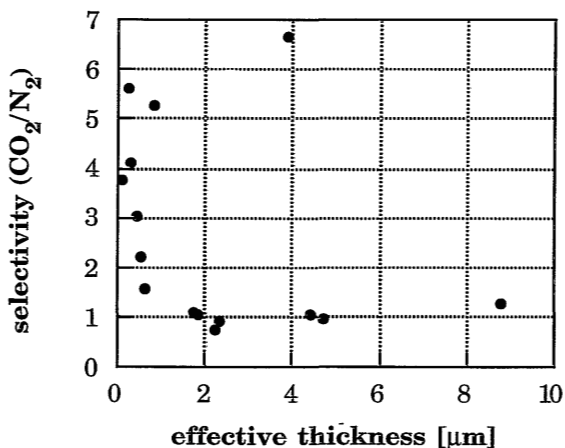


**Figure 4.9** Selectivity as a function of the effective thickness for composite membranes prepared from solutions of 6.5 % PMMA 350 in chloroform on non-impregnated APC11 fibers

#### Hollow fibers with impregnation

The dependency of the  $P/l$ -values on the coating velocity of the prepared composite membranes with impregnated supports is shown in Figure 4.10. Contrary to the experiments performed with dry supports it seems that there is a slight increase of the  $P/l$  values with increasing coating velocity. However, the trend is not very clear

from the results, because the reproducibility of the results is not that good. Furthermore, it can be seen that the P/l values for impregnated and non-impregnated fibers are about the same (see Figure 4.10).

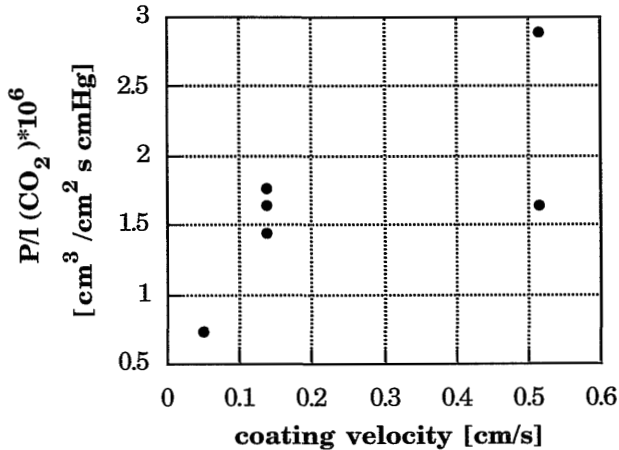


**Figure 4.10** Influence of the coating velocity on the P/l-values of composite membranes prepared from solutions of 6.5 % PMMA 350 in chloroform on impregnated APCII fibers

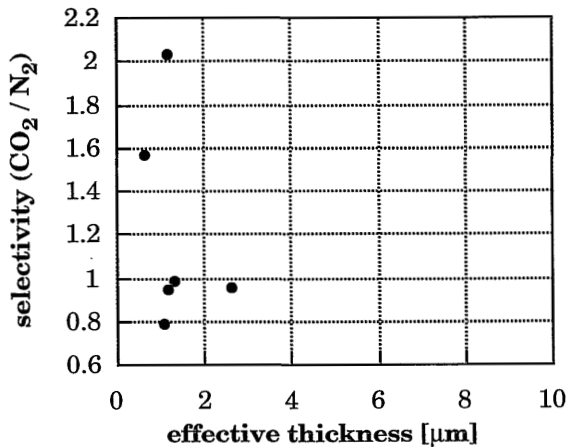


**Figure 4.11** Selectivity as a function of the effective thickness for composite membranes prepared from solutions of 6.5 % PMMA 350 in chloroform on impregnated APCII fibers

## 4. 5. 2. INFLUENCE OF THE POLYMER CONCENTRATION

### *Flat membranes*

Various coating solutions have been used and the different concentrations and the corresponding specific viscosities (equation 4.3) are given in table 4.3. The intrinsic viscosity  $[\eta]$  can be determined from these data and the value for PMMA/chloroform has been estimated too. The specific viscosities were determined with an Ubbelohde viscosimeter according to standard procedure<sup>[11]</sup> at 25 °C.

$$\eta_{sp} = \frac{t_p - t_s}{t_s}, \quad (4.3)$$

with

$t_p, t_s$  times necessary to pass a certain distance in the capillary of the Ubbelohde viscosimeter for the polymer solution and the solvent, respectively

**Table 4.3** Concentrations and specific viscosities of the used PMMA 350 solutions in chloroform

polymer concentration [wt %]	specific viscosity
2	7.96
3	17.44
5	58.52
6.7	86.48
7.8	105.6

The specific viscosities of the polymer solutions increase with increasing polymer concentration which implies that pore penetration is reduced as well. Indeed, successful coating experiments could be performed with coating solutions of 5 % and 6.7 % PMMA 350 in chloroform indicating that a minimum viscosity is required. Also the polymer coils will be more entangled with increased polymer concentration. With lower or higher concentrated solutions it was not possible to prepare composite membranes useful for permeation measurements. The defects in the coating layers were probably too large to be covered with silicone rubber. For the solutions with 7.8 % PMMA 350 the relatively high viscosity of the solution might cause an inhomogeneously coated film. However, no typical defects could be found on the surface of the coating layer by electron microscopy.



### 4. 5. 3. INFLUENCE OF THE COATING SOLVENT AND MOLECULAR WEIGHT

The molecular dimension of a polymer in a coating solution is an important variable to obtain thin toplayers in a composite membrane. A measure for the dimension of the polymer chain is the radius of gyration which depends on the molecular weight of the polymer and on the interaction between polymer and solvent. Four solvents, chloroform, toluene, tetrahydrofuran (THF) and 1,2-dichloroethane (1,2-DCE) have been investigated. The radii of gyration of PMMA in different solvents were given in Appendix B to Chapter 3.

Composite membranes with layers of PMMA 350 could be prepared from solutions in chloroform, THF and 1,2-DCE (see table 4.4).

**Table 4.4** Gas permeation results of composite membranes prepared from PMMA 350 in different solvents on GFT membranes

solvent	radius of gyration [nm] <sup>a</sup>	P/I (CO <sub>2</sub> ) ·10 <sup>7</sup> #*	selectivity (CO <sub>2</sub> /N <sub>2</sub> )	remarks
<b>PMMA 350</b>				
chloroform	-	25.4	6.1	associates in the solution
toluene	14.9	-	-	high intrinsic viscosity
1,2-DCE	24.3	1.91	1	-
THF	23.1	81	8.5	associates in the solution
<b>PMMA 100</b>				
chloroform	12.2	2.9	1.1	-
toluene	8.9	-	-	-
1,2-DCE	10.7	3.4	4.5	-
THF	9.6	-	-	-
<b>PMMA 75</b>				
chloroform	12.4	-	-	-
toluene	8.3	13.8	7	-
1,2-DCE	9.8	122	2.4	-
THF	10	-	-	-

<sup>a</sup> determined from GPC measurements

# [cm<sup>3</sup>/cm<sup>2</sup> s cmHg]

\* all membranes are prepared on GFT supports

Both from solution characterization<sup>[7]</sup> and gel permeation chromatography (GPC) the highest radii of gyration were determined, which are of about the same dimension as the maximum pore size of the GFT membranes. If toluene was used as solvent the defects in the coating layer seemed to be too big to be covered with silicone rubber and the fluxes were still too high to be measured with the gas

separation set-up. For this solvent the smallest radius of gyration (14.9 nm) of PMMA 350 was determined which allows pore penetration. The reproducibility of the results is still not satisfying. The experimental error in the results is in the case of chloroform solutions about 30 % and in the case of 1,2-DCE solutions 40 %. If PMMA 100 was used as the coating polymer only with chloroform and 1,2-dichloroethane measurable composite membranes could be prepared. In these solvents the highest radii of gyration were determined (12.2 nm in chloroform and 10.7 nm in 1,2-DCE), which are, however, smaller than the pore size of the GFT supports. In the case of PMMA 75 as the coating polymer only solutions with toluene and 1,2-DCE resulted in composite membranes which could be measured (see table 4.4). It should be noted, however, that for every solvent only one membrane showed measurable permeation behaviour. Solutions of PMMA 75 in chloroform did not result in defect free coating layers although in this solvent the largest radius of gyration (12.4 nm) was found, which is, however, still smaller than the maximum pore size of the GFT membranes.

The results show that it is possible to prepare composite membranes with poly(methyl methacrylate) as the coating polymer. A very important factor is the dimension of the polymer chain in the coating solution. This conformation is strongly dependent on the molecular weight of the polymer and on the interaction between polymer and solvent. If coating solutions were used in which the dimension of the PMMA chain was at least as big as the maximum pore size of the GFT supports composite membranes could be prepared, however, the obtained selectivities are far below the intrinsic values given in Table 4.2. The best reproducible results with respect to the P/l values were obtained with nonimpregnated APCI1 fibers coated with a solution of 6.5 % PMMA 350 in chloroform (see Figure 4.10).

#### **4. 5. 4. INFLUENCE OF THE DRYING PROCEDURE**

The drying procedure can have a big influence on the solidification process of the coating layer. If the drying rate is slow the polymer chains will relax to the most favorable conformation (see also section 4. 2). Therefore composite membranes have been prepared in saturated chloroform atmosphere and then the chloroform concentration was slowly decreased after 15, 20, 30 and 300 seconds, respectively until the solvent activity became zero, i. e. a pure nitrogen atmosphere was obtained. Some of the membranes have been dried immediately in a nitrogen atmosphere. The results of the gas permeation experiments are given in Table 4.5

**Table 4.5** Influence of different drying procedures on the P/l-values of composite membranes prepared from solutions of 6.7 % PMMA 350 in chloroform on impregnated GFT supports

drying procedure	P/l (CO <sub>2</sub> ) [cm <sup>3</sup> /cm <sup>2</sup> s cmHg]	selectivity (CO <sub>2</sub> /N <sub>2</sub> )	effective thickness* [μm]
100 % N <sub>2</sub>	9.7 10 <sup>-7</sup>	1.2	0.2
10 % N <sub>2</sub> /15 s	1.4 10 <sup>-7</sup>	1.7	1.4
10 % N <sub>2</sub> /20 s	2.7 10 <sup>-7</sup>	2.9	0.7
10 % N <sub>2</sub> /30 s	1.2 10 <sup>-7</sup>	1.1	1.6
10 % N <sub>2</sub> /300 s	30 10 <sup>-7</sup>	1.6	0.06

As can be seen from these experiments the different drying procedures did not result in improved selectivities for the composite membranes. A drastic increase in the P/l-value is obtained for membranes where the solvent activity was changed every 300 seconds. The selectivities of the prepared membranes are still far below the intrinsic value of 61.3.

#### 4. 5. 5. INFLUENCE OF THE POST-TREATMENT PROCEDURE

Post-treatment in a solvent vapour atmosphere is a method to improve the quality of a polymeric coating layer<sup>[4]</sup>. A number of membranes were subjected to a post-treatment. A fully solvent saturated nitrogen stream was applied to the membrane. The solvent activity was then stepwise lowered by the addition of nitrogen to the stream after different time intervals (30 seconds and 300 seconds, respectively). The results of the two different procedures are shown in Table 4.6. An increase in the P/l-value can be observed for the post-treatment procedure in which the activity is changed every 300 seconds. This effect is comparable to the one observed for different drying procedures (see Table 4.7) and might also be caused by an entrainment of the coating layer from the support. This also seems to be reasonable if the effective thicknesses are compared. Surprisingly, the membrane with the lower effective thickness shows the better selectivity, which is an indication that partial improvements of the gas separation performance of composite membranes by post-treatment can be obtained.

**Table 4.6** Influence of the post-treatment procedure on the gas separation performance of composite membranes prepared from solutions of 6.7 % PMMA 350 in chloroform on impregnated GFT supports

post-treatment	P/l (CO <sub>2</sub> ) [cm <sup>3</sup> /cm <sup>2</sup> s cmHg]	effective thickness [μm]	selectivity (CO <sub>2</sub> /N <sub>2</sub> )
10 % N <sub>2</sub> /30 s	1.2 10 <sup>-7</sup>	1.6	2.1
10 % N <sub>2</sub> /300 s	25.4 10 <sup>-7</sup>	0.075	6.1

The best result so far was obtained for a composite membrane prepared from a solution of 6.5 % PMMA 350 in chloroform on a dry Stork 3010 support. After drying the coating layer in pure nitrogen a post-treatment (10 % N<sub>2</sub>/300 s) was applied resulting in a composite membranes with almost intrinsic selectivity. The permeation results are given in Table 4.7.

**Table 4.7** Gas permeation properties of a composite membrane prepared from a solution of PMMA 350 in chloroform on a Stork 3010 support, dried in pure nitrogen and post treated (10 % N<sub>2</sub>/300 s); coating velocity: 0.075 cm/s

P/l (CO <sub>2</sub> )*	1.78-10-6
P/l (N <sub>2</sub> *)	3.39-10-8
selectivity (CO <sub>2</sub> /N <sub>2</sub> )	52.5
effective thickness [μm]#	1.06

\* cm<sup>3</sup>/cm<sup>2</sup> s cmHg

# calculated from the carbon dioxide flux

#### 4. 5. 6. ROLE OF THE SUPPORT

Because of the poor reproducibility no influence of the different supports with respect to the performance of the composite membranes could be determined. However, it seems that the GFT membranes give better results, while most of the membranes with Stork supports were leaking. An exception is the composite membrane with a Stork 3010 support which gave almost intrinsic selectivity of PMMA 350 (see Table 4.7). This is rather surprising because from the characterization of the supports smaller pores were determined<sup>[12]</sup> for the Stork membranes which should be easier covered by the polymer than the more open GFT membranes. However, the characterization showed also that always pores bigger than 20 nm are present, which can not be determined by the used methods. For the APCI1 fibers relatively

good reproducible P/l values were obtained. For nonimpregnated fibers coated with solutions of 6.5 % PMMA 350 in chloroform the highest P/l values for carbon dioxide were obtained. This corresponds to the permeation properties of the uncoated fiber which shows the highest P/l values compared to the other supports (see Chapter 2 of this thesis).

#### **4. 6. CONCLUSIONS**

Composite membranes have been prepared from poly(methyl methacrylate). The used polymers differ in molecular weight, however, no significant difference between these polymers with respect to the reproducibility of the prepared composite membranes could be observed.

Composite membranes with thin effective layers ( $< 1 \mu\text{m}$ ) have been prepared. The pore penetration could be prevented by using high molecular weight polymers and a good solvent. Coating experiments with nonimpregnated APC11 fibers resulted in membranes with relatively high P/l values, which were good reproducible.

Drying of the coating layers with low drying rate did not result in better quality of the coating layers.

Post-treatment of composite membrane with solvent vapour can improve the performance of the composite membranes. For a membrane coated on Stork 3010 and treated with chloroform vapour almost intrinsic selectivity for carbon dioxide over nitrogen and an effective thickness of about  $1 \mu\text{m}$  was obtained.

For the majority of the prepared membranes selectivities far below the intrinsic values were obtained. A reason for the defective coating layers is probably the high stress which is built up in the layer during the drying process. This will be discussed in the next chapter.

#### **4. 7. REFERENCES**

- [1] C. M. Hansen; Polymer coatings. Concepts of solvent evaporation; Ind. Eng. Chem. Prod. Res. Develop. 9 (1970), 283-286
- [2] J. Crank; The mathematics of diffusion; Oxford University Press 1975
- [3] R. H. B. Bouma; Relaxation phenomena in dense glassy polymer membranes; PhD-thesis University of Twente (1995)
- [4] M. E. Rezac, J. D. Le Roux, H. Chen, D. R. Paul, W. J. Koros; Effect of mild solvent post-treatments on the gas transport properties of glassy polymer membranes; J. Membr. Sci. 90 (1994) 213-229
- [5] Williams, S. C., Bikson, B., Nelson, J. K.; Composite membranes for enhanced fluid separation; EP 0 286 091  
Williams, S. C., Bikson, B., Nelson, J. K., Burchesky, R. D.; Method for preparing composite membranes for enhanced gas separation; U. S. Patent 4,840,819
- [6] Macdonald, W., Park, S., Pan, C.-Y., Albata, E.; Method for drying water-wet membranes; U. S. Patent 3,842,515

- Manos, P.; Gas separation membrane drying with water replacement liquid;  
U. S. Patent 4,080,744
- Manos, P.; Solvent/exchange drying of membranes for gas separation; U. S. Patent 4,120,098
- [7] Appendix B to chapter 3 of this thesis
- [8] Henis, J. M., Tripodi, M. K.; Multicomponent membranes for gas separation;  
U. S. Patent 4,230,463
- Henis, J. M., Tripodi, M. K.; Composite hollow-fibre membranes for gas separation: The  
resistance model approach; *J. Membr. Sci.*, 8 (1981) 233
- [9] I. Blume, R. W. Baker; U. S. Patent 4,952,751 (1990)
- [10] J. A. van't Hof; Wet spinning of asymmetric hollow fiber membranes for gas separation;  
PhD-thesis University of Twente (1988)
- [11] H.-G. Elias; *Makromoleküle*; Hüthig & Wepf Verlag Basel (1971)
- [12] Chapter 2 of this thesis

# 5

---

## **STRESS MEASUREMENTS IN COATING LAYERS UPON DRYING**

---

### ***Summary***

*A new method has been developed to measure the mechanical stress in polymeric coating layers during the drying process. Significant differences in the stress development could be observed between glassy and rubbery polymers.*

*The influence of the molecular weight of the coating polymer, the polymer concentration of the coating solution as well as the influence of the support have been investigated. The stress measurements were carried out on two different supports, an asymmetric polyacrylonitrile membrane and a thin aluminium film. On the aluminium film higher stresses were determined due to the lower mechanical resistance to shrinkage.*

*The influence of a post-treatment with solvent vapour on the stress development was investigated as well. With increasing number of post treatment steps an increase in the stress was observed. This increase is explained with the increase in deformation of the polymer chains*

## 5. 1. INTRODUCTION

During drying of a coated layer volume reduction occurs due to the evaporation of the solvent. This volume reduction causes mechanical stresses in the coating layer. This stress may effect the coating layer in different ways: firstly, it leads to a certain orientation of the polymer chains which in fact may result into an increase of the selectivity due to a higher packing density. On the other hand, if the stress is too high it may lead to defects (cracks) in the coating layer which causes unacceptable loss in selectivity. Therefore, it is important to follow the stress development during the drying (evaporation) process to understand which factors are important to prevent the occurrence of cracks.

A number of methods are available to measure the mechanical stress in thin polymeric and ceramic layers; X-ray diffraction<sup>[1]</sup>, DSC<sup>[2]</sup> and cantilever beam technique<sup>[1,3]</sup>. The first two methods are especially applicable for stress measurements in polymeric layers during a temperature treatment. Kumar<sup>[3]</sup> followed the drying process of alumina and titania layers on a ceramic support with the cantilever beam technique. However, until now no research work has been published to follow the stress upon the drying of a polymeric layer on a polymeric support after a dip coating procedure. In this work a method has been developed which allows to follow the stress development during drying of polymeric coating layers on a porous polymeric support. An important parameter in this respect is the glass transition temperature  $T_g$ . If the coating polymer is a glassy polymer, there will be a transition in the film from a rubbery state to a glassy state upon evaporation of the solvent. On the other hand, if the coating polymer is an elastomer then the system remains always in the rubbery state during evaporation of the solvent.

## 5. 2. MECHANICAL PROPERTIES OF POLYMERS

A measure for the elasticity of a material is given by the Young's modulus (E-modulus). The E-modulus can be obtained from the stress-strain behaviour of the material<sup>[4]</sup> and is defined as the initial slope of the stress-strain curve (see figure 5.1) It indicates the force per unit area required to achieve a certain deformation. Figure 5.1 gives some characteristic stress-strain curves for polymeric materials. As can be seen from this figure the E-modulus depends on whether the polymer is in the rubbery or in the glassy state. In the case of glassy polymers a relatively high force must be applied to obtain a small deformation. If the material is brittle it will break after a certain deformation. Generally, the E-moduli of elastomers are about three orders of magnitude lower than for glassy polymers. Table 5.1 summarizes the E-moduli and glass transition temperatures of some polymers.



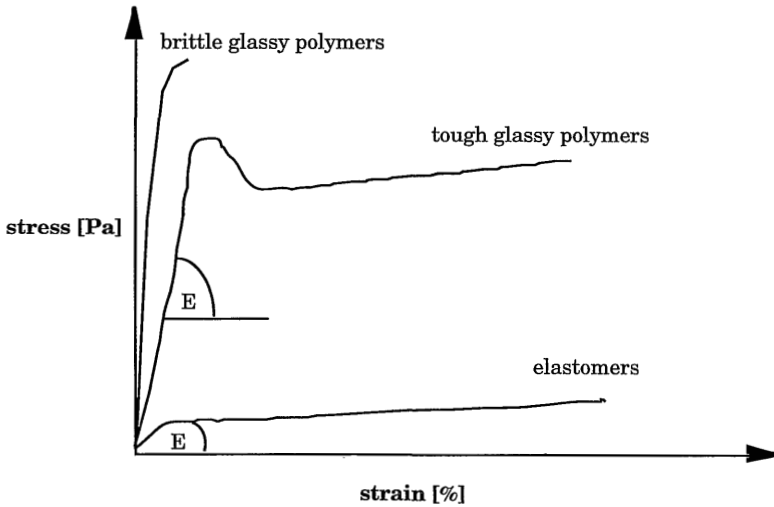


**Figure 5.1** Schematic drawing of the stress-strain behaviour of different types of polymers

**Table 5.1** E-moduli and glass transition temperatures of some polymers

polymer	T <sub>g</sub> [°C]	E-modulus [MPa]
polyisoprene	~73 <sup>[5]</sup>	~1
poly(methyl methacrylate)	105 <sup>[5]</sup>	3,300
polyacrylonitrile	120 <sup>[6]</sup>	7,000
polycarbonate*	153 <sup>#</sup>	97,000 <sup>#</sup>

\* Makrolon 3200

# own measurements

The differences in mechanical behaviour may effect the film properties. Solidification of a coating layer occurs by the evaporation of the solvent. This loss of solvent causes a volume reduction as indicated by the vectors x, y and z (see figure 5.2). Starting from a certain volume element of a coating layer two possibilities can be distinguished. In the case of a free layer the change in volume due to the evaporation may be considered to be isotropically, i. e. the reduction in the direction of the vectors x, y and z is equal. If the coating layer is fixed on a substrate the volume reduction can only take place in the direction of the vector z. The stress in the direction of the vectors x and y can be compensated by relaxation of the polymer chains, which eventually, results in the formation of crazes and cracks or loss of adhesion to the support.

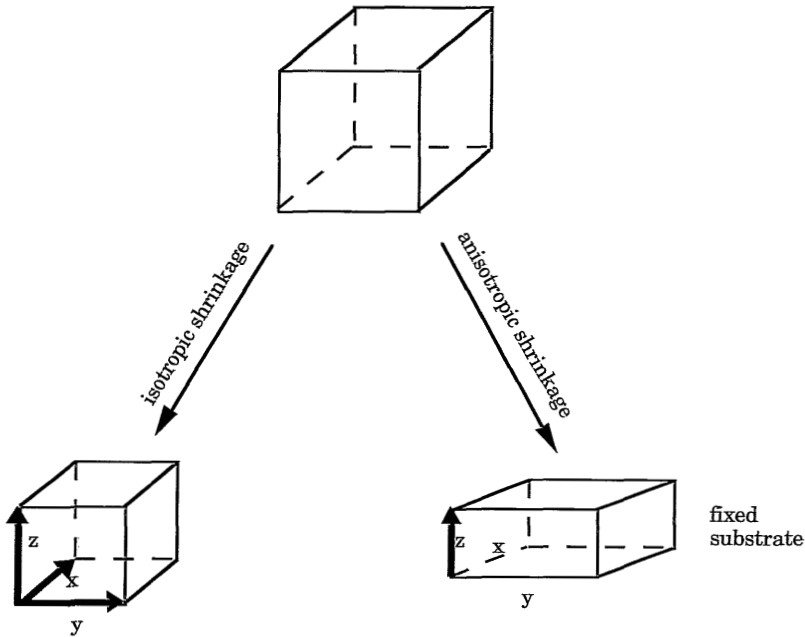


**Figure 5.2** Schematic drawing of the stress which may develop in coating layers of a free and a fixed substrate during drying<sup>[7]</sup>

Croll<sup>[8]</sup> stated that the stress in a coating can be related to the difference between the volume fraction of solvent at which the film solidifies and the volume fraction of retained solvent in the “dry” coating. The solidification of a polymer solution corresponds to the point at which this solution reaches its glass transition. The flexibility of the chains is then drastically decreased and due to further loss of solvent stresses will arise further. At this point the stress in the drying layer increases drastically due to the reduced flexibility of the polymer chains. The relation between stress and solvent loss is given below

$$\sigma = \frac{E_c}{(1 - \nu)} \frac{\phi_s - \phi_r}{3(1 - \phi_r)} \quad (5.1)$$

where

$\sigma$  residual stress [Pa]

$E_c$  E-modulus of the coating polymer [N/m<sup>2</sup>]

$\phi_s$  volume fraction of solvent at which the film solidifies [-]

$\phi_r$  volume fraction of retained solvent in the dry film[-]

$\nu$  Poisson's ratio [-] (ratio between the change in length and in width)

Because usually  $\phi_r \ll 1$  equation (5.1) can be simplified to

$$\sigma = \frac{E_c}{1 - \nu} \frac{\varphi_s - \varphi_r}{3} \quad (5.2)$$

To obtain a defect free layer the polymer chains must be able to release the stress. Therefore the polymer chains must bridge by extension the free volume which arises from the loss of solvent (see figure 5.3). This is much easier for a rubbery polymer with a relatively low E-modulus while the chains of a glassy polymer show a much higher resistance to this deformation. Therefore it can be expected that the stress in a dry coating layer is much higher for a glassy polymer compared to a rubbery polymer.

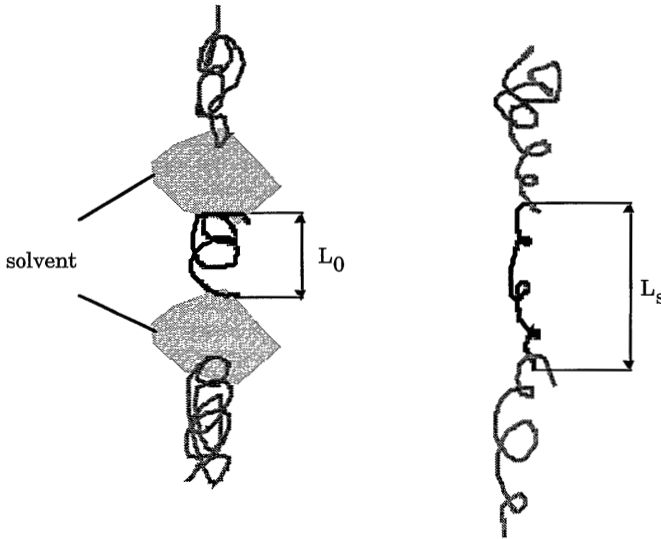


**Figure 5.3** Schematic drawing of the deformation of the polymer chains during the drying process;  $L_0$  represents the initial extension of the polymer chain,  $L_s$  is the extension of the chain after the solvent has been evaporated.

Once, the layer has been solidified a relaxation of stress can be observed. The rate of stress relaxation depends whether the polymer is in the rubbery or in the glassy state. The process of molecular relaxation can be described by the reptation model<sup>[9,4]</sup>. A polymer chain in the glassy state or in higher concentrated solutions can only move within a hypothetical tube (see figure 5.4). Relaxation occurs by chain disengaging at the ends of the tube.

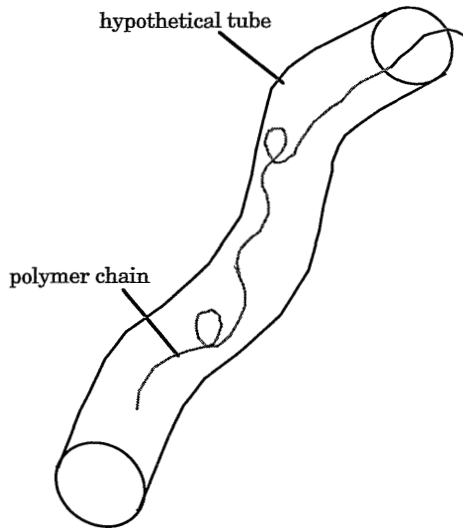


**Figure 5.4** Schematic drawing of a polymer chain in a hypothetical tube according to Doi and Edwards<sup>[9]</sup>

The chain reaches its equilibrium configuration when it diffuses out of the tube. Thereby at one end a part of the tube ‘disappears’ while at the other end a new part ‘develops’. The time in which this diffusion process occurs is proportional to the length of the hypothetical tube. The characteristic time  $T_0$  (see equation 5.3) is constant for a given polymer

$$T_0 \approx M_e^2, \quad (5.3)$$

with

$T_0$  disengagement time [s]

$M_e$  molecular weight of a segment of the polymer chain involved in the diffusion process [g/mol].

Another important characteristic of the relaxation process is the Rouse relaxation time  $T_R$  (see equation 5.4). This time describes how long it takes until a force applied to one end of the polymer chain will cause a retraction

$$T_R \approx T_0^2. \quad (5.4)$$

The reptation can be described by the disengagement time  $T_r$  of a polymer given by the following equation

$$T_r \approx T_0 M_w^3, \quad (5.5)$$

with

$M_w$  molecular weight of the polymer chain [g/mol].

The relaxation process is strongly dependent on the molecular weight of the polymer, i. e. the higher the molecular weight the longer the time necessary to relax the polymer chains. An important role in the relaxation process plays the mobility of the polymer chains, which is different for polymers in the rubbery and in the glassy state. The relaxation process is slow below the glass transition temperature while for temperatures above the glass transition temperature the relaxation process is much faster. This shows that the difference for these two different relaxation processes is quite significant: below  $T_g$  only segments of the chain can move (described by the time  $T_0$ ), above  $T_g$  whole chains can move (described by the time  $T_r$ ). An estimation of the characteristic relaxation time for polymer solutions, i. e., the minimum time necessary to relax, can be made by using equation (5.6)<sup>[10,11]</sup>.

$$\tau_{char} \approx \frac{1}{2} \frac{(\eta_0 - \eta_s) M}{c R T}, \quad (5.6)$$

where

- $\eta_0$  viscosity of the solution at zero shear rate [Pa s]
- $\eta_s$  viscosity of the solvent [Pa s]
- $M$  molecular weight of the coating polymer [g/mol]
- $c$  concentration of the polymer solution [g/m<sup>3</sup>]
- $R$  gas constant [J/mol K]
- $T$  temperature [K].

As can be seen from this equation the characteristic time  $\tau_{char}$  depends on the molecular weight, on the concentration and the viscosity of the solution. Depending on the viscosity increase with increasing polymer concentration an increase in  $\tau_{char}$  can be expected. For the stress development in a drying polymer film this means that the higher the characteristic time of the solution the higher the stress in the film will be. Because the drying process is often carried out very fast, i. e. within a few seconds, the polymer solution reaches its glass transition before the characteristic time and then relaxation can only take place by reptation which occurs very slowly for glassy polymers.

### 5. 3. METHODS FOR THE DETERMINATION OF THE STRESS IN A THIN LAYER

Different methods are known to determine the stress build-up in a thin layer. The most commonly used method is the cantilever beam technique. For this method the

coating layer is deposited on a support. During drying the layer will shrink and this causes bending of the support. From the curvature of the substrate (deflection  $\delta$ ) and the mechanical property of the support material (E-modulus) the stress in the coating layer can be calculated. Two main variations of the method are used (see figure 5.5): firstly, the support is fixed at one end and the deflection of the free end is measured; secondly, the substrate is deposited on the edges of two knives. From the bending of the substrate the stress can be determined. Both methods should give the same results.

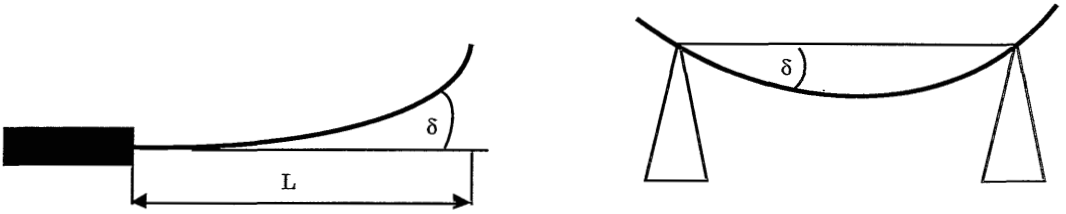


**Figure 5.5** Schematic drawing of the two variations of the cantilever beam technique

The stress in the layer can be calculated by equation (5.7)<sup>[12]</sup>. Two theories are combined to obtain this equation<sup>[12]</sup>: *firstly*, the plate theory which describes that a coating is under stress in a plane in two directions and *secondly*, the beam theory which implies an uniaxial stress situation in a cylindrical deformation of the substrate. For equation (5.7) it is assumed that i) a good adhesion exists between support and coating layer, ii) the elastic properties of the coating polymer and the support are isotropically, iii) the elastic limit of the support is not exceeded and iv) the internal stress is constant through the coating thickness.

$$\sigma = \frac{\delta E_s t^3}{3L^2 d(t+d)(1-\nu_s)} + \frac{\delta E_c(t+d)}{L^2(1-\nu_c)} \quad (5.7)$$

with

- $\sigma$  stress in the coating layer [Pa]
- $\delta$  deflection of the support [m]
- $E_s$  E-modulus of the support [N/m<sup>2</sup>]
- $t$  thickness of the cantilever support [m]
- $L$  length of the support between the point at which it is clamped and the point at which the deflection is measured [m]
- $d$  thickness of the coating [m]
- $\nu_s$  Poisson ratio of the support [-]
- $E_c$  E-modulus of the coating material [N/m<sup>2</sup>]
- $\nu_c$  Poisson ratio of the coating material [-]

If  $E_s \gg E_c$  and  $t \gg d$ , equation (5.7) can be simplified to

$$\sigma = \frac{\delta E_s t^3}{3 L^2 d (t + d)(1 - \nu_s)} \quad (5.8)$$

By continuously measuring the bending of the support during the drying process the stress development in the coating layer can be determined. This method has been applied successfully for ceramic membranes<sup>[3]</sup>. In the case of a polymeric support, e. g. a non-woven or an ultrafiltration membrane, however, this method fails because usually this support has not enough mechanical strength. As a result of the developed stress in the coating layer the support rolls. Therefore a modified cantilever beam method has been developed which will be discussed in the next section.

#### 5. 4. PRINCIPLE OF THE NEW METHOD

A schematic drawing of the revised cantilever beam method is shown in figure 5.6. The support is fixed at one end to a rigid clamp while the other one is connected to a microbalance. During the drying process the coated layer tends to shrink and, consequently, the support will bend to the side of the coated layer. The force necessary to keep the coated support in the initial (vertical) position is now measured.

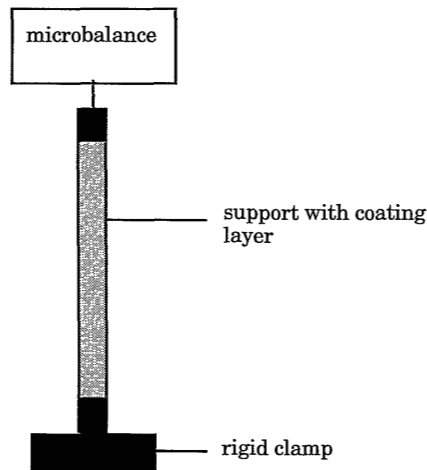


**Figure 5.6** Schematic drawing of the measurement set-up

This measured force  $F$  can be directly related to the mechanical stress in the coating layer

$$F = m * g \quad (5.9)$$

where  $m$  is the mass detected by the microbalance [kg] and  $g$  is the gravitational constant [ $m/s^2$ ]. The measured force acts on the “cross-section” of the coated strip or connection to the microbalance due to the change in length of the coated layer caused by volume reduction. The extent of the deformation is dependent on the E-modulus of the material. This can be described by equation (5.10) in which the subscripts  $c$  and  $s$  refer to coating layer and support, respectively.

$$F = (b * d_c * E_c * \epsilon_c) + (b * d_s * E_s * \epsilon_s) \quad (5.10)$$

where

$$\epsilon = l_0/l_d = \epsilon_c = \epsilon_s \quad (5.11)$$

with

- $b$  width of the support [m]
- $d_c$  thickness of the coated layer [m]
- $E_c$  E-modulus of the coating polymer [ $N/m^2$ ]
- $E_s$  E-modulus of the support [ $N/m^2$ ]
- $d_s$  thickness of the support layer [m]
- $\epsilon$  deformation in length of the coating layer [-]
- $l_0$  length of the coated layer before drying [m]
- $l_d$  length of the coating layer after drying [m].

For the used system we can assume

$$d_c * E_c \gg d_s * E_s.$$

With this assumption equation (5.10) can be simplified to

$$F = b * d_c * E_c * \epsilon_c. \quad (5.12)$$

The stress  $\sigma$  in the polymer layer can be defined as

$$\sigma = E_c * \epsilon_c. \quad (5.13)$$

By combination of equations (5.12) and (5.13) the stress in the layer can be calculated from equation (5.14)

$$\sigma = \frac{F}{b * d_c} \quad (5.14)$$

It should be noted that during the evaporation process the thickness of the coated



layer reduces. However, because of practical limitations this change in thickness could not be followed. For the calculation of stress the final thickness of the dried coating layer as determined by electron microscopy has been used.

## 5. 5. EXPERIMENTAL

Strips of GFT membranes have been used for the stress measurements (1.1 cm by 7 cm). The characteristics of these membranes have been given in chapter 2. The strips have been coated with approximately 0.6 ml of solutions of poly(methyl methacrylate) (PMMA) and polydimethyl siloxane (PDMS). These polymers have also been used for the coating experiments described in chapter 4, where the properties of the polymers are given. The polymer solutions were applied with a syringe.

## 5. 6. RESULTS AND DISCUSSION

### 5. 6. 1. INFLUENCE OF THE SUPPORT ON THE FINAL STRESS

To determine the influence of the support on the measured stress an experiment was carried out in which the supports were “coated” with the pure solvent which was in this case chloroform. The solution was then allowed to evaporate and the measured values are plotted against the time (see Figure 5.7). It should be noted that the values given on the y-axis are the measured masses, because a calculation of the stress with Equation (5.14) is not possible in this case.

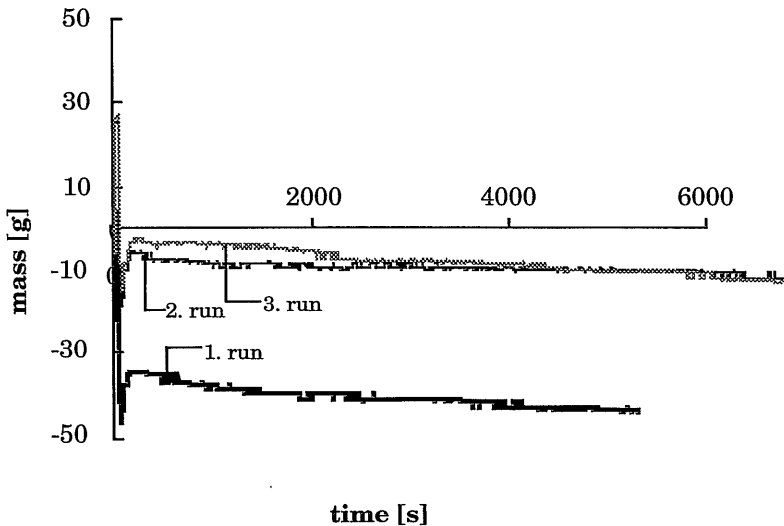


*Figure 5.7 Mass-time diagram for a GFT support “coated” with chloroform*

It can be seen that the mass increases initially when the chloroform is applied on the support. This might be due to a temperature decrease which is caused by the evaporation of the solvent. This temperature decrease causes a contraction of the polymeric material of the support. It can be seen that the “negative” stress in the support remains constant once the solvent was applied. Further treatment with solvent results in an equal final stress.

The results with an aluminium film as support are shown in Figure 5.8. Similar to the measurement carried out with the GFT support the mass increases after the solvent is applied. After about 2000 seconds a constant value has been reached which is lower than the initial value when the measurement was started. This value is negligible compared to the values measured when the polymer coatings are applied. This will be shown later in this Chapter.

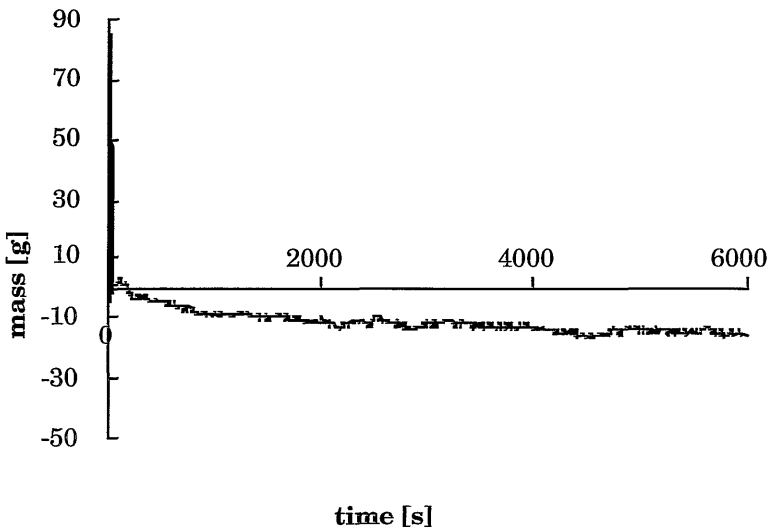


**Figure 5.8** Mass-time diagram for an aluminium film “coated” with chloroform

If polymer solutions are coated on the supports then the increase in the mass is about 200 to 300 g as will be shown later in this chapter. Therefore, it can be concluded that the influence of the support on the stress measurements can be neglected.

### 5. 6. 2. INFLUENCE OF THE MOLECULAR WEIGHT

For the coating experiments as described in chapter four PMMA of different molecular weights were used. The stress-time behaviour and the characteristic relaxation times of the different polymers are shown in figure 5.9.

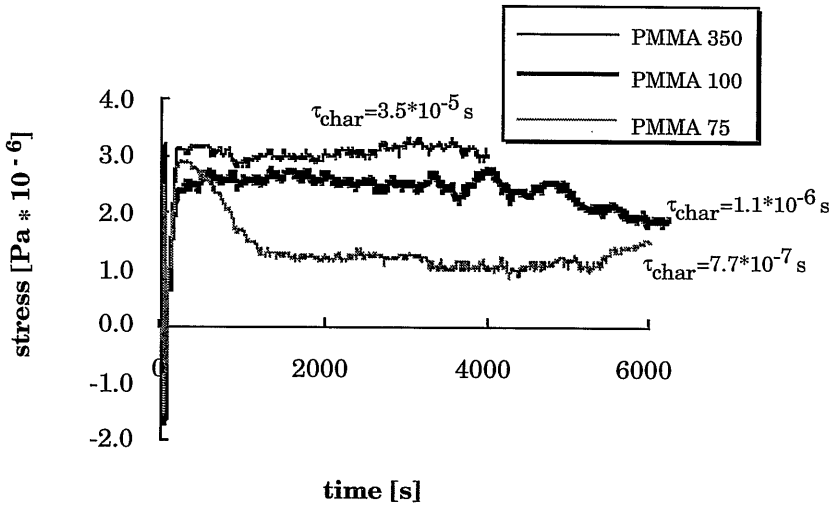


**Figure 5.9** Stress-time diagram for PMMA 350, PMMA 100 and PMMA 75 on GFT supports. The supports were coated with solutions of 4 % polymer in chloroform.

From this figure differences in the final stress for the different polymers can be observed. The layer of PMMA 350 has the highest stress, while for PMMA 75 the lowest stress was found. This corresponds with the characteristic times  $\tau_{\text{char}}$  for the polymers which are given in figure 5.9 as well. The characteristic times increase with increasing molecular weight indicating that chains with higher molecular weights need more time to carry out a certain movement. As can be seen from the curves the stress increase is very high in the beginning. Probably, there is some stress relaxation taking place because the characteristic times are quite low. However, the differences between the different molecular weights are obvious. Furthermore, the differences in the stress development are an indication for the influence of the molecular weight on the mechanical behaviour, i. e., stress-strain behaviour. From literature<sup>[13,14]</sup> it is known that the E-modulus decreases (see figure 5.10) and the yield stress (stress at which the polymer breaks) increases with increasing molecular weight.

The reason therefore is the entanglement of the chains which is higher for high molecular weight chains. These entanglements give the polymer chains more mechanical strength, i. e., the interaction between the chains is much higher. Hence, compared to a polymer with lower molecular weight, a higher force is necessary to break this interactions. As a result polymers with higher molecular weight can compensate more stress before they break.

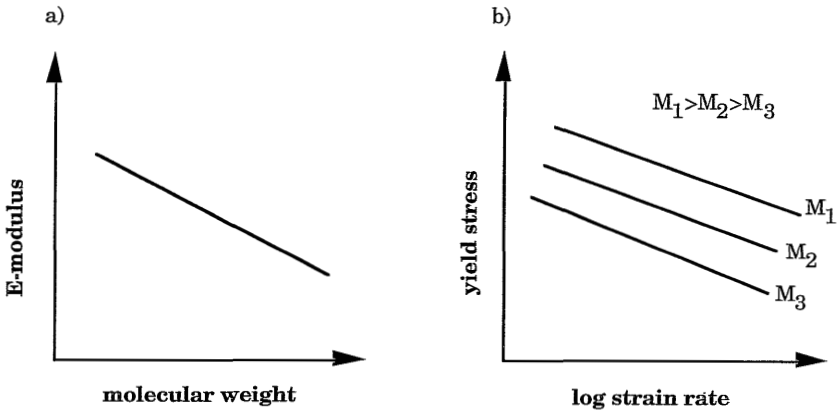


**Figure 5.10** Schematic drawing of a) the dependency of the E-modulus on the molecular weight and b) the influence of the molecular weight on the yield stress at a certain strain rate ( $M_1$ ,  $M_2$  and  $M_3$  indicate different molecular weights)

Furthermore, one can observe in the shape of the stress curve differences between the three polymers. While for PMMA 350 and PMMA 100 the stress almost immediately reaches a high level at which it remains almost constant there is a stress maximum in the first period of drying for PMMA 75. The stress remains then almost constant at a low level and increases again after about 5500 seconds. An explanation for the differences in the stress development has not been found yet. It might be due to the formation of small cracks in the layer of PMMA 75. Nevertheless, the film formation occurs within a few seconds in which the polymer solution passes its glass transition temperature. And this transition determines the development of stress in the layer. The changes in stress at longer drying times might be due to molecular relaxation processes in the case of PMMA 350 and PMMA 100, where at about 4000 seconds a decrease in stress can be observed.

For the aluminium film higher stress values were determined (see figure 5.11) which is caused by the lower mechanical strength of the aluminium film. The aluminium film has less resistance to withstand the shrinkage of the coating layer. Nevertheless, the assumptions made for equation (5.14) were applied for the GFT support too. Also here the highest stress was found for PMMA 350. Also the starting peak which is referred to as a temperature peak is much higher than in the case of the GFT supports and also higher than the stress in the coating layers. No negative stress can be observed indicating that the negative peaks obtained in the case of GFT supports are caused by some swelling or penetration of solvent into the pores.

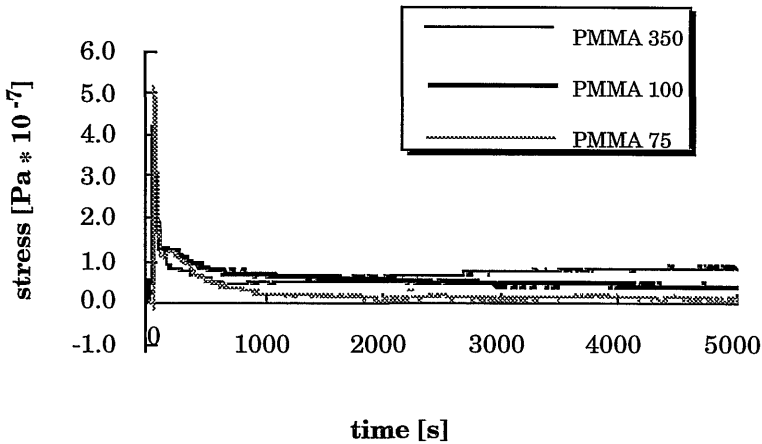


**Figure 5.11** Stress-time diagram for PMMA 350, PMMA 100 and PMMA 75 on aluminium films. Coating solutions of 4 % polymer in chloroform were applied.

A completely different behaviour in the stress development can be observed with polydimethyl siloxane (PDMS). The stress increases in the beginning to a level comparable to that of PMMA ( $\sim 10^6$  Pa), but then continuously decreases to negative values (see Figure 5.12). This might probably, be caused by interaction of the solvent hexane with the support membrane. This figure very clearly shows that a rubbery polymer can compensate the stress by relaxation at the same time scale as the evaporation of the solvent occurs. The relaxation time for these polymers is much shorter than for glassy polymers<sup>[4]</sup>.

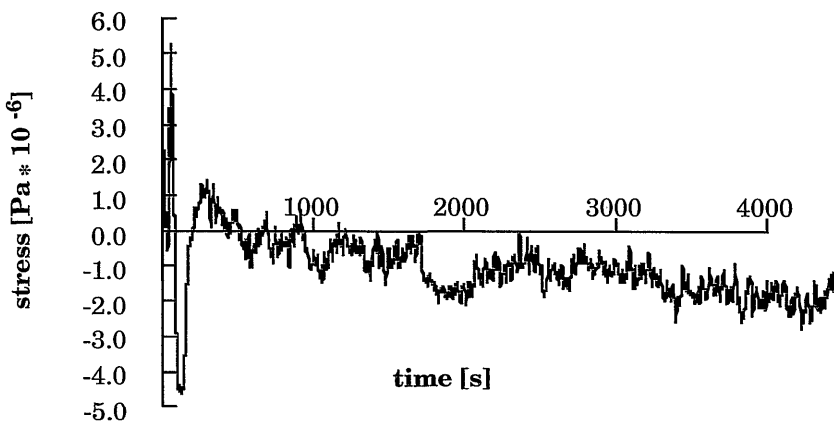


**Figure 5.12** Stress-time diagram of a PDMS layer coated from a solution of 5 % PDMS in hexane on nonimpregnated GFT support

### 5. 6. 3. INFLUENCE OF THE COATING THICKNESS

To investigate the influence of the coating thickness on the stress different concentrated solutions of PMMA 350 in chloroform were applied on GFT supports. Generally, it can be seen from figure 5.13 the higher the concentration in the coating solution the higher will be the stress in the dry film. In the case of 7.8 % and 6.5 % PMMA 350 in chloroform it seems that the stress values will approach the same value. The stress obtained for solutions with 5 % and 2 % polymer is much lower than that for the higher concentrated solutions. This can be understood if the characteristic relaxation times of the different solutions are compared. The characteristic times for the solutions with 7.8 % and 6.5 % polymer have almost the same value and are higher than those for the lower concentrated solutions. This means that the lower concentrated solutions can relax faster during the drying process. The results agree very well with measurements carried out by Perera<sup>[12]</sup>, who also obtained different stresses in layers of poly(isobutyl methacrylate) (PIBM) which were cast with different thicknesses. The results, however, disagree with those published by Croll<sup>[8]</sup>, who observed an independency of the stress on the casting thickness for layers of PIBM. Generally, the stress in the dry film may depend on the coating thickness if, for example, the E-modulus and the Poisson's ratio are affected by the concentration<sup>[8]</sup>.

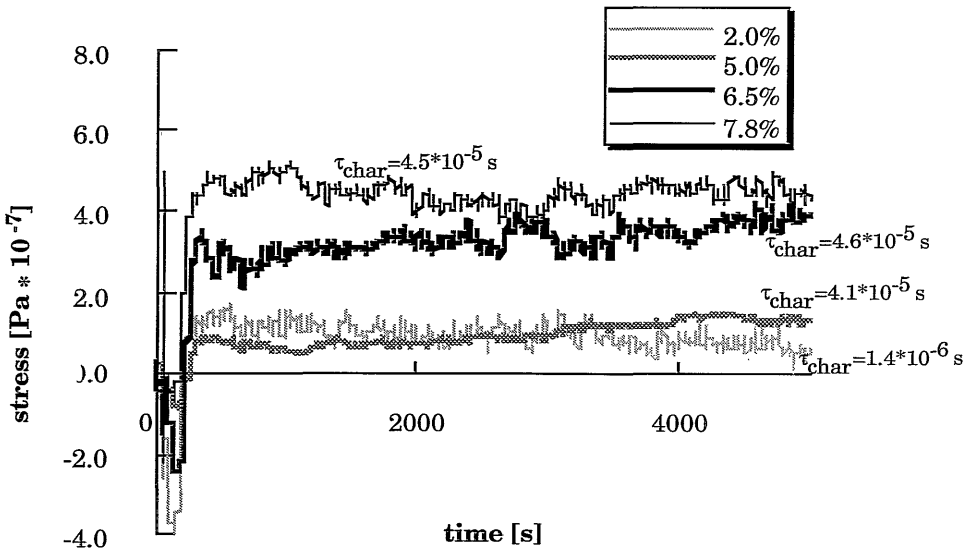


**Figure 5.13** Stress-time diagram for coating layers of PMMA 350 of different thicknesses. The coatings were applied from solutions of 2 %, 5 %, 6.5 % and 7.8 % polymer in chloroform

## 5. 6. INFLUENCE OF THE DRYING PROCEDURE

Figure 5.14 shows the stress measurements of layers of PMMA 350 which were dried in air and in a controlled atmosphere of chloroform vapour. No difference between the initial stress and the stress after the drying procedure can be observed. At a chloroform activity of about 0.4 the stress increases which might be due to the fact that the solution passes its glass transition. At an activity of 0.1 the stress increases very drastically up to the the initial stress value. The longer drying procedure does not result in bridging defects due to solvent loss, otherwise the stress would be higher compared to the one of the air dried layer. This result could be expected from the coating experiments discussed in chapter 4, where differences in the drying procedure did not result in differences in the performance of the composite membranes.

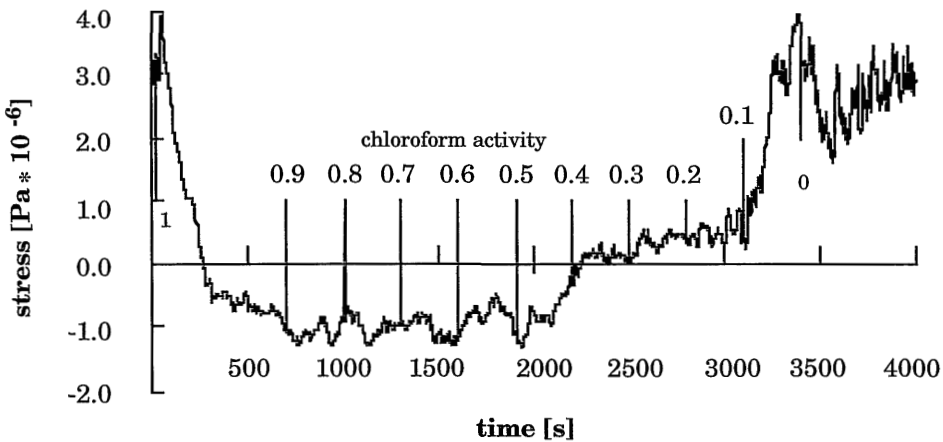


**Figure 5.14** Stress-time diagram for a layer of PMMA 350 coated from a solution of 6.5 % PMMA 350 in chloroform and dried in a controlled atmosphere of chloroform vapour. The activity of the chloroform was lowered about every 300 seconds as indicated.

### 5. 6. 4. INFLUENCE OF POST-TREATMENT

As was shown in Chapter 4 a post-treatment with solvent vapour can improve the gas separation performance of a composite membrane. Due to a partial dissolution the coated polymer is below its glass transition temperature. The polymer chains have a much higher mobility to rearrange due to the presence of solvent and in this way defects in the film can be repaired.

In Figure 5.15 the stress-time diagram is shown for a coating layer of PMMA 350 on GF'T support with a sequence of post-treatments with chloroform vapour. The

coating layer was applied from a solution of 4 % PMMA 350 in chloroform and then every 300 seconds (similar to the conditions described in Chapter 4) the activity of the surrounding was changed between solvent activity zero (pure nitrogen) and solvent activity 1. It can be clearly seen that during the vapour treatment the stress in the coating layer disappears due to the relaxation of the polymer chains. As the membrane is dried hereafter, the stress develops again, however, it does not reach its initial value. For the different cycles of post-treatment it seems that there is a slight increase in the stress with increasing number of treatments. This might be caused by the fact that after every post-treatment procedure further and further defects in the layer are bridged by polymer chains. This means that the polymer chains are more and more extended (see Figure 5.3). The resistance of the chains to follow this extension results in stresses which are higher the more defects in the layer are repaired.

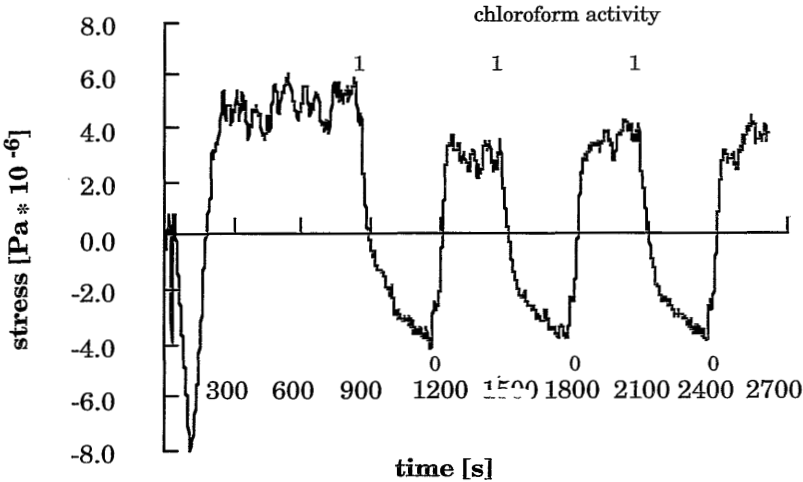


**Figure 5.15** Stress-time diagram for PMMA 350 post treated with vapour of chloroform

**5. 7. CONCLUSIONS**

A new method to measure the stress in polymeric coating layers during drying has been developed. It allows to measure differences in the residual stress depending on the molecular weight of the coating polymer. For PMMA 350, which has the highest molecular weight, one finds the highest stress in the dry coating layer. This shows the improved mechanical strength of the higher molecular weight polymer.

Significantly lower stress was found for a layer of PDMS. The residual stress in the layer of this rubbery polymer is about  $3 \cdot 10^6$  Pa times lower than in the layers of the PMMA.



A drying procedure with controlled change of the surrounding atmosphere did not result in a change in the stress values.

## 5. 8. REFERENCES

- [1] H. Tong, L. Nguyen; New characterization techniques for thin polymer films; Wiley-Interscience Publication, J. Wiley & sons, Inc. (1990)
- [2] C. L. Bauer, R. J. Farries; Polyimides: Materials, chemistry and characterization; Elsevier Science Publishers B. V., Amsterdam (1989), p. 549-562
- [3] K. P. Kumar; PhD thesis University of Twente, Chapter 3 (1993)
- [4] L. H. Sperling; Introduction to physical polymer science; 2nd edition, J. Wiley & sons, Inc. (1992)
- [5] J. Brandrup, E. H. Immergut; Polymer Handbook, 3rd ed. Wiley New York
- [6] H. F. Mark, N. M. Biklas, C. G. Overberger, G. Menges; Encyclopedia of polymer science and engineering; 2nd ed. Wiley, New York (1988)
- [7] G. P. Bierwagen; Film formation and mudcracking in latex coatings; J. Coat. Techn. 658 (51) (1979), 117-126
- [8] S. G. Croll; The origin of residual internal stress in solvent-cast thermoplastic coatings; J. Appl. Polym. Sci. 23, 847-858 (1979)
- [9] M. Doi, S. F. Edwards; The theory of diffusion; Oxford Science Publications, (1994)
- [10] T. C. Patton; Paint flow and pigment dispersion; Wiley & Sons, 2nd ed. (1970)
- [11] Appendix A to Chapter 3
- [12] D. Y. Perera, D. v. Eynde; Consideration on a cantilever (beam) method for measuring the internal stress in organic coatings; J. Coat. Techn. 53(677) 39-44 (1981)
- [13] J. H. Golden, B. L. Hammant, E. A. Hazell; Effects of molecular weight and strain rate on the flexural properties of polycarbonate; J. Appl. Polym. Sci., 12, 557-569 (1968)
- [14] J. R. Martin, J. F. Johnson, A. R. Cooper; Mechanical properties of polymers: The influence of molecular weight and molecular weight distribution; J. Macromol. Sci.-Rev. Macromol. Chem., C8(1), 57-199 (1972)



# 6

---

## **THE PREPARATION OF COMPOSITE MEMBRANES BY DIP-COATING; A SUMMARY**

---

### **6. 1. INTRODUCTION**

Membrane technology using composite membranes with a thin polymeric toplayer provides an alternative to other methods for the separation of gases. The applicability is determined by the permeability as well as by the selectivity. Generally, glassy polymers show low permeabilities in combination with relatively high selectivities, while this is vice versa for rubbery polymers. Because of the higher selectivities, which are necessary to produce pure gases, glassy polymers are preferred as coating material. However, to obtain economically attractive membranes, very thin dense layers are required to realize high fluxes through these membranes while maintaining the high selectivity. A relatively simple process to prepare such membranes is the dip-coating process, where a support membrane is withdrawn through a coating solution. The process is quite simple and can be carried out in a continuous mode, which is of great interest for the industrial production. However, the preparation of composite membranes provides certain difficulties since the prepared thin coating layers often are not defect-free. If the number of defects and the size of the defects are not too large an extra layer of a highly permeable rubber can be coated onto the selective layer to plug the defects<sup>[1]</sup>. The question remains how defect-free layers of the selective polymer can be obtained and which requirements with respect to the support, the coating polymer and the coating process must be fulfilled.

The answer to this question is very complex and can not be given straightforward. In this work some of the aspects of preparing composite membranes by dip-coating have been investigated. Some major conclusions can be drawn which may help to prepare better and more reproducible composite membranes.

## 6. 2. GENERAL ASPECTS

A composite membrane consists of at least two different layers, a porous substructure and a thin dense rate-determining toplayer. Both parts of the membrane can be optimized independently to obtain a membrane with the desired properties.

### *The support*

The support is required because the very thin coating layers do not possess any mechanical stability. Ideally, the support should not take part in the transport of gases, i. e. its porous structure should be as open as possible, or, in other words, its transport resistance should be negligible. On the other hand, if the pores on the surface are too big the coating solution can easily penetrate into these pores and block them. This leads to a drastic decrease of the flow through such a membrane<sup>[1,2]</sup>. If a support with too narrow pores is used then the capillary forces acting in these pores can cause defects in the toplayer. From these opposing effects it is clear that the support must be carefully chosen with regard to the separation problem and the properties of the coating polymer. Generally, as supports porous membranes with pore sizes in the ultrafiltration range are used. Furthermore, the material of the support must be chosen such, that it is not soluble in the solvent of the coating solution. Common polymers which are frequently used as supports are polysulfone<sup>[1,3-7]</sup>, polyacrylonitrile<sup>[2,8]</sup>, polyetherimide<sup>[9]</sup> and polyphenylene oxide<sup>[10]</sup>. Furthermore, the support and the coating polymer should be compatible in so far that adhesion between the two materials can occur.

### *The coating polymer*

Special attention so far has been paid toward the development of polymers with high selectivities for certain separation purposes. Generally, these polymers show rather low permeability coefficients. They consist of relatively large and stiff monomers, which are responsible for the restricted flexibility of the polymer chain. Typically, the flexibility of these polymers is not high which is indicated by their high glass transition temperatures. On the other hand, the E-moduli, which are in the range of about  $10^9$  N/m<sup>2</sup> for these polymers are quite high. As a comparison, the E-moduli for rubbery polymers are in the range of about  $10^6$  N/m<sup>2</sup>.

From stress measurements during the drying process of the coating layers<sup>[2]</sup> it seems that the mechanical properties of the coating polymer form a crucial parameter. During the drying process, i. e. the evaporation of solvent, two major processes occur: firstly, the coated film solidifies, which means for glassy polymers that at a certain polymer concentration the glass transition temperature of the solution is reached resulting in a very restricted flexibility of the polymer chains; secondly, a volume reduction occurs due to the loss of solvent in the coating layer

leading to a stress development in the layer. To obtain a defect-free layer the formed stress must be released, i. e. by the relaxation of the polymer chains. Therefore, flexible polymers or flexible parts in the main polymer chain are required. In the case of a rubbery polymer the flexible chains can change their conformation and thereby bridge the spaces arising from solvent loss. From the results of the coating experiments shown in chapters 3 and 4 and from the stress measurements discussed in chapter 5 it can be concluded that in the development of polymers for gas separation also the mechanical behaviour of these polymers should be included. The mechanical flexibility must be increased while maintaining the separation properties of the selective polymer. A possibility to obtain polymers with improved mechanical properties is the preparation of block copolymers with flexible spacers (see figure 6.1). These flexible spacers might be methylene- or siloxane groups, the number of them depending on the desired mechanical properties. It should be realized, however, that in most cases the separation performance changes as well.

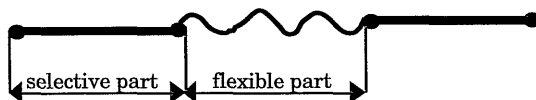


**Figure 6. 1** *Schematic drawing of the segments of an “ideal” coating polymer consisting of a selective (and stiff) part which determines the separation properties and a flexible part which is responsible for the mechanical properties*

### ***Prevention of pore penetration***

A problem which often occurs in the preparation of composite membranes is the penetration of the coating polymer into the pores of the support. This leads to a drastic decrease of the flux through the composite membrane and secondly, it can be the reason for defects. Pore penetration can be prevented by different methods. Firstly, an intermediate layer of a highly permeable rubber can be applied directly on the support creating an intermediate layer or “gutter” layer. The difficulty with this variant is that the compatibility between the intermediate layer and the actual separation layer must be good, because otherwise defects can be created by incomplete wetting<sup>[2]</sup>.

Another possibility might be the use of higher concentrated and, therefore, higher viscous coating solutions. However, this route has two main disadvantages; firstly, due to the higher concentration thicker coating layers are obtained and secondly, if the viscosity of the coating solution becomes too high, no continuous film can be formed<sup>[11]</sup>. The results obtained from the coating experiments with different concentrated solutions of poly(methyl methacrylate)<sup>[11]</sup> and literature data<sup>[12]</sup> indicate that there is an optimum range of viscosity.

The third method to prevent pore penetration is the use of polymers with higher molecular weights and the use of good solvents. From literature<sup>[12]</sup> and the coating experiments performed in this work<sup>[11]</sup> it is clear that the molecular weight of the coating polymer should be relatively high and a good solvent should be used to obtain a maximum radius of gyration to avoid a penetration of the polymer into the pores of the support.

A very effective method to prevent pore penetration is impregnating the pores of the support with a liquid, which is a nonsolvent for the coating polymer and immiscible with the coating solution (in our case water)<sup>[2,13]</sup>. The effective thicknesses of composite membranes prepared from solutions of 2 % Makrolon 3200 in chloroform on dry and impregnated GFT supports are shown in Figure 6.2. It can clearly be seen that in the case of impregnated supports the effective thickness could be reduced.

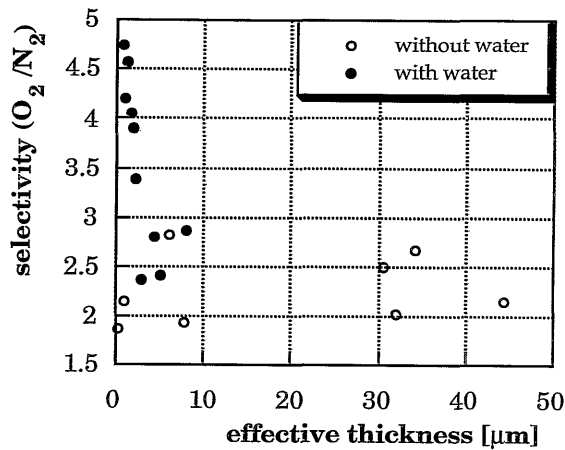


**Figure 6.2** Comparison of the effective thicknesses for layers prepared from a 2 % solution of Makrolon 3200 in chloroform on dry and impregnated GFT supports<sup>[2]</sup>

### **Drying and post-treatment**

No influence of the drying procedure on the quality of the prepared composite membranes could be observed. This is also indicated by the stress measurements which show no difference in the final stress for coating layers dried by different procedures (see chapter 4 of this thesis).

A post-treatment in a solvent vapour may improve the gas permeation selectivities. This procedure can be repeated several times to improve the quality of the coating

layer<sup>[10]</sup>. The effect can also be seen from the stress measurements which show an increase in the final stress in the coating layer after the post-treatment procedure indicating that the stress increases due to less defects in the layer the stress increases<sup>[14]</sup>.

### 6.3 CONCLUSIONS

The coating experiments performed in this work show that it is possible to prepare composite membranes with ultrathin toplayers. To obtain high flux membranes pore penetration of the coating polymer into the pores of the support must completely be avoided. This can be achieved by firstly using a polymer with a molecular weight of at least 300,000 g/mol<sup>[10,11]</sup> and secondly, by using a coating solvent in which the molecular dimension of the polymer chain is a maximum.

The mechanical properties of the coating polymer seem to be crucial for the quality of the coating layer. Glassy polymers with relatively high E-moduli are not flexible enough to compensate the stress which is built up in the layer upon drying. Therefore, in the development of new polymers for the separation of gases the elasticity should be taken into account.

The main criteria which have to be considered in the preparation of composite membranes can be summarized as follows:

- the coating polymer with:
  - high selectivity and permeability for a certain separation problem
  - relatively flexible chains
  - high molecular weight
- the use of a solvent which creates a high radius of gyration
- the porous support which is not soluble in the coating solvent
- the application of a post-treatment with solvent vapour to repair defects

### 6. 4. REFERENCES

- [1] Henis, J. M., Tripodi, M. K.; Multicomponent Membranes for gas separation; U. S. Patent 4,230,463  
Henis, J. M., Tripodi, M. K.; Composite hollow-fibre membranes for gas separation: The resistance model approach; J. Membr. Sci., 8 (1981) 233
- [2] chapter 3 of this thesis
- [3] J. D. Le Roux, D. R. Paul; Preparation of composite membranes by a spin coating process; J. Membr. Sci., 74 (1992), 233-252
- [4] I. Cabasso, K. A. Lundy; Method for making membranes for gas separation and the composite membranes; U. S. Patent 4,602,922  
K. A. Lundy, I. Cabasso; Analysis and construction of multilayer membranes for the separation of gas mixtures; Ind. Eng. Chem. Res., 28(6) (1989), 742-756
- [5] I. Pinnau; Ultrathin ethylcellulose/poly(4-methylpentene-1) permselective membranes; U. S. Patent 4,871,378

- [6] I. Blume, I. Pinnau; Composite membranes, method of preparation and use; U. S. Patent 4,963,165
- [7] S. Ohyabu, S. Kawai, T. Okamoto, T. Migaki; Composite hollow fibre-type separation membranes, process for the preparation thereof and their use; U. S. Patent 4,664,669
- [8] T. Chung, E. R. Kafchinsky, R. S. Kohn, P. Foley, R. S. Straff; Fabrication of composite hollow fibers for air separation; *J. Appl. Polym. Sci.*, 53 (1994), 701-708
- [9] K. Kneifel, K. V. Peinemann; Preparation of hollow fiber membranes from polyetherimide for gas separation; *J. Membr. Sci.*, 65 (1992), 295-307
- [10] G. A. Polotskaya, Y. P. Kuznetsov, K. A. Romashkova, M. Bleha, J. Schauer, J. Urban; Gas permeability through composite membranes based on polyamideimide; in *Polyimides and other high temperature polymers*, ed. by M. J. M. Abadie, B. Sillion; Elsevier Science Publishers B. V., Amsterdam (1991)
- [11] Chapter 4 of this thesis
- [12] M. E. Rezac, W. J. Koros; Preparation of polymeric-ceramic composite membranes with thin defect-free separating layers, *J. Appl. Polym. Sci.*, 46 (1992), 1927-1938)
- [13] S. C. Williams, B. Bikson, J. K. Nelson; Composite membranes for enhanced fluid separation; EP 0 286 091  
S. C. Williams, B. Bikson, J. K. Nelson, R. D. Burchesky; Method for preparing composite membranes for enhanced gas separation; U. S. Patent 4,840,819
- [14] chapter 5 of this thesis



## SUMMARY

The application of polymeric composite membranes can be very interesting in the field of gas separation. The two main parameters which determine the applicability of membranes are the selectivity and the permeability. Good selectivities can be achieved by developing proper materials, high permeation rates can be obtained by minimizing the thickness of the separation layer. Special attention is paid so far for glassy polymers which generally show higher selectivities than rubbery polymers. However, caused by the often rigid structure of the glassy polymers, defects in the these layers can occur which have a dramatic influence on the selectivity. The objective of this thesis is to investigate, which parameters may influence the preparation of composite membranes. The membranes were coated by the dip-coating method. Polycarbonate (Makrolon 3200) and poly(methyl methacrylate) (PMMA) were used as coating polymers. Three commercial polyacrylonitrile ultrafiltration membranes (GFT, Stork 3010, Stork 5010) were used as support materials.

Chapter 1 gives a short introduction into the preparation of composite membranes. The given literature review is restricted to the dip-coating method.

The support material is an important part of a composite membrane. Special requirements with respect to chemical resistance and porous structure must be fulfilled. In Chapter 2 the support membranes are characterized with different techniques, such as gas permeation, electron microscopy, permporometry and liquid-liquid displacement and the results are compared. Significant differences between methods carried out in the dry or in the wet state were obtained.

The appendixes A and B to Chapter 2 give the mathematical derivation of the pore size distribution from permporometry and liquid-liquid displacement measurements.

In Chapter 3 the preparation of composite membranes with polycarbonate as the coating polymer is described. The membranes were prepared with polymer solutions of different concentrations and different coating velocities. A significant improvement was obtained by impregnation of the support membrane with water, thereby avoiding pore penetration. Pore penetration is one of the major problems with composite membranes, because it firstly, may lead to defects and secondly, it may lead to dramatic decrease of the gas permeation rate through the membrane. The latter was shown with a simple calculation using the resistance model of Henis and Tripodi. For some of the impregnated membranes selectivities higher than the intrinsic selectivities were obtained.

In Appendix a to Chapter 3 the rheological properties of the coating solutions were investigated. For all of the used solutions Newton behaviour can be assumed.

Appendix B to Chapter 3 shows the results of the characterization of the coating solutions with respect to the conformation and association behaviour. The solutions were characterized with viscosity measurements, gel permeation chromatography

and static light scattering.

In Chapter 4 the preparation of composite membranes with PMMA as the coating polymer is described. For the PMMA with the highest molecular weight in chloroform, tetrahydrofuran and 1,2-dichloroethane pore penetration could be avoided, because the dimension of the polymer chains in these solutions is at least as big as the dimension of the pores of the support membrane. Some of the prepared membranes were post treated with solvent vapour leading to partially improved performance and effective thicknesses of less than 1  $\mu\text{m}$ . In one case almost intrinsic selectivity was obtained.

An important reason for the occurrence of defects in coating layers of composite membranes is the development of mechanical stress during the drying process. The stress is much higher for glassy polymers than for rubbery polymers. In Chapter 5 a new method is introduced which allows the measurement of stress during the drying process.

Chapter 6 is an attempt of a summary of important aspects which have to be considered during the preparation of composite membranes. Special attention is paid to the influence of the support, the coating polymer, the prevention of pore penetration and the drying and post-treatment process.

## SAMENVATTING

Polymere membranen bieden interessante mogelijkheden voor het scheiden van gassen. Twee parameters die bepalend zijn voor de toepasbaarheid van membranen zijn de selectiviteit en de permeabiliteit. Hoge selectiviteiten kunnen bereikt worden door de ontwikkeling van specifieke op het proces toegesneden materialen terwijl hoge permeabiliteiten bereikt kunnen worden door een goede materiaal keuze en het minimaliseren van de dikte van de scheidende laag. Bij gasscheidingsmembranen gaat de aandacht voornamelijk uit naar glasachtige polymeren daar deze in het algemeen een hogere selectiviteiten bezitten dan rubberachtige polymeren. Een probleem bij het maken van dunne lagen van glasachtige polymeren is dat deze polymeren een nogal starre structuur hebben waardoor defekten in de laag kunnen optreden. Deze defekten hebben een drastische verlaging van de selectiviteit tot gevolg. Het doel van de in dit proefschrift beschreven onderzoek is proberen inzicht te krijgen in de parameters die in het laagjes vormingsproces van belang zijn zodat dunnere en defektvrije laagjes kunnen worden gemaakt.

De in dit proefschrift gebruikte komposietmembranen bestonden uit een dragermateriaal met daarop een polymere coating, die werd aangebracht met de dip-coating methode. Polycarbonaat (Makrolon 3200) en poly(methylmethacrylaat) (PMMA) werden als coating polymeer gebruikt. Als dragermateriaal werden drie commercieel verkrijgbare ultrafiltratiemembranen gebruikt (GFT, Stork 3010, Stork 5010).

Hoofdstuk 1 geeft een korte introductie op het gebied van het vervaardigen van komposietmembranen. De nadruk ligt daarbij op de dip-coating methode.

Het dragermateriaal is een belangrijk deel van een komposietmembraan. Het moet aan specifieke eisen voldoen inzake chemische stabiliteit en poriestructuur. In Hoofdstuk 2 worden de dragermembranen gekarakteriseerd met verschillende technieken, zoals gaspermeatie, elektronenmicroscopie, permoporometrie en vloeistof-vloeistof verdringing. De resultaten die met deze technieken verkregen zijn worden met elkaar vergeleken. Er zijn belangrijke verschillen gevonden tussen die karakteriseringsmethoden die de membranen in droge toestand gebruiken en die waarbij de membranen in natte toestand gebruikt worden.

In de Appendices A en B bij Hoofdstuk 2 wordt de poriegrootteverdeling wiskundig afgeleid uit de resultaten van permoporometrie en vloeistof-vloeistof verdringing.

In Hoofdstuk 3 wordt de vervaardiging van komposietmembranen met polycarbonaat als coatingpolymeer beschreven. Er werden membranen gemaakt met verschillende concentraties van het coatingpolymeer en met verschillende coatingsnelheden. Een belangrijke verbetering van de kwaliteit van de coating is bereikt door het impregneren van het dragermembraan met water. Hierdoor is penetratie van de coating in de poriën van het dragermembraan tegengegaan. Poriepenetratie is een van de belangrijkste problemen bij het maken van komposietmembranen, omdat het, ten eerste, kan leiden tot defekten in de toplaag en, ten tweede, kan zorgen voor een afname van de gaspermeatie door het membraan. Dit laatste blijkt ook uit een berekening aan de hand van het weerstandsmodel van Henis en Tripodi. Sommige geïmpregneerde membranen hadden hogere selectiviteiten dan de intrinsieke selectiviteit van het coating polymeer.

In Appendix A bij Hoofdstuk 3 wordt het onderzoek naar de rheologische eigenschappen van de coatingoplossingen beschreven. Voor alle oplossingen kan Newtoniaans gedrag worden aangenomen. Appendix B bij Hoofdstuk 3 beschrijft de resultaten van de karakterisering van de coatingsoplossingen betreffende het configuratie- en associatiegedrag. De oplossingen werden

gekaracteriseerd door viscositeitsmetingen, gelpermeatie chromatografie en statische lichtverstrooiing. In Hoofdstuk 4 wordt de vervaardiging van komposietmembranen met PMMA als coatingpolymeer beschreven. Wanneer het hoogste molgewicht PMMA wordt opgelost in chloroform, tetrahydrofuraan of 1,2-dichloorethaan, kan er geen penetratie in de poriën plaatsvinden, omdat de afmetingen van de polymere ketens tenminste zo groot zijn als die van de poriën in het dragermateriaal. Sommige membranen zijn nabehandeld met oplosmiddeldamp, wat in bepaalde gevallen leidt tot verbetering van de scheidingseigenschappen en tot effectieve dikten van minder dan 1  $\mu\text{m}$ . Voor één membraan is een selectiviteit gevonden die vrijwel gelijk was aan de intrinsieke selectiviteit van PMMA.

Een belangrijke reden voor het ontstaan van defekten in dunne lagen glasachtige polymeer is de opbouw van mechanische spanningen tijdens het drogen van de polymere laag. Deze spanningen zijn relatief hoog in vergelijking met die die optreden bij rubberachtige polymeren. In Hoofdstuk 5 wordt een nieuwe methode geïntroduceerd waarmee de mechanische spanningen die tijdens het droogproces optreden gevolgd kunnen worden.

In Hoofdstuk 6 is gepoogd om de voornaamste aandachtspunten die van belang zijn bij het maken van komposietmembranen aan te geven. Daarbij is vooral ingegaan op de invloed van het dragermembraan, het coating polymeer, het verhinderen van poriepenetratie en het droog- en nabehandelingsproces.

## ZUSAMMENFASSUNG

Komposietmembranen bieten eine gute Ergänzung herkömmlicher Gastrennungsmethoden. Besonders wichtig für die Wirtschaftlichkeit einer solchen Membran sind der Trennfaktor und der Gasfluß durch die Membran. Der Trennfaktor ist eine Materialeigenschaft, welcher durch die Entwicklung spezieller Polymere erhöht werden kann. Der Gasfluß kann erhöht werden, indem die Dicke der Trennschicht verringert wird. Spezielles Interesse liegt dabei bei den glasartigen Polymeren, die generell höhere Selektivitäten als Elastomere zeigen. Ein Problem bei der Herstellung dünner Schichten mit diesen Polymeren ist, daß, bedingt durch die teilweise steife Struktur der Polymere, Fehlstellen entstehen, die zur Unbrauchbarkeit der Membran führen. Das Ziel der vorliegenden Arbeit ist es, zu untersuchen, welche Parameter einen Einfluß auf die Herstellung von Komposietmembranen ausüben können. Beim Anbringen der Polymerschicht auf die Trägersubstanz wurde ausschließlich die dip-coating-Methode angewandt. Als Beschichtungspolymere wurden Polykarbonat (Makrolon 3200) sowie ataktisches Polymethylmethacrylat (PMMA) verwendet. Als Trägermaterialien wurden drei kommerzielle Ultrafiltrationsmembranen aus Polyacrylnitril (GFT, Stork 3010, Stork 5010) ausgewählt.

Kapitel 1 gibt eine kurze Einleitung in die Problematik der Herstellung von Komposietmembranen. Besonderes Augenmerk wurde dabei auf die dip-coating-Methode gelegt.

Das Trägermaterial spielt eine wichtige Rolle sowohl bei der Herstellung als auch für das Trennungsvermögen einer Komposietmembran. Es ist deshalb besonders wichtig, die Struktur der Trägermembran zu charakterisieren. In Kapitel 2 werden die Ergebnisse verschiedener Charakterisierungsmethoden (Gasflußmessungen, Elektronenmikroskopie, Permporometrie und Flüssigkeit-Flüssigkeit-Verdrängungsmethode) verglichen.

Die Anhänge A und B zu Kapitel 2 geben die mathematische Ableitung der Porengrößenverteilung aus den Meßwerten von Permporometrie und Flüssigkeit-Flüssigkeit-Verdrängungsmethode.

In Kapitel 3 wird die Herstellung von Komposietmembranen mit Polykarbonatschichten auf GFT-Trägermembranen beschrieben. Es wurden Membranen mit verschiedenen konzentrierten Beschichtungslösungen und unterschiedlichen Beschichtungsschnelligkeiten hergestellt. Eine wesentliche Verbesserung der Beschichtungsqualität konnte durch impregnieren der Trägermembran mit Wasser erreicht werden, wodurch verhindert werden konnte, daß die Beschichtungslösung in die Poren der Trägermembran eindringt. Das Eindringen von Polymerlösung in die Trägermembran ist nicht nur eine der wesentlichen Ursachen für das Entstehen von Fehlstellen, sondern kann auch erheblich zur Reduzierung der Transportes von Gas durch die Komposietmembran führen. Letzteres wird anhand

einer Berechnung mit dem Widerstandsmodell deutlich aufgezeigt. Für einige der Komposietmembranen konnten Sauerstoff/Stickstoff-Selektivitäten erreicht werden, die über der intrinsischen Selektivität für Polykarbonat liegen.

Im Anhang A zu Kapitel 3 werden die rheologischen Eigenschaften der Beschichtungslösungen untersucht. Für alle verwendeten Lösungen kann Newtonsches Verhalten angenommen werden.

Anhang B zu Kapitel 3 beschäftigt sich mit der Charakterisierung von Polymerlösungen mit verschiedenen Methoden (Viskositätsmessungen, Gelpermeationschromatographie, Lichtstreuung). Anhand der erhaltenen Informationen über Viskosität, Ausdehnung der Polymermoleküle in der Lösung und deren Assoziationsverhalten kann der Einfluß der Beschichtungslösungen auf die Qualität der Beschichtungen bestimmt werden.

Kapitel 4 beschreibt die Herstellung von Komposietmembranen mit PMMA als Beschichtungspolymer. Es wurden PMMA mit verschiedenen Molekulargewichten verwendet. Für das PMMA mit dem höchsten Molekulargewicht (PMMA 350) in Chloroform, Tetrahydrofuran und 1,2-Dichlorethan konnte das Eindringen der Beschichtungslösungen in den porösen Träger verhindert werden, da die Ausdehnung der Polymermoleküle zumindest ebenso groß ist wie die Poren des Trägers. Einige der hergestellten Komposietmembranen wurden einer Nachbehandlung mit Lösungsmitteldampf unterzogen, wobei partiell eine Verbesserung der Trenneigenschaften und in einem Fall auch fast intrinsische Selektivität erreicht werden konnte.

Ein wichtiger Grund für die Entstehung von Fehlstellen bei glasartigen Polymeren sind mechanische Spannungen, die sich während des Trocknungsprozesses in der Schicht entwickeln. Diese Spannungen können im Vergleich zu Elastomeren hohe Werte erreichen. In Kapitel 5 wird eine Methode vorgestellt, die es erlaubt, diese Spannungen zu messen. Dabei wurde für das PMMA mit dem höchsten Molekulargewicht auch die höchste Spannung in der Schicht gemessen.

Kapitel 6 ist der Versuch, einer Zusammenfassung wichtiger Aspekte, die bei der Herstellung von Komposietmembranen beachtet werden sollten. Anhand der Resultate wird auf die Einflüsse des Trägermaterials, des Beschichtungspolymeres, das Impregnieren des Trägers sowie des Trocknungs- und Nachbehandlungsprozesses eingegangen.



## **CURRICULUM VITAE**

Katrin Ebert was born on september 17, 1965 in Dresden (Germany). She graduated at the Kant-Gymnasium in 1984. In the same year she entered the Technical University of Merseburg and in 1987 the Technical University of Dresden. In 1989 she took her Diplom-Chemiker degree. The diploma-thesis were carried out in the group of Prof. Dr. G. Glöckner on the characterization of polymer solutions by means of light scattering and viscosity measurements.

After graduation she worked as a Senior Research Scientist at Chemieanlagenbau, Dresden and at Constab-Polymerchemie Rüthen. There she was responsible for the mechanical tests of polymers as well as for the analysis of polymer batches.

In July 1991 she entered in the membrane group of prof. dr. C. A. Smolders and later prof. ing. H. Strathmann and worked there on the preparation of composite membranes of glassy polymers. The research is finished with a doctor degree on September 15, 1995.





